Mixing State of the Aqueous Solution of Ionic Liquid $[P_{4,4,4,4}]CF_3COO$ Near the Critical Point

臨点近傍におけるイオン液体 $[P_{4,4,4,4}]CF_3COO$ 水溶液の混合状態

Doctor Thesis

January 2017

Ayako Nitta

Department of Nanomaterial Science
Division of Nanoscience
Graduate School of Advanced Integration Science

CHIBA UNIVERSITY

(千葉大学審査学位論文)

Mixing State of the Aqueous Solution of Ionic Liquid $[P_{4,4,4,4}]CF_3COO$ Near the Critical Point

臨点近傍におけるイオン液体 $[P_{4,4,4,4}]CF_3COO$ 水溶液の混合状態

Doctor Thesis

January 2017

Ayako Nitta

Department of Nanomaterial Science
Division of Nanoscience
Graduate School of Advanced Integration Science

CHIBA UNIVERSITY

Contents

Chapter 1 General introduction

1. 1. Ionic liquids

Ionic liquids (ILs) are novel types of liquids composed of only cations and anions which show the melting points below 100 ºC. [1], [2] ILs have the unique properties [3]–[5] such as non-volatility, non-flammability, high thermal and chemical stability, high solubility towards a large number of solutes and good electric conductivity. Furthermore, some authors claimed that ILs show inhomogeneity in liquid structure [6]–[9] while other observed anomalous kinetic behaviors associated with freezing/melting processes [10], [11]. There have been an extensive activities on investigating such special characteristics of ILs in recent years.

There have been extensive efforts to lower the melting points of salts for various purposes including the environmental issue. [12] Now that new room temperature ILs have been gradually discovered, they are indeed environmentally friendly solvents. ILs have high solubility and selectivity towards gases and are expected as good CO_2 absorbents. [13] They are also electrolytes and can be utilized for electrochemical applications. [14] Non-volatility and non-flammability of ILs are useful for electrolytes in car batteries. [15] Recently, dissolution for cellulose is one of the most attractive topics related to the issues of bioethanol. [16]

Figure 1-1 shows typical cations and anions composing ILs. Afore mentioned properties depend on the combination of constituent cations and anions and the nature of each ions. Because many ILs are composed of large organic ions, their final properties can be regulated for the given target functions by designing the side chains or the functional groups of the cations and the anions. For example, extending alkyl chains and etherifying a part of the chains bring about an increase in hydrophobicity. That is, a large number of combinations of cations and anions can be possibly tried out. Thus, we could obtain various ILs with the variety of desired functions. [14] As a result such ILs as those containing metal complexes. [17] Furthermore, zwitterionic ILs [18], polymerized and gelatinized ILs [19] and liquid-crystal type ILs [20] have been synthesized.

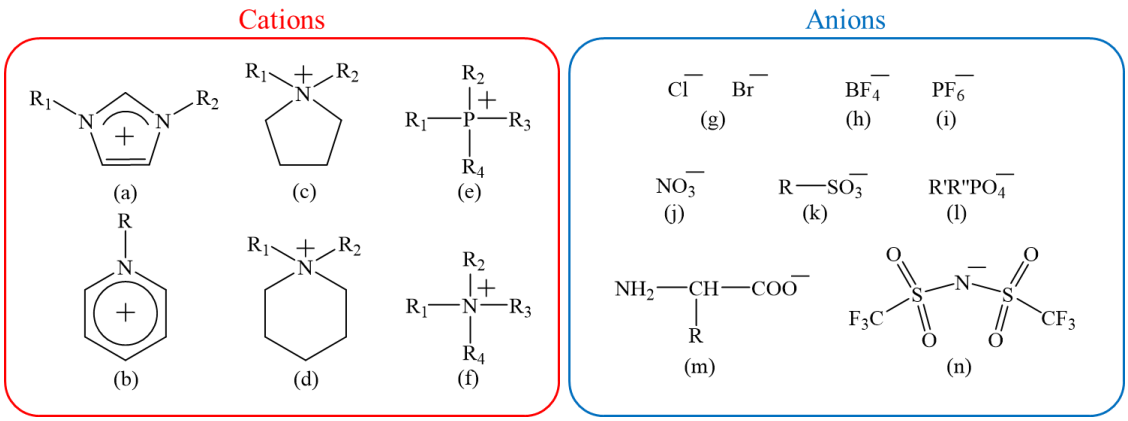

Figure 1-1 Typical ions composing ionic liquids. Cations; (a)imidazolium, (b)pyridinium, (c)pyrrolidinium, (d)piperidinium, (e)phosphonium, (f)ammonium. Anions; (g)halides, (h)tetrafluoroborate, (i)hexafluorophosphate, (j)nitrate, (k)sulfonate, (l)phosphate, (m)amino acid anion and (n)bis(trifluoromethansulfonyl)imide.

1. 2. Mixtures of ionic liquids and other materials

ILs' solubility for other solvents is important [21]–[23] because a small amount of impurities tends to change the properties of the pure ILs rather drastically. Liquid-liquid equilibrium properties for binary or ternary mixtures of ILs and alcohols or water have been reported from the view point of removing contaminants. [24]–[27]

On the other hand, ILs tend to be highly viscous, and cause disadvantage for mass transfer or some difficulty in treating them. To overcome such difficulties, mixtures of IL with molecular liquids are often used. For example, the mixtures of 1-butyl-3-methylimidazolium bis(trifluoromethylsulfonyl)imide, $[C_4mim]NTf_2$, with alcohols or water show a much lower viscosity than the pure ILs. [28] Furthermore, by mixing, new properties are obtained and the drastic change of those properties of the IL mixtures are depending on its concentration. They could be used to our advantage. [29] Mixing is another technique to control their functions and the properties may be predicted. For the mixture of two kinds of ILs, similar advantages were discussed. [30], [31]

1. 3. Study on aqueous solutions of ionic liquids

Because water is the most important liquid for living matters, aqueous solutions of ILs have been studied for biochemical reactions and chemical extractions media. [32] Also, water itself has the unique characteristics based on three dimensional hydrogen bonding. The mixtures of two peculiar materials thus attract increasing attention for fundamental investigations.

The solubility of ILs in water depends on the combination of cations and anions of ILs. ILs composed of imidazoliums with short alkyl chain and halides, for example, 1-ethyl-3-methylidazolium chloride, $[C_2mim]Cl$, and BF_4^- with the same cation, $[C_2mim]BF_4$, are miscible with water in the complete mole fraction. On the other hand, ILs composed of imidazoliums with a longer alkyl chain such as $[C_6mim]^+$, and/or a bulky anion as NTf_2^- are water immiscible and show biphasic systems at room temperature. Some aqueous solutions of ILs show temperature dependent reversible phase separations. [32]–[34] For example, the aqueous solution of 1-butyl-3-methylimidazolium tetrafluoroborate, $[C_4mim]BF_4$, was observed to exhibit phase separation with the upper critical solution temperature, UCST, [33], [34] showing the single phase (mixing) at higher temperatures and the biphasic system (separating) at lower temperatures. Also some aqueous solution of phosphonium-based ILs showing phase separation with the lower critical solution temperature, LCST, also have been reported. [35], [36] Using the mixtures with those properties are expected as a possible extraction and reaction solvents. Figure 1-2 is one of the applications for aqueous solutions of IL with the LCST-type phase separation as a reaction solvent [32], as explained in the figure caption of figure 1-2.

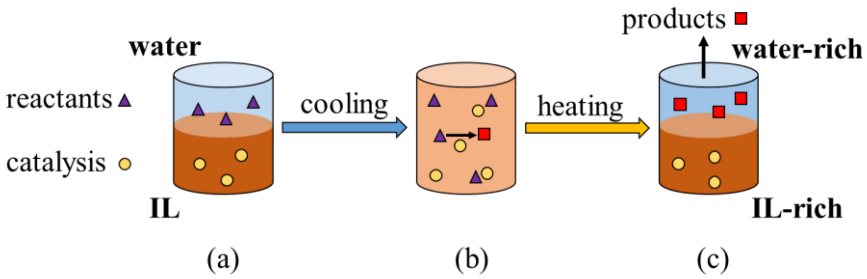

Figure 1-2 An application for a binary systems of ILs and water with LCST relies on the reversible phase separation. [32] (a)Reactants and catalysts are dissolved in the water and the IL layers separately. (b)By cooling, the system becomes one phase and the chemical reactions occur. (c)By heating the system, the biphasic mixture appears with the water-rich phase and the IL-rich phase. Thus the products and the catalysts are separated.

A large number of investigations for physicochemical properties of aqueous solution of ILs have been reported [37], [38] such as density [39]–[41], surface tension [39], viscosity [42], thermophysical quantities [43]–[45] and electrical conductivity [46]–[48]. Mixing state of them also have been studied by molecular dynamics simulation [49], [50], NMR method [51], [52] and X-ray or neutron scattering method [53]–[55]. Even in dilute region, ion pair formations were discussed. [52], [56]–[59] At higher concentration region, aggregation of ILs [55], [60]–[62] and unique behavior of water molecules [63]–[66] were reported. In some aqueous solutions of ILs, "water pocket" which confine water molecules in ILs was demonstrated by molecular dynamics simulation. [61] For the mixture of 1-butyl-3-methyl nitrate, $[C_4mim]NO_3$, and water, the evidence of water pocket was observed by neutron scattering. [53] The aqueous solution of $[C_4mim]BF_4$ which shows UCST-type phase separation was reported a drastic change of mixing state by small-angle neutron scattering. [54]

1. 4. Aqueous solution of $[P_{4,4,4,4}]CF_3COO$

The most of the sample ILs in previous studies are based on ILs with imidazolium cations although there are many other kinds of cations as shown in figure 1-1. Recently, phosphonium-based ILs which has four alkyl chains draw much attentions. Their properties depend heavily on their symmetries. Also their high solubility for organic solvents is advantageous for chemical reactions. [67], [68] The mixtures of phosphonium-based ILs and water show various behaviors depending on the counter anions. Combinations of tetrabutylphosphonium, $[P_{4,4,4,4}]^+$ and NTf_2^-, BF_4^- and trifluoromethanesulfonate are immiscible with water and form liquid/liquid biphasic systems. On the other hand, combinations of $[P_{4,4,4,4}]^+$ and Br^-, NO_3^- and benzenesulfonate are miscible with water completely. Combinations of $[P_{4,4,4,4}]^+$ with p-methylbenzenesulfonate, 2,4-dimethylbenzensulfonate and 2,4,6-trimethylbenzen-sulfonate are reported to show the LCST-type phase separation. [69] Using the temperature-induced phase transition, the mixtures of IL and water are used as extraction of biopolymers. The aqueous solution of tetrabutylphosphonium *N*-trifluoromethanesulfonyl leucine was reported their effectiveness for protein extraction. [32] Furthermore, based on the investigation of aqueous solutions of ILs, such functional materials as thermoresponsive polyelectrolyte hydrogels have been synthesized. [70]–[72]

Now we selected the aqueous solution of tetrabutylphosphonium trifluoroacetate, $[P_{4,4,4,4}]CF_3COO$, because the structure of composing ions are relatively simple. It shows

the phase separation with the LCST and its critical point is at x_{IL}= 0.025 and at T= 302.35 K [69], where x_{IL} is mole fraction of $[P_{4,4,4,4}]CF_3COO$ and T is the absolute temperature. Figure 1-3 shows the phase diagram of the aqueous solution of $[P_{4,4,4,4}]CF_3COO$ and the black solid curve indicates the phase boundary. [69]

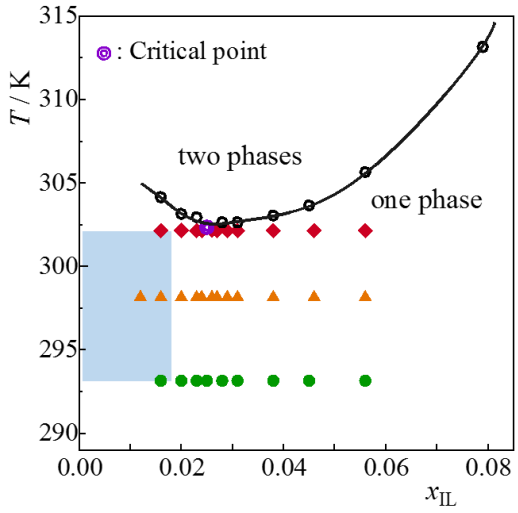

Figure 1-3 Phase diagram of aqueous solution of tetrabutylphosphonium trifluoroactate, $[P_{4,4,4,4}]CF_3COO$. [69] Black line is phase boundary and purple symbol indicate the critical point at x_{IL}= 0.025 and at T= 302 K. Red diamonds, orange triangles and green circles represent observed points for SAXS measurement at 293, 298 and 302 K. The light blue region indicates the mole fraction/temperature region where differential thermodynamic studies were applied.

The objective of this study is to learn the mixing state of aqueous solutions of IL. Mixing state is important to design the functional systems using IL. Especially, aqueous solution with temperature dependent reversible phase transition have great potential as biochemical reaction and extraction media. Furthermore, in the previous studies[73], [74], the unique properties near the critical points in aqueous solutions of molecular liquids which have UCST- or LCST-type phase separation were studied. We applied the concept of fluctuation which have been used for studying on liquid structure of various solution with the critical points on the aqueous solution of $[P_{4,4,4,4}]CF_3COO$ using small-angle X-ray scattering technique near the critical point. Also from the view point of differential thermodynamics established by Koga, we learned the intermolecular interactions of $[P_{4,4,4,4}]CF_3COO$ and water in dilute concentration region.

Chapter 2 Fluctuations

2. 1. Fluctuations for binary systems

Fluctuation, the variation from the global average, is an important concept for fundamental investigations. [73], [75] Super critical pure fluids, a good example, have both properties of gas-like and liquid-like and show large degree of fluctuation [76]. For aqueous solutions of molecular liquids, the systems show a large fluctuation near the de-mixing critical point. [77]–[80] The mixtures with a temperature-dependent phase separation were reported to show a large fluctuation near the critical point. For example, the aqueous solution of acetonitrile [81] showed the UCST-type phase separation and that of 2-butoxyethanol [82] exhibited the LCST-type phase separation.

Now consider a binary system of component A and B. Figure 2-1 (a) shows the schematic view of density fluctuation. The number of particles in a fixed volume V is fluctuating. Density fluctuation, $\langle(\Delta N)^2\rangle/\bar{N}$, is defined as the mean square of the difference of the local or instantaneous particle number from the average particle number ($\bar{N}$), ΔN. On the other hand, concentration fluctuation, $\bar{N}\langle(\Delta x)^2\rangle$, expresses the contrast of component A and B defined as the mean square difference of concentration from the global average, Δx. The correlation term of the density fluctuation and the concentration fluctuation, $\langle(\Delta N)(\Delta x)\rangle$, is also defined as shown in equation (3) below.

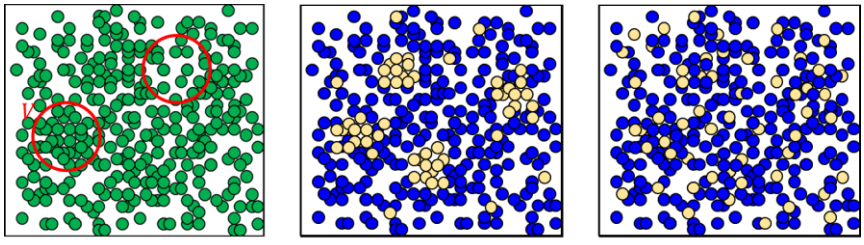

Figure 2-1 Schematic views of fluctuations for binary systems. (a)Density fluctuation, $\langle(\Delta N)^2\rangle/\bar{N}$, and (b)larger and (b')smaller concentration fluctuation, $\bar{N}\langle(\Delta x)^2\rangle$.

These fluctuations are the second derivative quantities of Gibbs energy, G, written as,

$$\bar{N}\langle(\Delta x_{\mathrm{A}})^2\rangle = \bar{N}k_{\mathrm{B}}T \Big/ \left(\frac{\partial^2 G}{\partial x_{\mathrm{A}}^2}\right)_{T,p,N}, \tag{1}$$

$$\frac{\langle(\Delta N)^2\rangle}{\bar{N}} = \left(\frac{\bar{N}}{V}\right)k_{\mathrm{B}}T\kappa_T + \left\{\frac{\bar{N}}{V}(v_{\mathrm{A}} - v_{\mathrm{B}})\right\}^2 \bar{N}\langle(\Delta x_{\mathrm{A}})^2\rangle, \tag{2}$$

$$\langle(\Delta N)(\Delta x_{\mathrm{A}})\rangle = -\left\{\frac{\bar{N}}{V}(v_{\mathrm{A}} - v_{\mathrm{B}})\right\}\bar{N}\langle(\Delta x_{\mathrm{A}})^2\rangle, \tag{3}$$

where k_{B} is Boltzmann's constant and μ_{A} is chemical potential of component A which is the first derivative of G. κ_T is the isothermal compressibility of the mixture and v_{i} is the partial molar volume of component i. Both κ_T and v_{i} are also the second derivatives.

2. 2. Small-angle X-ray scattering method

Small-angle X-ray Scattering (SAXS) method is one of the powerful tools to observe the structure at nanoscopic level (1-100 nm). Mainly SAXS methods have been used for structure analysis of nanomaterials and proteins in solution. [83], [84] X-ray is scattered by electrons in the sample material and the diffracted image corresponds to the Fourier transformation of electron density distribution. Scattering intensity is expressed as a function of scattering parameter, s, defined as,

$$s = \frac{4\pi \sin\theta}{\lambda}, \tag{4}$$

where λ is the wavelength of X-ray and 2θ is the scattering angle. The signals from electron density variation appear at certain s region according to the scale of the shape of materials. For materials without specific structures such as fluids and polymer solutions, SAXS intensity still gives information of their spatial characteristics. Figure 2-3 shows the relationship between the region of scattering parameter and the information of material structures. [85]

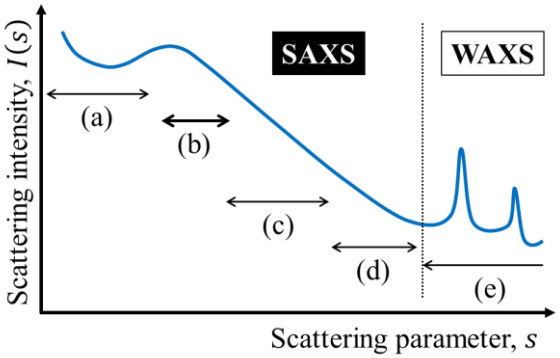

Figure 2-3 The information of materials obtained by small-angle and wide-angle X-ray scattering intensity against scattering parameter [85]; (a)interactions between molecules, (b)size of colloids, (c)shape of colloidal particles, (d)surface structure of particles and (e)crystal structures.

Bhatia and Thornton connected the SAXS intensity to fluctuations of binary systems. [75], [86] Consider a mixture composed of component A and B. Generally X-ray scattering intensity from the system, $I(s)$, is written as,

$$I(s) = \overline{N_\mathrm{A}} f_\mathrm{A}(s)^2 + \overline{N_\mathrm{B}} f_\mathrm{B}(s)^2 + \frac{\overline{N_\mathrm{A}}^2 f_\mathrm{A}(s)^2}{V}\int\left(g_{\mathrm{AA}}^{(2)} - 1\right)\frac{\sin sr}{sr}dV + \frac{\overline{N_\mathrm{B}}^2 f_\mathrm{B}(s)^2}{V}\int\left(g_{\mathrm{BB}}^{(2)} - 1\right)\frac{\sin sr}{sr}dV + 2\frac{\overline{N_\mathrm{A}}\,\overline{N_\mathrm{B}} f_\mathrm{A}(s) f_\mathrm{B}(s)}{V}\int\left(g_{\mathrm{AB}}^{(2)} - 1\right)\frac{\sin sr}{sr}dV \quad (5)$$

where N_i is the number of particles (molecules) of component i in a volume, V, and $f_\mathrm{i}(s)$ is the form factor of component i. $g_{\mathrm{ij}}^{(2)}$, two body correlation function, is defined as correlation between component i and j at a distance of $r = |r_\mathrm{j} - r_\mathrm{i}|$, namely, the probability of existence of component j around i. The value of $g_{\mathrm{ij}}^{(2)}$ approaches to 1 with increase of r. Superscript bar indicates the average.

First, Bhatia and Thornton defined Fourier transformations of variations from the average for the total number density of particles, $n = N/V$, $\Delta n(r)$, and for the mole fraction variation between A and B, $\Delta c(r)$ with distance r apart. They named the resulting Fourier transformations as $\mathcal{N}(s)$ and $\mathcal{C}(s)$, respectively. [75]

$$\mathcal{N}(s) = \int \exp(is \cdot r)\,\Delta n(r)\mathrm{d}r, \quad (6)$$

$$\mathcal{C}(s) = \int \exp(is \cdot r)\,\Delta c(r)\mathrm{d}r, \quad (7)$$

The density fluctuation, the concentration fluctuation and their correlation term within the reciprocal space are written using $\mathcal{N}(s)$ and $\mathcal{C}(s)$ as,

$$\frac{\langle \mathcal{N}(s)^* \mathcal{N}(s) \rangle}{\bar{N}}, \tag{8}$$

$$\bar{N} \langle \mathcal{C}(s)^* \mathcal{C}(s) \rangle, \tag{9}$$

$$\mathrm{Re} \langle \mathcal{N}(s)^* \mathcal{C}(s) \rangle. \tag{10}$$

Superscript * indicates conjugate quantity. The intensity of scattered X-ray is then written as,

$$\frac{I(s)}{\bar{N}} = \bar{f}(s)^2 \frac{\langle \mathcal{N}(s)^* \mathcal{N}(s) \rangle}{\bar{N}} + (f_\mathrm{A} + f_\mathrm{B})^2 \bar{N} \langle \mathcal{C}(s)^* \mathcal{C}(s) \rangle$$

$$+2\bar{f}(f_\mathrm{A} - f_\mathrm{B}) \mathrm{Re} \langle \mathcal{N}(s)^* \mathcal{C}(s) \rangle, \tag{11}$$

where,

$$\bar{f} = x_\mathrm{A} f_\mathrm{A} + x_\mathrm{B} f_\mathrm{B}, \tag{12}$$

and x_A and x_B are the mole fractions of component A and B, respectively.

At the limit of long wavelength,

$$\lim_{s \to 0} \frac{\sin sr}{sr} \to 1, \tag{13}$$

the amplitudes of component i, f_i, approach to the number of electrons of component i, Z_i,

$$f_\mathrm{i} \to Z_\mathrm{i}, \tag{14}$$

$$\bar{Z} = x_\mathrm{A} Z_\mathrm{A} + x_\mathrm{B} Z_\mathrm{B}. \tag{15}$$

Each term of equation (11) approaches to the fluctuations defined in equation (1), (2) and (3) as shown in equation (16), (17) and (18).

$$\frac{\langle \mathcal{N}(s)^* \mathcal{N}(s) \rangle}{\bar{N}} \to \frac{\langle (\Delta N)^2 \rangle}{\bar{N}}, \tag{16}$$

$$\bar{N} \langle \mathcal{C}(s)^* \mathcal{C}(s) \rangle \to \bar{N} \langle (\Delta x)^2 \rangle, \tag{17}$$

$$\mathrm{Re} \langle \mathcal{N}(s)^* \mathcal{C}(s) \rangle \to \langle (\Delta N)(\Delta x) \rangle. \tag{18}$$

Namely, the scattering intensity at s= 0, $I(0)$, shows the information of the system described by thermodynamic quantities. Therefore $I(0)$ is written as,

$$\frac{I(0)}{\bar{N}} = \bar{Z}^2 \frac{\langle(\Delta N)^2\rangle}{\bar{N}} + (Z_{\mathrm{A}} + Z_{\mathrm{B}})^2 \bar{N}\langle(\Delta x_{\mathrm{A}})^2\rangle + 2\bar{Z}(Z_{\mathrm{A}} - Z_{\mathrm{B}})\langle(\Delta N)(\Delta x_{\mathrm{A}})\rangle. \quad (19)$$

Using thermodynamic expressions,

$$\frac{I(0)}{\bar{N}} = \bar{Z}^2 \left(\frac{\bar{N}}{V}\right) k_{\mathrm{B}} T \kappa_T + \left\{\bar{Z}(v_{\mathrm{A}} - v_{\mathrm{B}})\frac{\bar{N}}{V} - (Z_{\mathrm{A}} + Z_{\mathrm{B}})\right\}^2 \bar{N}\langle(\Delta x_{\mathrm{A}})^2\rangle. \quad (20)$$

Thus, the density fluctuation, the concentration fluctuation and their correlation term are determined by combination of $I(0)$, κ_T and v_{A} and v_{B} measured experimentally. In SAXS method, we are able to observe the fluctuation in the volume defined by the coherent length of X-ray (about 10000 Å).

By equation (1), the concentration fluctuation can also be calculated by measuring chemical potentials as a function of mole fraction, and taking its derivative. However, as discussed extensively before [87] and in reference [88], the error bar for the thermodynamic route near the maximum tends inevitably quite large. Hence, the SAXS route to obtain the concentration fluctuation [74] is more advantageous.

2. 3. Individual density fluctuations

To see more details of the mixing state of mixtures, the individual density fluctuations which are the density fluctuations focusing on one component in the complex system are calculated using Kirkwood-Buff parameters. Figure 2-3 shows a schematic view of the individual fluctuations. Kirkwood-Buff parameters [89] connect the microscopic quantities to the macroscopic quantities. They are also one of expressions of fluctuation defined as,

$$G_{\mathrm{ij}} = \int \left(g_{\mathrm{ij}} - 1\right) 4\pi r^2 \mathrm{d}r\,, \quad (21)$$

where g_{ij} is the two body distribution function of component i and j, and r is interparticle distance between i and j. Kirk-wood parameters are the integral of the variation from the convergent value, 1, in total space. For a binary system composed of component A and B, Ben-Nam introduced the relationship between thermodynamic quantities and those parameters. [90]

Kirkwood-Buff parameters, G_{AA}, G_{BB} and G_{AB}, are connected to fluctuations by scattering intensity, $I(0)$, as, [91]

$$\frac{I(0)}{\bar{N}} = x_A {Z_A}^2 + x_B {Z_B}^2 + x_A{}^2 {Z_A}^2 \left(\frac{\bar{N}}{V}\right) G_{AA} + x_B{}^2 {Z_B}^2 \left(\frac{\bar{N}}{V}\right) G_{BB} + 2 Z_A Z_B \left(\frac{\bar{N}}{V}\right) G_{AB}. \quad (22)$$

Comparing the coefficients of each terms of equations (19) and (22),

$$G_{AA} = -\left(\frac{V}{N_A}\right) + \kappa_T k_B T + \left(\frac{v_B}{x_A}\right)^2 \left(\frac{\bar{N}}{V}\right) \cdot \bar{N} \langle (\Delta x_A)^2 \rangle, \quad (23)$$

$$G_{BB} = -\left(\frac{V}{N_B}\right) + \kappa_T k_B T + \left(\frac{v_A}{x_B}\right)^2 \left(\frac{\bar{N}}{V}\right) \cdot \bar{N} \langle (\Delta x_A)^2 \rangle, \quad (24)$$

$$G_{AB} = \kappa_T k_B T + \left(\frac{v_A v_B}{x_A x_B}\right) \left(\frac{\bar{N}}{V}\right) \cdot \bar{N} \langle (\Delta x_A)^2 \rangle. \quad (25)$$

When $i = j$, the individual density fluctuation of component i is written using the number of component i, N_i, as,

$$\frac{\langle (\Delta N_i)^2 \rangle}{\bar{N}_i} = \left(\frac{\bar{N}_i}{V}\right) G_{ii} + 1. \quad (26)$$

On the other hand, when $i \neq j$, the correlation terms between the individual density fluctuations of i and j are obtained as,

$$\frac{\langle \Delta N_i \Delta N_j \rangle}{\bar{N}_j} = \left(\frac{\bar{N}_i}{V}\right) G_{ij}. \quad (27)$$

$\langle \Delta N_i \Delta N_j \rangle / \bar{N}_j$ indicates the affinity between component i and component j. Positive value of the cross term corresponds to high affinity.

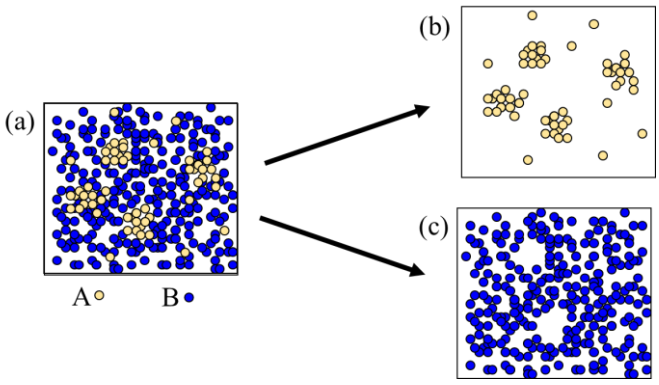

Figure 2-3 Schematic views of individual fluctuations for component (b)A, $\langle (\Delta N_A)^2 \rangle / \overline{N_A}$, and (c)B, $\langle (\Delta N_B)^2 \rangle / \overline{N_B}$, separated from (a)the total fluctuation.

Chapter 3 Experimental to determine fluctuations

3. 1. Sample preparation

The target ionic liquid $[P_{4,4,4,4}]CF_3COO$ was donated by Ohno's group (Tokyo University of Agriculture and Technology). $[P_{4,4,4,4}]CF_3COO$ was prepared by direct neutralization of aqueous solutions of the tetrabutylphosphonium hydroxide (Hokko Chem Co.) with trifluoroacetic acid (Wako Chem. Co.). After evaporating water, the product was added to a dichloromethane/water biphasic system, and the resulting mixture was washed several times with distilled water. The target salt was precipitates in the organic phase. The prepared $[P_{4,4,4,4}]CF_3COO$ was dried in vacuum for 24 h at 333 K prior to use. The structure and the purity of the salt were confirmed by ^{1}H NMR and elemental analyses.

$[P_{4,4,4,4}]CF_3COO$ was dried under vacuum more than 2 days at room temperature prior to use because of its high hygroscopicity. If the sample appears as glassy solid $[P_{4,4,4,4}]CF_3COO$ was turned into powder form by crushing. Then $[P_{4,4,4,4}]CF_3COO$ was mixed with ultrapure water (Milli-Q, Millipore) to the desired concentration gravimetrically. All experiments were performed at x_{IL}= 0.000-0.079 along isotherms at T= 293, 298 and 301 K within a week after preparing mixtures. Details for sample preparation is reported in Appendix A.

3. 2. SAXS measurements

3. 2. 1. Layout of apparatus

SAXS measurements were performed at the BL-6A station in Photon Factory (PF) at the National Laboratory for High Energy Accelerator Research Organization (KEK), Tsukuba. The high intensity X-rays whose wavelength is 1.5 Å (8.3 keV) and the highly accurate detector in the PF are powerful to measure scattering intensity for aqueous solutions to quantify fluctuations. Figure 3-1 shows the layout of BL-6A beam station. [92] X-rays are focused and monochromatized using a bent mirror and a monochromator. The monochromatic X-rays pass through three slits.

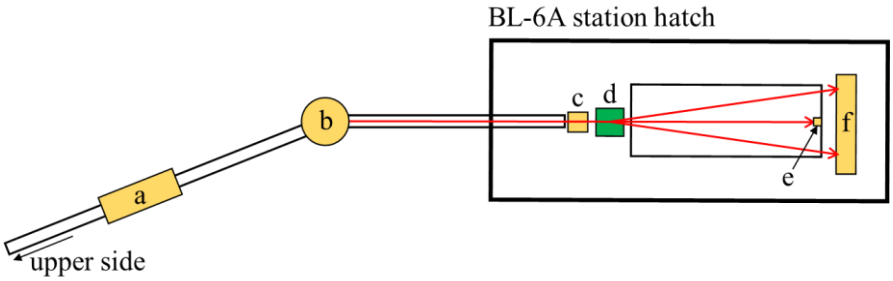

Figure 3-1 View of the beam line BL-6A layout [92]; (a)bent mirror, (b)monochromator, (c)ionization chamber, (d)sample holder, (e)beam stopper with photodiode detector and (f)scattered X-ray detector. Monchromatized X-rays drawn as red arrows are scattered by sample substance in (d).

The intensity of incident X-ray was monitored by the ionization chamber set before the sample holder. The transmitted X-ray was detected simultaneously by the photodiode set on the X-ray beam stopper, which enables determination of precise absorption coefficient of each sample to obtain the scattering intensity on absolute scale. [93] The X-rays scattered by sample materials passed through vacuum chamber and were detected by 2 dimensional semiconductor detector, PILATUS 1M (DECTRIS). The distance from the sample to the detector was set at 2 m and its correct value was determined by calibration using the silver behenate, AgBh, diffraction pattern. The exposure time was 300 seconds. Details of conditions are mentioned in Appendix B.

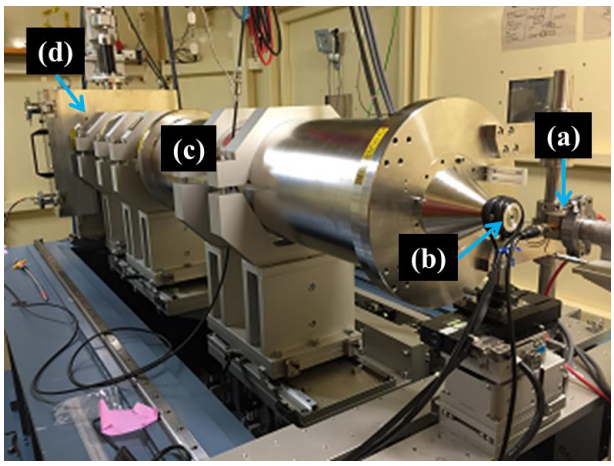

Figure 3-2 A snapshot of the BL-6A station hatch. Right hand side of figure is up stream; (a)ionization chamber, (b)sample holder, (c)vacuum chamber and (d)X-ray detector.

Sample holder was made of stainless steel (SUS 304) shown in figure 3-3. In SAXS measurement, the scattering volume depends on sample length, l, and decrease of scattered X-ray by absorption by sample materials follow Lambert-Beer law as,

$$\mu_{\mathrm{m}}\rho l = \ln\left(\frac{I_{\mathrm{inc.}}}{I_{\mathrm{trans.}}}\right), \tag{28}$$

where μ_{m} is the mass absorption coefficient, ρ is density of the sample materials and $I_{\mathrm{inc.}}$ and $I_{\mathrm{trans.}}$ are the intensities of the incident and transmitted X-rays, respectively. A large sample length causes high absorption and small scattering intensity. On the other hand, thin sample length results in weak scattering. When the optimum sample length, l_0, is selected, the intensity of scattered X-ray is maximum.

$$l_0 = \frac{1}{\mu_{\mathrm{m}}\rho}. \tag{29}$$

Mass absorption coefficient, μ_{m}, is specific originated from composing elements. Those for molecules are the sum of constituent mass absorption coefficients of elements, independent of their physical states. Consider a chemical compound $\mathrm{A_xB_y}$, A and B are composing elements whose atomic weights are M_{A} and M_{B}, respectively. When Mass absorption coefficients of A and B are known as $\mu_{\mathrm{m,A}}$ and $\mu_{\mathrm{m,B}}$, that of the compound $\mathrm{A_xB_y}$ is calculated as,

$$\mu_{\mathrm{m,comp.}} = \frac{\mu_{\mathrm{m,A}}M_{\mathrm{A}}x + \mu_{\mathrm{m,B}}M_{\mathrm{B}}y}{M_{\mathrm{A}}x + M_{\mathrm{B}}y}. \tag{30}$$

Similarly, the mass absorption coefficient for mixture composed of component 1 and 2, $\mu_{\mathrm{m,mix.}}$, is calculated as sum of products of $\mu_{\mathrm{m,comp.}}$ and mass fraction of each component, w_{i}.

$$\mu_{\mathrm{m,mix.}} = \mu_{\mathrm{m,comp.1}}w_1 + \mu_{\mathrm{m,comp.2}}w_2, \tag{31}$$

where subscripts 1 and 2 indicate component 1 and 2. Mass absorption coefficients of elements at the energy of X-ray used are obtained from XCOM, the database in National Institute of Standards and Technology, NIST, U. S. The required mass absorption coefficients are calculated on the website of NIST. [94], [95]

In this study of aqueous solutions, the sample length of the sample holder was based on the optimum sample length of water, 1.067 mm. To obtain sufficient scattered X-ray, the actual sample length of the sample holder was 1.6 mm. A pair of single crystal disks (Sumitomo Electric Hardmetal Co.) of diamond with thickness 0.3 mm and diameter 4.0 mm, were used as X-ray transmitting windows attached on both parts of P and Q in figure 3-3 by thermoset epoxy resin. Two parts of P and Q are assembled as shown in figure 3-3 (b) sealed by fluorinated O-ring (Morisei Kako Co.) of which the outer diameter is 10

mm and thickness is 1.0 mm. The parts P and Q are in touch with each other by their metal surfaces and the sample length is fixed.

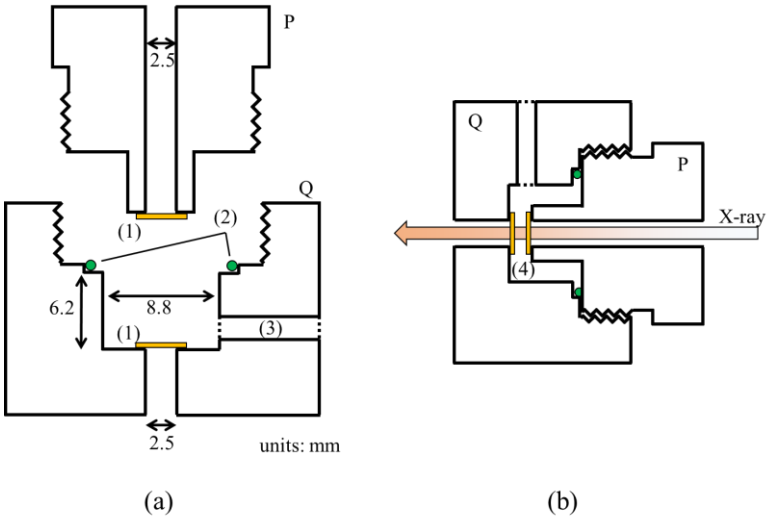

Figure 3-3 Design of sample holder composed of two parts P and Q. (a) shows details of each part; (1)diamond windows, (2)sealing O-ring and (3)sample injection hole. (b) shows the assembled sample holder with two parts of P and Q. Space (4) is the sample holding space and the distance between pair of diamond disks determines the sample length, 1.6 mm.

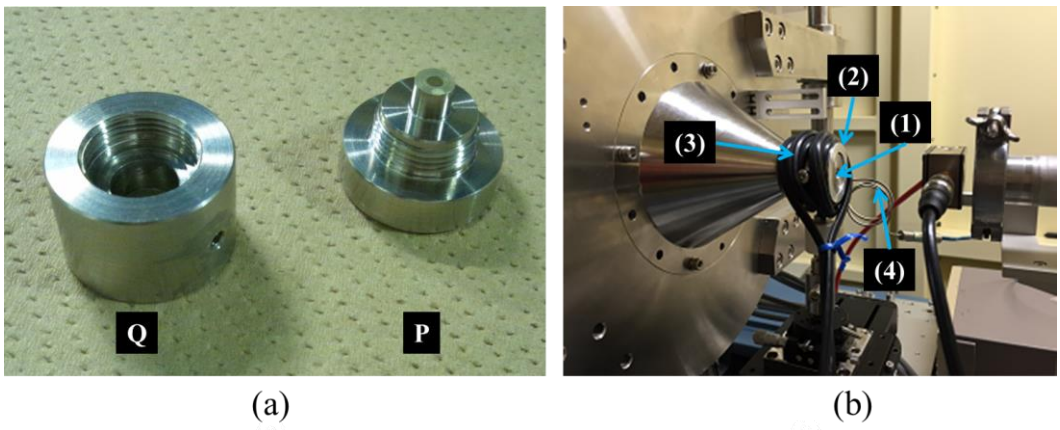

Figure 3-4 (a)A snapshot of the sample holder. (b)Setting of the sample stage on the beam line BL-6A; (1)the sample holder, (2)fixture of the sample holder, (3)rubber hose and (4)thermocouple.

For SAXS measurements, only 300 μl sample materials were required and injected in the space (4) in figure 3-3 (b) through sample injection hole (3) shown in figure 3-3 (a) with a micropipette. After checking the sample material was filled through diamond window, the sample holder was set at the sample stage on the beam line shown in figure 3-4. Temperature of sample materials were controlled by flowing circulating water in rubber hose with thermostat bath and monitored by K-type thermocouple set at the sample holder.

3. 2. 2. Procedure for data analysis

The 2-D images of intensity shown in figure 3-5 (a) were converted to 1-D intensity data versus scattering parameter shown in figure 3-5 (b) except for unnecessary signals by the program Fit2D [96], [97]. The color band shown below in figure 3-5 (a) represents the magnitude of SAXS intensity distinguished by color (white is the strongest). A variety of corrections were applied on the resultant raw data shown in figure 3-5 (b) to remove spurious scatterings from air and the diamond windows. And the effects of sample absorption was also corrected. Another correction is required to the raw data using measured incident and transmitted X-ray intensities.

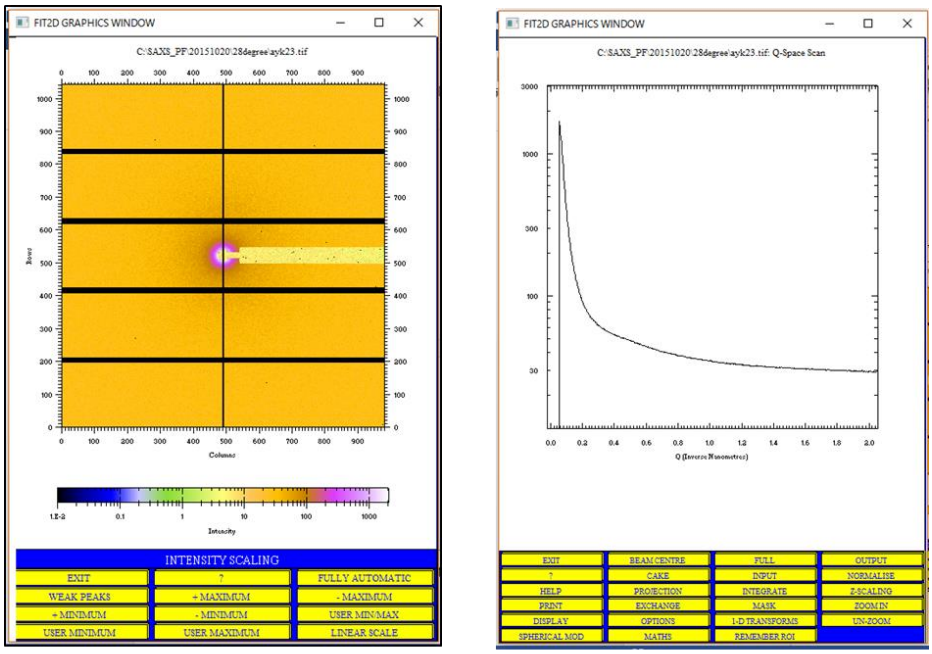

(a) (b)

Figure 3-5 Conversion of 2-D scattering intensity data to 1-D data using Fit2D program [96], [97]; (a)raw 2-D data and (b) converted raw 1-D data prior to various corrections.

First, because the intensity of incident X-ray fluctuates with time, the raw intensity, $I_{\mathrm{raw}}(s)$, is normalized by the average of incident X-ray intensity, $I_{\mathrm{inc.}}$, and the exposure time, t. Corrected scattering intensity, $I_{\mathrm{i}}(s)$, is written as,

$$I_{\mathrm{i}}(s) = \frac{I_{\mathrm{raw}}(s)}{I_{\mathrm{inc}} \cdot t}. \tag{32}$$

Next, consider the ratio of the transmitted intensity to the incident intensity, $A = I_{\mathrm{trans.}}/I_{\mathrm{inc}}$. To remove effects of absorption of X-ray by sample, correction is performed on $I_{\mathrm{i}}(s)$ as follows.

$$I_{\mathrm{ii}}(s) = I_{\mathrm{i}}(s) \cdot \left(\frac{A_{\mathrm{back}}}{A}\right). \tag{33}$$

A_{back} is the ratio of the transmitted intensity to the incident intensity for background. For scattering intensity of the back ground, the same correction is also applied and the corrected scattering intensity, $I_{\mathrm{ii}}(s)_{\mathrm{back}}$, is written as,

$$I_{\mathrm{ii}}(s)_{\mathrm{back}} = I_{\mathrm{i}}(s)_{\mathrm{back}} \cdot \left(\frac{A_{\mathrm{back}}}{A_{\mathrm{back}}}\right) = I_{\mathrm{i}}(s)_{\mathrm{back}}. \tag{34}$$

In the present measurements for aqueous solution of $[P_{4,4,4,4}]CF_3COO$, the intensity data of air (no material in the sample holder) at the temperature was used as background.

Finally to extract the scattering intensity only from the sample, the corrected scattering intensity of background, $I_{\mathrm{ii}}(s)_{\mathrm{back}}$, is subtracted from that of the measurement, $I_{\mathrm{ii}}(s)$. The scattering intensity of the sample, $I(s)$, is then obtained as,

$$I(s) = I_{\mathrm{ii}}(s) - I_{\mathrm{ii}}(s)_{\mathrm{back}}. \tag{35}$$

3. 2. 3. Forward SAXS intensity at zero-angle

Figure 3-6 shows the SAXS profiles against scattering parameter, s, of aqueous solutions of $[P_{4,4,4,4}]CF_3COO$ at 301 K. The vertical axis is the absolute scattering intensity, $I(s)$. The profile of water, blue plots, show flat behavior in this s range. By adding $[P_{4,4,4,4}]CF_3COO$, scattering intensity curls up toward s= 0 and the intensity at x_{IL}= 0.026, the nearest concentration to the critical concentration, exhibited the largest increase. And then beyond the critical concentration, scattering intensity comes down. However, the magnitudes of the intensities at 293 and 298 K were considerably weaker than those at 301 K.

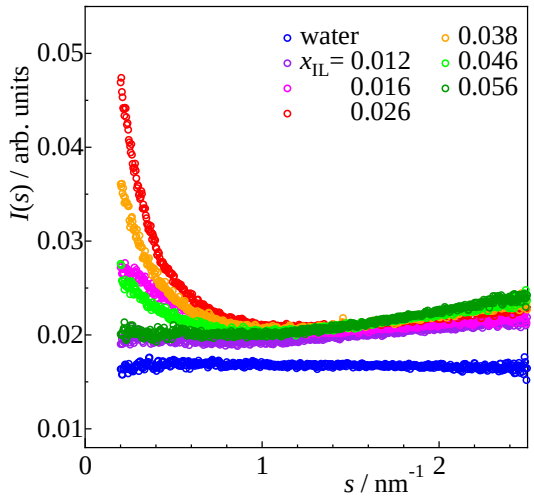

Figure 3-6 X-ray scattering profile of aqueous solutions of $[P_{4,4,4,4}]CF_3COO$ at 301 K. The blue symbols are results of pure water. Adding $[P_{4,4,4,4}]CF_3COO$, SAXS intensity, $I(s)$, increase toward s= 0 and that at x_{IL}= 0.026, $I(s)$ shows the greatest increase.

As discussed in 2. 2., the SAXS intensity at s= 0, $I(0)$, includes information of fluctuations. But in actual measurement, we are not able to obtain the value directly because direct beam stopper shade scattered X-rays at zero angle. Each value for $I(0)$ was obtained by extrapolation of the corresponding fitting curve obtained in the range 0.2 < s < 1.0 nm^{-1} to s= 0.

The SAXS intensity of the system near the critical point follows the Ornstein-Zernike equation [98] as,

$$I(s) = \frac{I(0)}{1 + \xi^2 s^2}, \tag{36}$$

where ξ is the correlation distance. This equation is applied on the systems which have various size clusters, namely highly fluctuating systems. Inverse of $I(s)$ should be linear against square of s. In the study of aqueous solution of acetonitrile, $I(0)$ s were determined following equation (36) near the critical point. Outside of this region, even functions were fitted instead. [81] However, for the present aqueous solution of $[P_{4,4,4,4}]CF_3COO$, the SAXS intensities did not follow equation (36) even the result at x_{IL}= 0.026 and at 301 K, only a degree lower than the critical point. Molecular dynamics simulation studies showed most ILs have strong interactions among themselves in pure state [6], [9], [99]. The X-ray scattering study showed broad peak generally at a certain s region larger than what is plotted in figure 3-6. [7], [8] Pure $[P_{4,4,4,4}]CF_3COO$ also showed an increase of the intensity at larger than s= 2 nm^{-1} [100] and a similar increase

was observed in X-ray scattering intensity of its aqueous solution at s > 1.2 nm^{-1} as shown in figure 3-6. Therefore, the effect of this intensity spilling over from high s region should be corrected. Thus instead of equation (36), we used equation (37) below to fit the present data. The attempt was reasonably successful. $I(0)$ was obtained as the sum of $I(0)'$ and α.

$$I(s) = \frac{I(0)'}{1 + \xi^2 s^2} + \alpha. \tag{37}$$

Figure 3-7 (a) is the examples of fitting curves using equation (37) applied on the result at x_{IL}= 0.026 and at 301 K. On the other hand, figure 3-7 (b) is the Ornstein-Zernike plot using equation (36) applied on the same data. The inverse of $I(s)$ data do not show linearity against square of s even at small s region. This indicates that the fitting function, equation (36), is unsuitable. Also Guinier plot which express the system with the same size clusters was found to be unsuitable. It indicated that the present aqueous solution is fluctuating and shows various size of aggregation. Figure 3-8 shows the concentration dependence for the zero-angle scattering intensities, $I(0)$, at 293, 298 and 301 K. All the SAXS profiles and the fitting curves are shown in Appendix C.

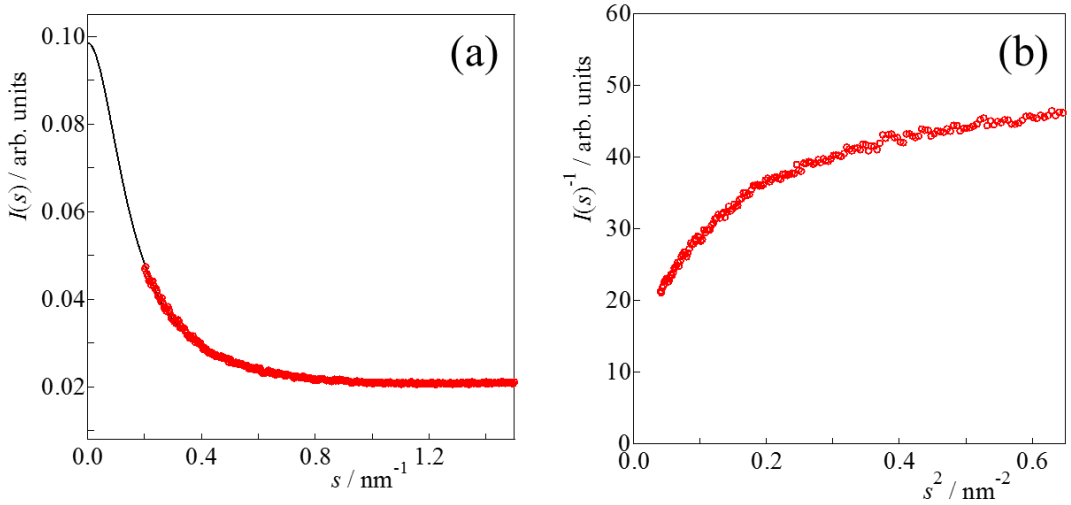

Figure 3-7 Example of fitting curves on the SAXS profile; (a)fitted by equation (37) and (b)fitted by equation (36).

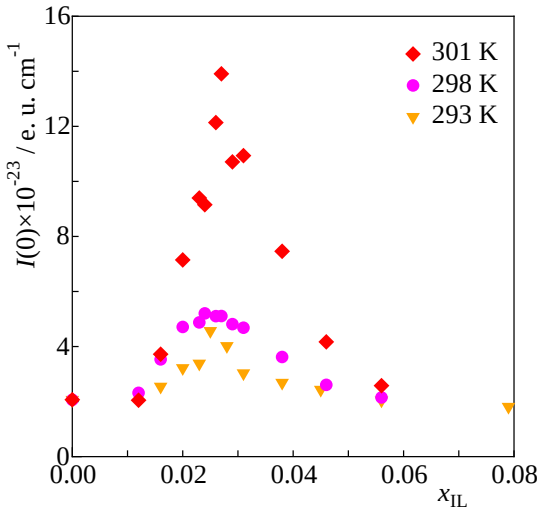

Figure 3-8 Concentration dependence of the zero-angle scattering intensity, $I(0)$, at 293, 298 and 301 K. $I(0)$s describe a peak near the critical concentration, x_{IL}= 0.025, at each temperature. Especially $I(0)$ at 301 K shows a drastic increase toward the critical concentration.

3. 3. Density measurements

3. 3. 1. Vibration tube density meter

In order to obtain the second derivative parameters in equation (20), the partial molar volumes of components and its isothermal compressibility were determined. For this purpose, we determined the density of the present aqueous solution as a function of mole fraction as well as pressure using the vibration tube density meter. We then take derivatives of the result in terms of mole fraction to obtain partial molar volumes, and in terms of pressure to determine isothermal compressibility.

The frequency of vibration tube, ω, is proportional to the sum of masses of the tube, m, and of the sample, ρV, where ρ is density and V is volume of the sample, as,

$$\omega = \left[\frac{k}{4\pi^2(m+\rho V)}\right]^{1/2}. \tag{38}$$

k represents the apparatus constant. From equation (38), density is written as a function of period, $\tau = \omega^{-1}$,

$$\rho = A\tau^2 + B, \tag{39}$$

$$A = \frac{k}{4\pi^2 V}, \tag{40}$$

$$B = -\frac{m}{V}. \tag{41}$$

Parameters A and B are the constants depending on temperature and pressure and determined by measuring τ of two reference materials, nitrogen or air and pure water, at the target temperatures and pressures.

Partial molar volume of component i, v_i, is defined as,

$$v_\mathrm{i} \equiv \left(\frac{\partial V}{\partial n_\mathrm{i}}\right)_{p,T,n_{\mathrm{j}\neq\mathrm{i}}}, \tag{42}$$

where V is volume of the system and n_i is the molar amount of component i. However, it is more convenient experimentally to use $\{x_\mathrm{i}$ (i= 1, 2, 3, …, k-1), $N\}$ variables in the k-component systems, rather than $\{n_\mathrm{i}$ (i= 1, 2, 3, …, k)$\}$ in which thermodynamic quantities are generally defined. Using x_i, equation (42) is rewritten as,

$$v_\mathrm{i} = (1 - x_i)\left(\frac{\partial V_\mathrm{m}}{\partial x_\mathrm{i}}\right)_{p,T} + V_\mathrm{m}, \tag{43}$$

where $V_\mathrm{m} = V/N$ is the molar volume of the mixture and N is the total molar amount. Partial molar volumes of $[P_{4,4,4,4}]CF_3COO$ and water in the solution were obtained using equation (43) by measuring concentration dependence of density. The apparatuses used for this were DMA 4500 and DMA 4100 (Anton Paar). Parameters A and B were determined using distilled pure water and dry air at 293 K. The corrections for other temperatures and also for viscosity were done automatically.

On the other hand, isothermal compressibility, κ_T, is defined as,

$$\kappa_T \equiv -\frac{1}{V}\left(\frac{\partial V}{\partial p}\right)_{T,x_\mathrm{i}}. \tag{44}$$

κ_T was obtained by measuring pressure dependence of density using high-pressure vibration tube density meter DMA HP (Anton Paar). Parameters A and B were determined using distilled pure water and nitrogen gas at all temperature and pressure according to the measurement points conditions. Detail of the apparatus is reported in Appendix D.

3. 3. 2. Partial molar volumes

Figure 3-9 shows the concentration dependence of density, ρ, and the molar volume of aqueous solution of $[P_{4,4,4,4}]CF_3COO$, V_m, at 293, 298 and 302 K and at x_IL= 0.000-0.079. All raw data are reported in Appendix E. Molar volume, V_m, was calculated as,

$$V_{\mathrm{m}} = \frac{M_{\mathrm{IL}} x_{\mathrm{IL}} + M_{\mathrm{W}}(1 - x_{\mathrm{IL}})}{\rho}. \tag{45}$$

M_{IL} and M_{W} are the formula weight of $[P_{4,4,4,4}]CF_3COO$, 372.46, and the molecular weight of water, 18.02, respectively. We note that V_{m} versus x_{IL} appears linear up to the maximum concentration in the present measurement.

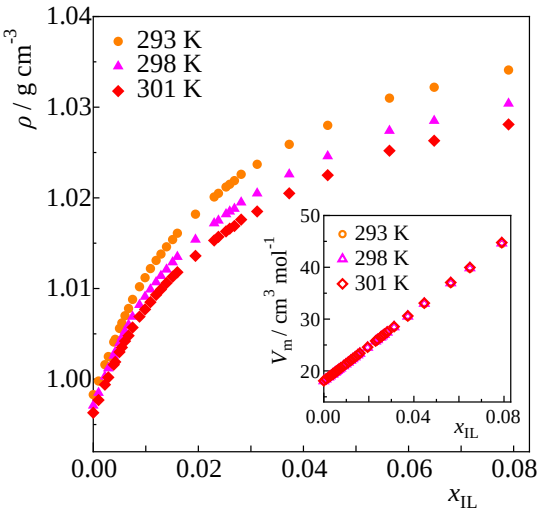

Figure 3-9 Concentration dependence of density, ρ, for the aqueous solution of $[P_{4,4,4,4}]CF_3COO$ at 293, 298 and 301 K. The inset shows the calculated molar volume, V_{m}.

Using the equation (43), the molar volume was differentiated with respect to mole fraction, x_{IL}. To see the effect of intermolecular interactions more clearly, the excess partial molar volumes should be evaluated. First, the excess molar volume, $V_{\mathrm{m}}^{\mathrm{E}}$, must be obtained, which can be calculated by,

$$V_{\mathrm{m}} = V_{\mathrm{m}}^{\mathrm{id}} + V_{\mathrm{m}}^{\mathrm{E}} = \{V_{\mathrm{IL}} x_{\mathrm{IL}} + V_{\mathrm{W}}(1 - x_{\mathrm{IL}})\} + V_{\mathrm{m}}^{\mathrm{E}}. \tag{46}$$

V_{IL} and V_{W} are the molar volumes of pure $[P_{4,4,4,4}]CF_3COO$ and water, respectively. Superscripts id and E represent ideal and excess quantities, excess quantities include all information about intermolecular interactions in the mixture. The partial molar volume of $[P_{4,4,4,4}]CF_3COO$, v_{IL}, is written as,

$$v_{\mathrm{IL}} = v_{\mathrm{IL}}^{\mathrm{id}} + v_{\mathrm{IL}}^{\mathrm{E}} = (1 - x_{\mathrm{IL}})\left(\frac{\partial V_{\mathrm{m}}^{\mathrm{id}}}{\partial x_{\mathrm{IL}}}\right) + V_{\mathrm{m}}^{\mathrm{id}} + (1 - x_{\mathrm{IL}})\left(\frac{\partial V_{\mathrm{m}}^{\mathrm{E}}}{\partial x_{\mathrm{IL}}}\right) + V_{\mathrm{m}}^{\mathrm{E}}, \tag{47}$$

$$v_{\mathrm{IL}}^{\mathrm{id}} = V_{\mathrm{IL}}. \tag{48}$$

And partial molar volume of water, v_{W}, is obtained in the same manner.

However, pure $[P_{4,4,4,4}]CF_3COO$ is solid at 293-302 K and it is difficult to obtain V_{IL} experimentally. We define the "apparent" ideal molar volume of $[P_{4,4,4,4}]CF_3COO$, $V_{\mathrm{m,ap}}^{\mathrm{id}}$, using the present data set from x_{IL}= 0.000 to 0.079, assuming that $V_{\mathrm{m,ap}}^{\mathrm{id}}$ is linear to x_{IL},

$$V_{\mathrm{m,ap}}^{\mathrm{id}}(x_{\mathrm{IL}}) = x_{\mathrm{IL}} \cdot \frac{V_{\mathrm{m}(x_{\mathrm{IL}}=0.079)} - V_{\mathrm{W}}}{0.079} + V_{\mathrm{W}}, \tag{49}$$

and the "apparent" molar volume of pure $[P_{4,4,4,4}]CF_3COO$ at x_{IL}= 1 is expressed as,

$$V_{\mathrm{IL,ap}} = \frac{V_{\mathrm{m}(x_{\mathrm{IL}}=0.079)} - V_{W}}{0.079} + V_{W}. \tag{50}$$

According to the equation (46), the "apparent" excess molar volume is written as,

$$V_{\mathrm{m,ap}}^{\mathrm{E}}(x_{\mathrm{IL}}) = V_{\mathrm{m}}(x_{\mathrm{IL}}) - V_{\mathrm{m,ap}}^{\mathrm{id}}(x_{\mathrm{IL}}). \tag{51}$$

Figure 3-10 shows the apparent excess molar volumes, $V_{\mathrm{m,ap}}^{\mathrm{E}}$, at 298 K. In this concentration region, $V_{\mathrm{m,ap}}^{\mathrm{E}}$ shows negative value and concave downward. The solid curve is fitting curve drawn with a flexible ruler. The reason why we chose to draw fitting curve with a flexible ruler is discussed in Appendix F. We read values off at every 0.01 mole fraction of $[P_{4,4,4,4}]CF_3COO$ and calculate partial molar volume of $[P_{4,4,4,4}]CF_3COO$ as,

$$v_{\mathrm{IL}} = V_{\mathrm{IL,ap}} + (1 - x_{\mathrm{IL}}) \left(\frac{\Delta V_{\mathrm{m,ap}}^{\mathrm{E}}}{\Delta x_{\mathrm{IL}}} \right) + V_{\mathrm{m,ap}}^{\mathrm{E}}. \tag{52}$$

$\Delta V_{\mathrm{m,ap}}^{\mathrm{E}}$ indicates the amount of change of $V_{\mathrm{m,ap}}^{\mathrm{E}}$ in Δx_{IL} corresponding to 0.01. Partial molar volume of water, v_{W}, is calculated by the same manner.

Figure 3-11 shows partial molar volumes of $[P_{4,4,4,4}]CF_3COO$, v_{IL}, and water, v_{W}, at 293, 298 and 301 K, calculated by equation (52). All resulting values and used fitting curves are reported in Appendix G. v_{IL} and v_{W} show respectively the minimum and the maximum at x_{IL}= 0.003. The behavior of partial molar volumes for a binary system in a dilute region is discussed in 5. 5. 1. In the concentration region x_{IL}= 0.016-0.06, v_{IL} increases with x_{IL}, whereas v_{W} decreases. These results can be attributed to the fact that the volume of a $[P_{4444}]CF_3COO$ ion pair is about approximately 20 times greater than that of a water molecule. Because $[P_{4444}]CF_3COO$ is very bulky and has a large steric hindrance, it requires large spaces. The water molecules, on the other hand, are likely to fill the voids formed by the $[P_{4444}]CF_3COO$ packing because of their size difference.

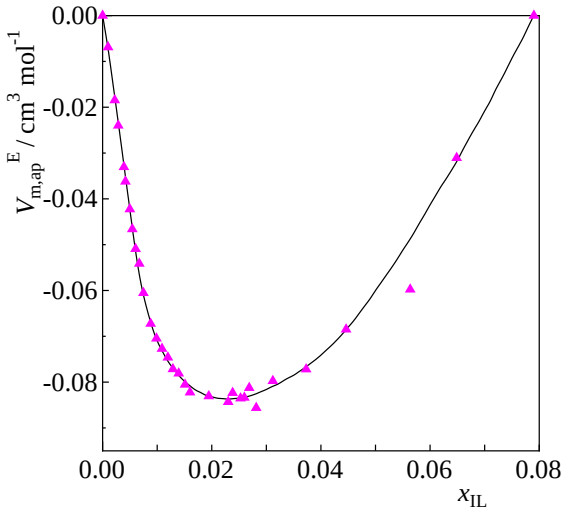

Figure 3-10 The apparent excess molar volume of the aqueous solution of $[P_{4,4,4,4}]CF_3COO$, $V_{m,ap}^{E}$, at 298 K against x_{IL}. The solid curve is the fitting curve drawn with a flexible ruler. The results at 293 and 301 K is shown in Appendix G.

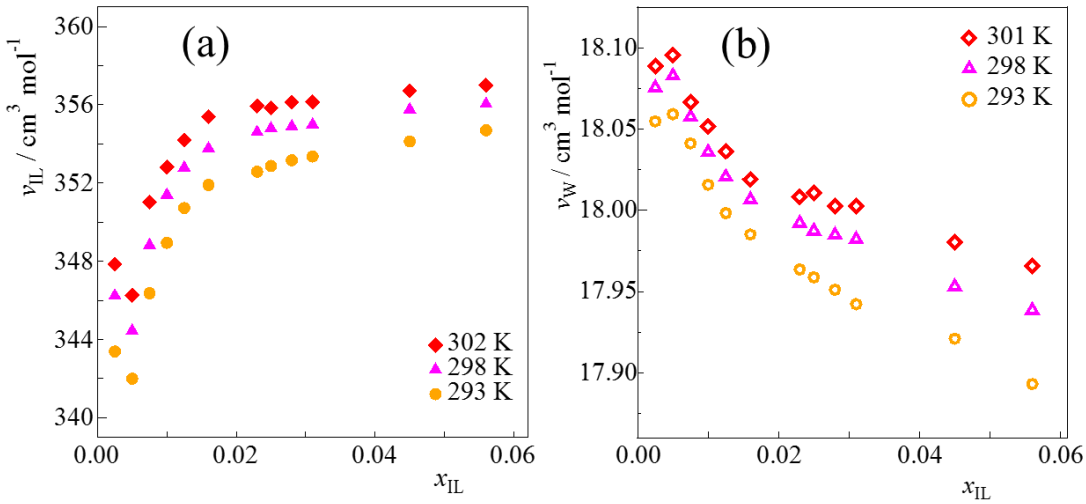

Figure 3-11 Concentration dependence of the partial molar volumes of (a)$[P_{4,4,4,4}]CF_3COO$, v_{IL}, and (b)water, v_W, at 293, 298 and 301 K.

3. 3. 3. Isothermal compressibility

Pressure dependence of density, ρ for aqueous solution of $[P_{4,4,4,4}]CF_3COO$ was measured at 293 and 301 K and the pressure range from 0.1 to 12.0 MPa at every 1.0

MPa. Figure 3-12 shows the results at 301 K. All raw data are shown in Appendix H. In this pressure range of 0.1-12.0 MPa, the increase of density or the decrease of molar volume, V_{m}, against pressure was too small to use the fitting functions introduced in a previous study [101]. We approximated the pressure dependence of molar volume, V_{m}, by a straight line. We then calculated isothermal compressibility, κ_T, which is equal to $\left[-V^{-1}(\partial V/\partial p)_{T,n_{\mathrm{i}}}\right]$, up to p= 12 MPa by using its slope. Figure 3-13 shows an example of linear fitting at 301 K and x_{IL}= 0.025.

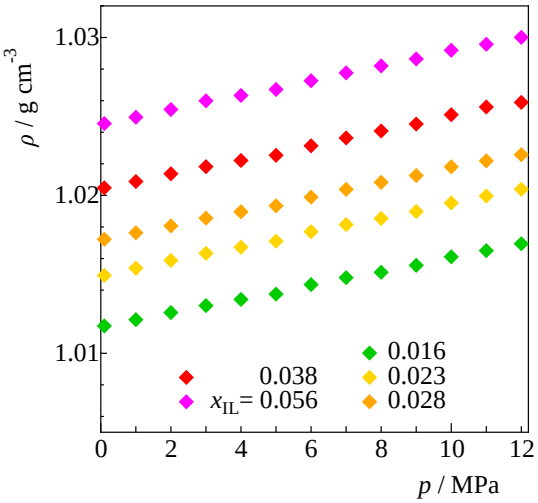

Figure 3-12 Pressure dependence for the density, ρ, for the aqueous solutions of $[P_{4,4,4,4}]CF_3COO$ at 301 K.

Figure 3-14 shows the concentration dependence of the isothermal compressibility of the aqueous solution of $[P_{4,4,4,4}]CF_3COO$, κ_T, at 293 and 301 K. Pure water has anomaly for isothermal compressibility which shows the minimum value around at 318 K [102] which is one of the anomalous behavior of liquid water. At x_{IL}= 0.000, the isothermal compressibility at 293 K was larger than that at 301 K. On the other hand, adding $[P_{4,4,4,4}]CF_3COO$, the isothermal compressibility at 293 K shows a smaller value than that at 301 K and the aqueous solution behaved like normal liquids. However, the contribution from the term of κ_T on numerical calculation of fluctuations turned out to be smaller than that of SAXS intensity; the values of $I(0)/\bar{N}$ 62.65 and $\bar{Z}^2(\bar{N}/V)k_{\mathrm{B}}T\kappa_T$ 9.41 at x_{IL}= 0.027 and 301 K. Thus the value at 298 K we calculated by interpolation between results at 293 and 301 K at a given mole fraction.

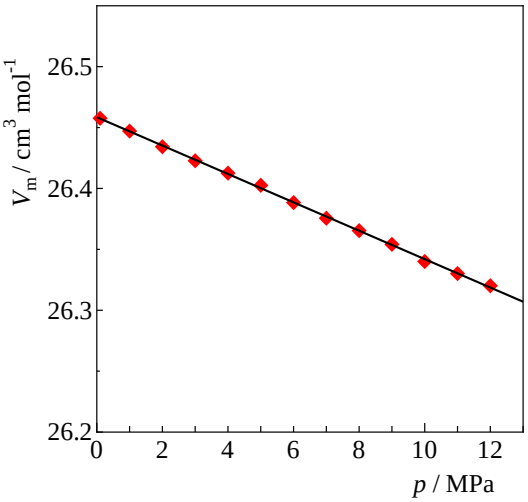

Figure 3-13 Pressure dependence the molar volume for the aqueous solution of $[P_{4,4,4,4}]CF_3COO$, V_m, at 301 K and x_{IL}= 0.025. Black solid line is the fitted linear line. Isothermal compressibility was determined using the slope up to 12.0 MPa.

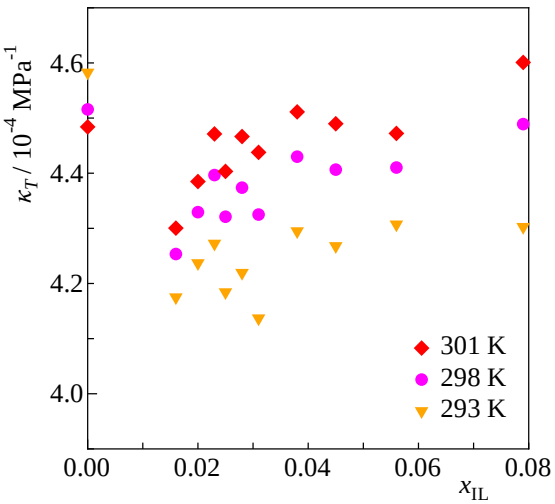

Figure 3-14 Concentration dependence of isothermal compressibility, κ_T, for the aqueous solution of $[P_{4,4,4,4}]CF_3COO$, κ_T, at 293 and 301 K were calculated by measured density data. That at 298 K was obtained by liner interpolation of the values at 293 and 301 K.

Chapter 4 Fluctuations in the aqueous solution

4. 1. Fluctuations of entire system

Figure 4-1 shows the density fluctuation, $\langle(\Delta N)^2\rangle/\bar{N}$, and the concentration fluctuation, $\bar{N}\langle(\Delta x)^2\rangle$, and figure 4-2 shows the cross term of them, $\langle(\Delta N)(\Delta x)\rangle$, for aqueous solution of $[P_{4,4,4,4}]CF_3COO$ at 293, 298 and 301 K against x_{IL} calculated by combination of $I(0)$, v_{IL} and v_W, and κ_T. The values of all fluctuations are reported in Appendix I. Both $\langle(\Delta N)^2\rangle/\bar{N}$ and $\bar{N}\langle(\Delta x)^2\rangle$ showed increase approaching to the critical point and sharp peaks at 301 K. These results show the high fluctuation towards the critical point at 302 K and x_{IL}= 0.025. Interestingly, the density fluctuation of the present mixture shows much larger value than that for aqueous solution of acetonitrile in the previous study [81]; at the respective critical mole fraction the present case shows about 1200 at 301 K, a degree lower than the LCST, while the aqueous solution of acetonitrile at 272 K, about 85 [81]. Comparison of fluctuations with previous studies is shown in Appendix O.

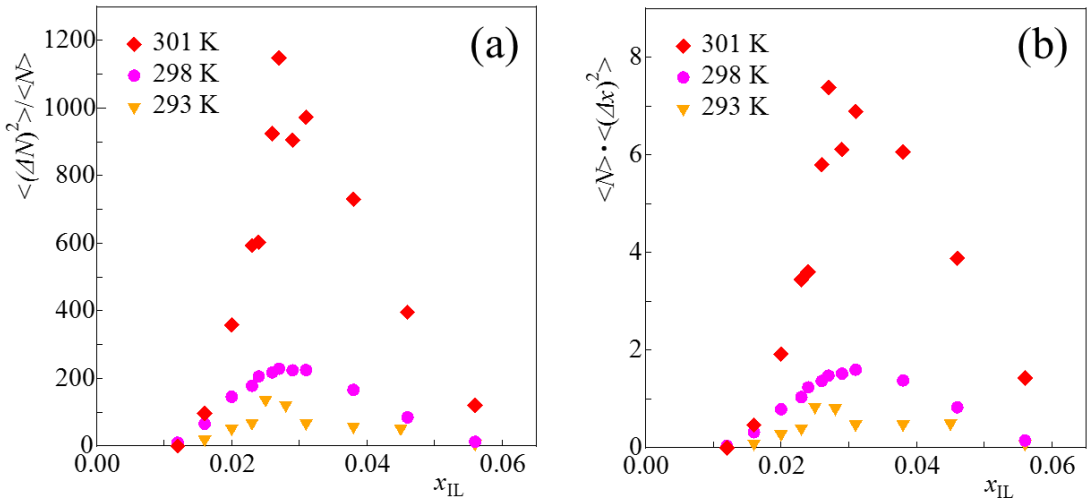

Figure 4-1 Fluctuations of the entire system for aqueous solution of $[P_{4444}]CF_3COO$ at 293, 298 and 301 K; (a)the density fluctuation, $\langle(\Delta N)^2\rangle/\bar{N}$, and (b)the concentration fluctuation, $\bar{N}\langle(\Delta x)^2\rangle$.

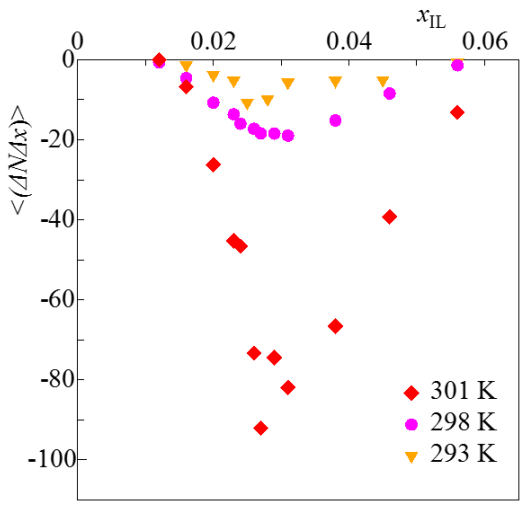

Figure 4-2 The cross term of density and concentration fluctuations for the entire system of the aqueous solution of $[P_{4444}]CF_3COO$ at 293, 298 and 301 K, $\langle(\Delta N)(\Delta x)\rangle$.

4. 2. Individual density fluctuations of $[P_{4,4,4,4}]CF_3COO$ and water

Using Kirkwood-Buff parameters, the individual density fluctuations for $[P_{4,4,4,4}]CF_3COO$, $\langle(\Delta N_{IL})^2\rangle/\overline{N_{IL}}$, and for water, $\langle(\Delta N_W)^2\rangle/\overline{N_W}$, at 293, 298 and 301 K as functions of x_{IL} were calculated and shown in figure 4-3. Calculated values are shown in Appendix J. Both components showed a large fluctuation near the critical point and a drastic change at 301 K. However, the individual density fluctuation for water was 10 times greater than that for $[P_{4,4,4,4}]CF_3COO$. The correlation terms of those two individual density fluctuations were also calculated by Kirkwood-Buff parameters and shown in figure 4-4. Figure 4-4 (a)$\langle\Delta N_{IL}\Delta N_W\rangle/\overline{N_{IL}}$ and (b)$\langle\Delta N_{IL}\Delta N_W\rangle/\overline{N_W}$ represent affinity between $[P_{4,4,4,4}]CF_3COO$ and water. The cross terms showed positive values at entire concentrations and temperatures. These results indicated that the water molecules in the aqueous solution of $[P_{4444}]CF_3COO$ were distributed inhomogeneously near the critical point and there is a strong affinity between $[P_{4,4,4,4}]CF_3COO$ and water.

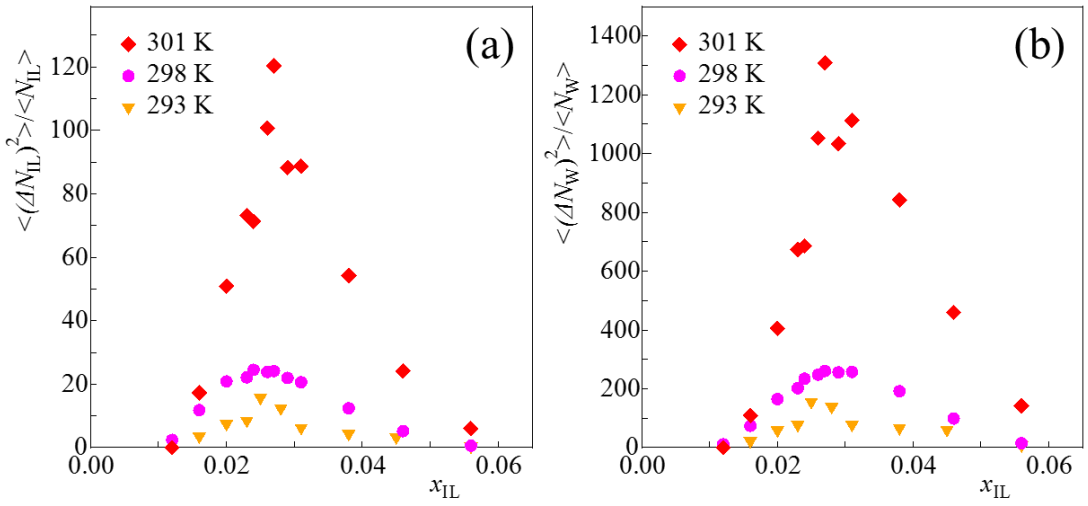

Figure 4-3 Individual density fluctuations for (a)[P_{4444}]CF_3COO, $\langle(\Delta N_{IL})^2\rangle/\overline{N_{IL}}$, and (b)water, $\langle(\Delta N_W)^2\rangle/\overline{N_W}$, as a function of x_{IL} at 293, 298 and 301 K.

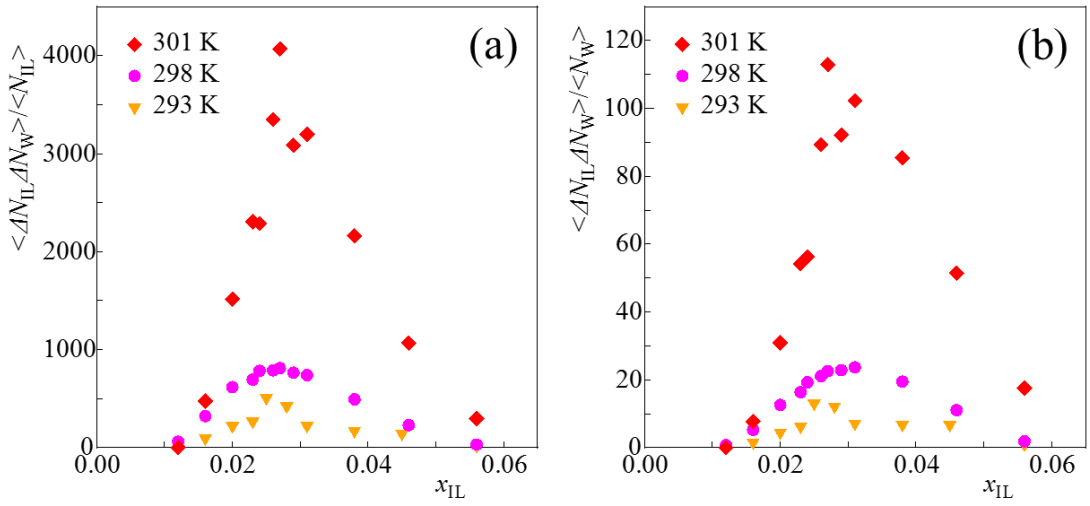

Figure 4-4 Correlation terms of individual density fluctuations as a function of x_{IL} at 293, 298 and 301 K; (a)$\langle\Delta N_{IL}\Delta N_W\rangle/\overline{N_{IL}}$, and (b)$\langle\Delta N_{IL}\Delta N_W\rangle/\overline{N_W}$.

4. 3. Discussion

Figure 4-5 are the contour maps of fluctuations drawn on the phase diagram of the aqueous solution of $[P_{4,4,4,4}]CF_3COO$. Approaching to the critical point, respective fluctuation functions show large fluctuations, toward the macroscopic phase separation, as is clearly indicated in the figure.

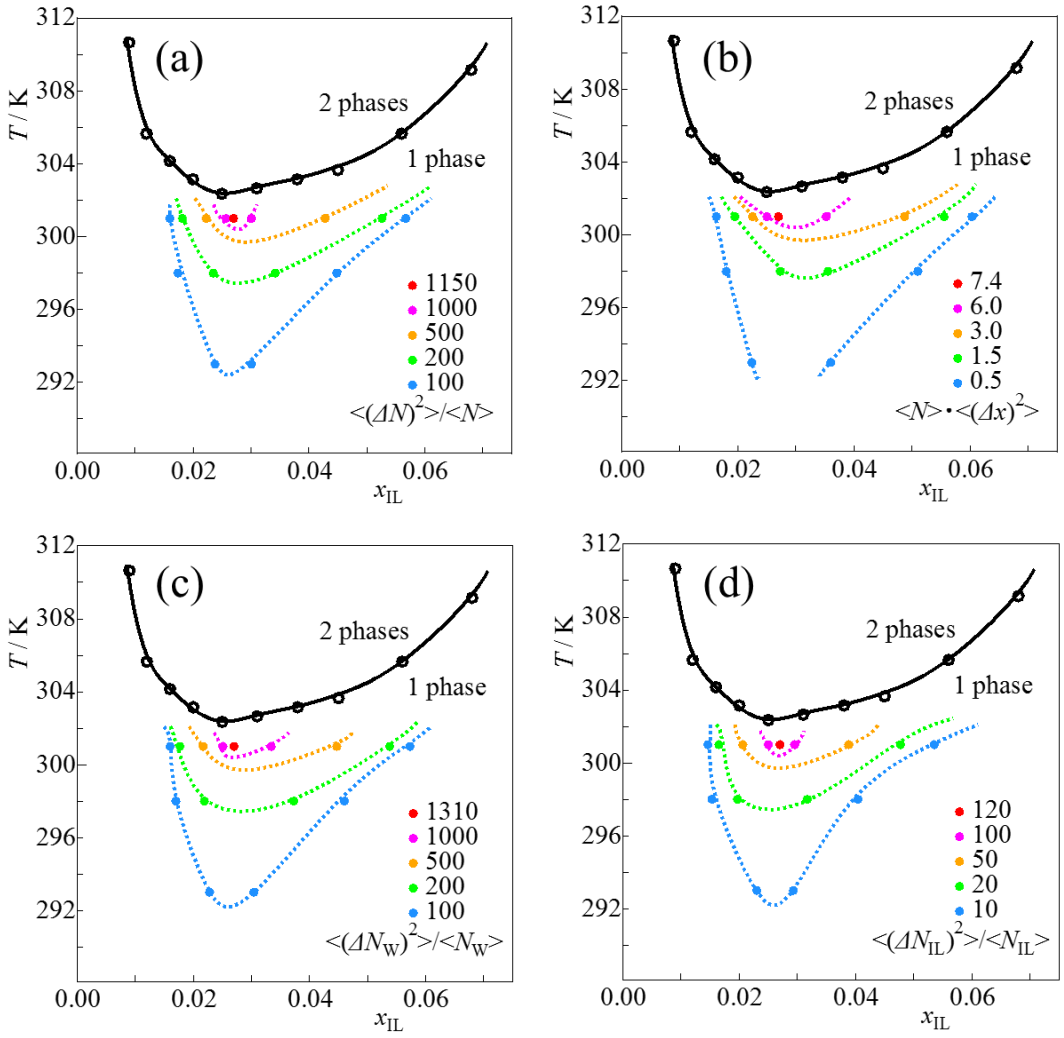

Figure 4-5 Contour maps of fluctuations drawn on the phase diagram of aqueous solution of $[P_{4,4,4,4}]CF_3COO$; (a)the density fluctuation for the entire system, $\langle(\Delta N)^2\rangle/\overline{N}$, (b)the concentration fluctuation, $\overline{N}\langle(\Delta x)^2\rangle$, (c)the individual density fluctuation for water, $\langle(\Delta N_W)^2\rangle/\overline{N_W}$, and (d)the individual density fluctuation for $[P_{4,4,4,4}]CF_3COO$, $\langle(\Delta N_{IL})^2\rangle/\overline{N_{IL}}$.

A large difference in the partial molar volumes of $[P_{4,4,4,4}]CF_3COO$ and water was observed, as discussed in 3. 3. 2. The difference between the two increased as the concentration of $[P_{4,4,4,4}]CF_3COO$ increased as shown in figure 3-11. The term related to the partial molar volume difference, $(v_{IL} - v_W)\,\bar{N}/V$, contributes to the fluctuations as shown in equation (20). In the area where $[P_{4,4,4,4}]CF_3COO$ ion pairs show gathering in the process of fluctuation, the total number of both $[P_{4,4,4,4}]CF_3COO$ and water per unit volume, N, becomes much less than that in the water-rich area because of the large difference in partial molar volumes. Thus, the density fluctuation in aqueous solution of $[P_{4,4,4,4}]CF_3COO$ is particularly sensitive to the distribution of $[P_{4,4,4,4}]CF_3COO$, when the total number, N, is considered. The individual density fluctuations indicated that the water molecules were largely localized near $[P_{4,4,4,4}]CF_3COO$ even more so near the critical point.

The aqueous solution of $[C_4mim]BF_4$ which shows a UCST-type phase separation was reported a large concentration fluctuation near its critical point, x_{IL}= 0.08, T= 277 K. [54] The increase of fluctuations toward the critical point was also observed for the same IL aqueous solution. [103] However, one of Kirkwood-Buff parameters, G_{IL-W}, which indicates the correlation between $[C_4mim]BF_4$ and water was negative which suggests that IL and water molecules are repulsive [54], contrary to the present case where G_{IL-W} is positive as discussed above. In the mixture below the LCST, therefore, it is considered that $[P_{4,4,4,4}]CF_3COO$ clusters are hydrated by a larger number of water molecules. Hence, it is proposed that the $[P_{4,4,4,4}]CF_3COO$ gather with a large number of hydration water molecules, and $[P_{4,4,4,4}]CF_3COO$ and water do not completely separate at any instance. As approaching to the critical point, the gathering grow drastically. In a recent investigation, it was found that 7-14 water molecules exist per $[P_{4,4,4,4}]CF_3COO$ ion pair, even in the separated IL-rich phase above the LCST, and that the number of water molecules in the IL-rich phase decreases with increasing temperature. [69] It was argued that a mixture which has a tendency for phase separation with an LCST shows a stronger entropic attraction than enthalpic repulsion. [88] In the next section, the enthalpic contribution of $[P_{4,4,4,4}]CF_3COO$ in the aqueous solution is discussed. However, we are not able to determine the driving force of the phase separation because there is no data of entropic situation for the mixture. For the aqueous solution of $[C_4mim]BF_4$ which shows the UCST-type phase separation, enthalpy-entropy compensation was discussed.[44]

Chapter 5 Concentration dependent mixing schemes

5. 1. Differential thermodynamics

Higher order derivative quantities of Gibbs energy contain deeper information. The differential thermodynamic approach for aqueous solutions have been studied by Koga *et al*. [88], [104], [105] Now, we choose pressure, p, temperature, T, and the molar amount of component i, n_{i}, as the independent variables of state functions. Gibbs energy, $G(p,T,n_{\mathrm{i}})$, is the 0-th derivative quantity and determines the macroscopic nature of the system. The first derivative quantities of Gibbs energy with respect to p or T are volume, V, entropy, S, and enthalpy, H, which describe the average properties of the system. Chemical potential of component i is also the first derivative of G with respect to n_{i} and express the contribution of component i on the system in terms of Gibbs energy. Partial molar quantities of volume, v_{i}, entropy, S_{i}, and enthalpy, H_{i}, are defined as differentiation of V, S and H with respect to n_{i}. They are the second derivatives of G and express the contribution of component i on the system in terms of volume, entropy and enthalpy, respectively. Thus, they signify the actual volumetric, entropic and enthalpic situation of component i in the mixture.

Furthermore, partial molar quantities are differentiated with respect to n_{j} again as,

$$F_{\mathrm{i-j}} \equiv N\left(\frac{\partial F_{\mathrm{i}}}{\partial n_{\mathrm{j}}}\right)_{p,T,n_{\mathrm{k}\neq\mathrm{j}}} . \tag{53}$$

F is V, S or H and F_{i} are the respective partial molar quantities. The defined $F_{\mathrm{i-j}}$ is the third derivative quantity of Gibbs energy and expresses the effects of component j on F_{i}, namely, the interaction between component i and j in terms of appropriate thermodynamic quantity. To learn the characteristics of the intermolecular interactions more clearly, the excess functions should be used, excess over the sum of thermodynamic quantities of all pure components. Thus, they are expressed similarly,

$$F^{\mathrm{E}}_{\mathrm{i-j}} \equiv N\left(\frac{\partial F^{\mathrm{E}}_{\mathrm{i}}}{\partial n_{\mathrm{j}}}\right)_{p,T,n_{\mathrm{k}\neq\mathrm{j}}} . \tag{54}$$

It is easy to define higher order derivative quantities of Gibbs energy by mathematical expression. The deeper and more important information may be expected from the behavior of higher order derivatives. However, determination of them experimentally is problematic.

5. 2. Mixing schemes in aqueous solutions

Generally, aqueous solutions are divided into three concentration regions in each of which the “mixing scheme”, mixing scenario at molecular level, is qualitatively different from the other. [88] We name them “mixing scheme I, II, III” from the water-rich side. In mixing scheme I, liquid water retains its integrity, the highly fluctuating three dimensional hydrogen bond network system. Although the hydrogen bond probability remains high enough to keep the hydrogen bond percolation. Solutes are isolated and interact with each other via the water hydrogen bond network. In this concentration region, ion pairs are completely dissociated and all the effects of solutes must be additive. On increasing solute to the threshold of bond-percolation, solutes begin interacting with each other directly. In the region of mixing scheme II, there are two types of clusters, one rich in water and the other in solute. The most solute-rich region, mixing scheme III is operative in which solute aggregates as in pure liquid and gas-like water molecules interact with them.

In the mixing scheme I, the interaction between solute i-i are apparent in the mole fraction dependence pattern of the third derivative of Gibbs energy, $F_{\mathrm{i-i}}^{\mathrm{E}}$, the interaction function. The boundaries between the regions of mixing scheme are also appeared on $F_{\mathrm{i-i}}^{\mathrm{E}}$ as the change of slope. Figure 5-1 shows relationship between the mixing scheme and the $F_{\mathrm{i-i}}^{\mathrm{E}}$ pattern against mole fraction of solutes i for various kinds of solutes in aqueous solutions. Three different kinds of solute, “hydrophobes”, “hydrophiles” and “amphiphiles”, are found out as shown in figure 5-1. From a number of previous studies [106]–[109], we suggested that the first changing point of slope in figure 5-1, indicates the end of mixing scheme I, the threshold of bond percolation of water network, called point X, and the second point reflects the beginning of mixing scheme II, called point Y. When solute i is a hydrophobe, $F_{\mathrm{i-i}}^{\mathrm{E}}$ shows a peak type behavior and the peak top corresponds to point X. The details of the behavior is discussed below. On the other hand, the behavior of $F_{\mathrm{i-i}}^{\mathrm{E}}$ show no distinction among various solutes in the regions of mixing scheme II and III.

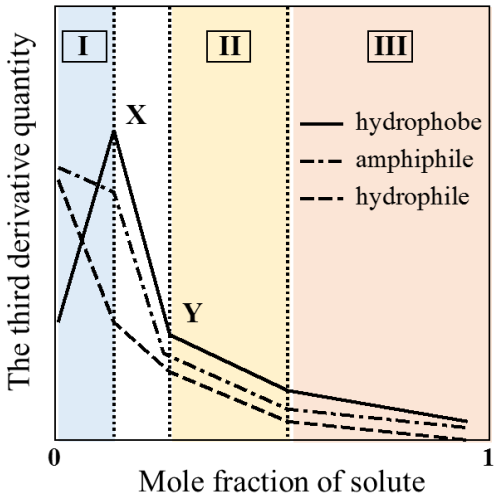

Figure 5-1 Relationship between the mixing schemes and the behavior of $F_{\mathrm{i-i}}^{\mathrm{E}}$, interaction between solite i-i for the three kinds of solutes, hydrophobes, hydrophiles and amphiphiles against concentration of the solute. [88] Point X corresponds to the end of the region of mixing scheme I and point Y is the beginning of mixing scheme II.

From various analyses of higher derivative thermodynamic quantities for aqueous solutions including the 1-prpanol probing methodology discussed below in 5. 5., an additional kind of solutes, [110], [111] “hydration centers” was discovered. Thus in total four kinds of solutes were identified in the mixing scheme I according to the solutes’ effects on the water network, defined as “hydrophobes”, “hydrophiles”, “amphiphiles” and “hydration centers”. Hydrophobesv[106]–[108] are recognized as strangers by water and water molecules form hydration shells around them. The hydrogen bond probability in the hydration shells is slightly higher than pure liquid water. [112]–[114] However, that in bulk water away from hydration shells becomes lower gradually. On increasing the solute mole fraction x_{i}, $F_{\mathrm{i-i}}^{\mathrm{E}}$ increases sharply to the point X, at which the bond percolation of the water network starts to break down, i. e. the system arrives at the hydrogen bond percolation threshold. [115] This process of crossover continues to the next break point, point Y, where the mixing scheme II sets in. [115], [116] This mole fraction width from point X to Y reflects the fact that the wide distribution of the hydrogen bond strength is prevalent in water. Hydrophiles [104], [117], [115], on the other hand, make hydrogen bonds directly to the water network. Then the characteristic high fluctuation of water network becomes smaller. When the mole fraction of hydrophiles reach about 0.1, they remains no bulk water to form bond percolating hydrogen bond network, and the mixing scheme II sets in. Amphiphiles [104], [115] have contributions

of both hydrophobic and hydrophilic moieties additively on water. [118]–[120] Hydration centers [111], [121] are similar to hydrophobes. They form hydration shells, but they do not lower the probability of hydrogen bond in bulk water away from hydration shells.

We applied this thermodynamic technique on studying on the aqueous solution of $[P_{4444}]CF_3COO$. We focused on partial molar volume and partial molar enthalpy of $[P_{4444}]CF_3COO$, the second derivative quantities of Gibbs energy. Then we performed differentiation with respect to n_{IL}, the molar amount of $[P_{4444}]CF_3COO$ to obtain the third derivative quantities.

5. 3. Volumetric analysis

Partial molar volumes for $[P_{4,4,4,4}]CF_3COO$ and water are discussed in 3. 3. 2. As mentioned above, the partial molar volume of component $[P_{4,4,4,4}]CF_3COO$, v_{IL}, is the second derivative of Gibbs energy.

$$v_{IL} \equiv \left(\frac{\partial V}{\partial n_{IL}}\right)_{p,\,T,\,n_W} = \left\{\frac{\partial}{\partial n_{IL}}\left(\frac{\partial G}{\partial p}\right)\right\}_{p,\,T,\,n_W} . \quad (55)$$

Figure 5-2 shows the apparent excess partial molar volume of $[P_{4,4,4,4}]CF_3COO$, $v^E_{IL,ap}$, and that of water, $v^E_{W,ap}$, at 298 K in dilute region, x_{IL}= 0.000-0.025. The subscripts ap indicate apparent value as mentioned in 3. 3. 2. $v^E_{IL,ap}$ shows a minimum at x_{IL}= 0.003. As can been seen from Gibbs-Duhem relation, $v^E_{W,ap}$ shows a maximum at the same concentration. Their behaviors suggest that $[P_{4,4,4,4}]CF_3COO$ has hydrophobic contribution on the water network according to previous studies. [88], [106] When $[P_{4,4,4,4}]CF_3COO$ which is much more bulky than water is added in pure water, water molecules fill the void of $[P_{4,4,4,4}]CF_3COO$. An apparent volume of $[P_{4,4,4,4}]CF_3COO$ in the infinite dilution is smaller than that in pure $[P_{4,4,4,4}]CF_3COO$ and $v^E_{IL,ap}$ is negative. As mentioned above, a hydrophobic solute forms hydration shells and reduce the probability of hydrogen bond probability of the bulk water away from the hydration shells. Furthermore, water is not just a small molecule. The net size of water is a little larger due to hydrogen bonds. This contributes positively at the infinite dilution. However, the existence of a hydrophobic solute reduces the hydrogen bond probability of bulk water away from hydration shells, where the next incoming solute settles in. Thus the positive contribution is reduced gradually, resulting in an apparent decrease in partial molar volume of a hydrophobic solute. [122] $v^E_{IL,ap}$ in figure 5-2 shows the same behavior as a typical hydrophobic solute, 2-butoxyethanol in its aqueous solution [122].

By applying differentiation on the partial molar volume of $[P_{4,4,4,4}]CF_3COO$ with respect to the molar amount of $[P_{4,4,4,4}]CF_3COO$, v^E_{IL-IL}, the volumetric IL-IL interaction

the third derivative quantity of Gibbs energy is calculated by,

$$v^{\mathrm{E}}_{\mathrm{IL-IL}} \equiv N\left(\frac{\partial v^{\mathrm{E}}_{\mathrm{IL}}}{\partial n_{\mathrm{IL}}}\right)_{p,T,n_{\mathrm{W}}} = (1-x_{\mathrm{IL}})\left(\frac{\partial v^{\mathrm{E}}_{\mathrm{IL}}}{\partial x_{\mathrm{IL}}}\right)_{p,T,N}, \tag{56}$$

where N is the total molar amount of $[P_{4,4,4,4}]CF_3COO$ and water, $N = n_{\mathrm{IL}} + n_{\mathrm{W}}$. $v^{\mathrm{E}}_{\mathrm{IL-IL}}$ was obtained in the same manner as determination of v_{IL} in 3. 3. 2. Black solid curve in figure 5-2 (a) is the fitting curve drawn by a flexible ruler. All $v^{\mathrm{E}}_{\mathrm{IL,ap}}$ values and fitting curves are shown in Appendix F.

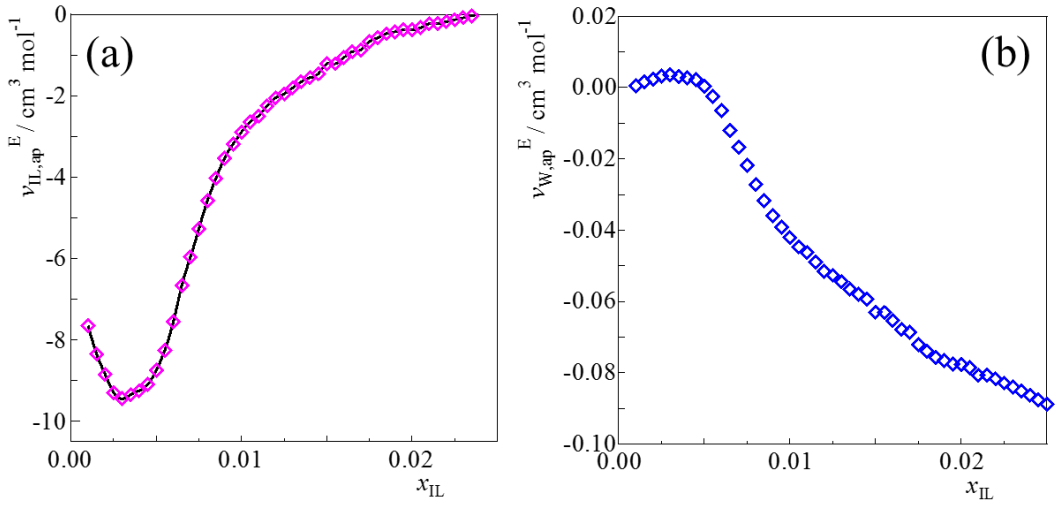

Figure 5-2 Excess partial molar volumes of (a)$[P_{4,4,4,4}]CF_3COO$, $v^{\mathrm{E}}_{\mathrm{IL,ap}}$, and (b)water, $v^{\mathrm{E}}_{\mathrm{W,ap}}$, in dilute region at 298 K. The solid curve in (a) is the fitting curve drawn with a flexible ruler.

Figure 5-3 shows the third derivative quantities of Gibbs energy in terms of volume, $v^{\mathrm{E}}_{\mathrm{IL-IL}}$, at 293, 298 and 301 K. $v^{\mathrm{E}}_{\mathrm{IL-IL}}$ at each temperature is approximated with three straight lines and shows peak type behavior against mole fraction. The calculated values are shown in Appendix G. The results indicate clearly that $[P_{4,4,4,4}]CF_3COO$ has a strong hydrophobic effect on the water network and water molecules make hydration shells around it in the mixing scheme I. These contribution of $[P_{4,4,4,4}]CF_3COO$ should be the sum of contributions of each constituent ions, $[P_{4,4,4,4}]^+$ and CF_3COO^-, because salts are dissociate into cations and anions completely and their contributions are additive in the mixing scheme I. From the viewpoint of the third derivative, there is no anomaly at x_{IL}= 0.003 ($v^{\mathrm{E}}_{\mathrm{IL-IL}}$= 0) where the partial molar volumes of $[P_{4,4,4,4}]CF_3COO$, the second derivatives, show the minimum. The water network remains bond percolation and

$[P_{4,4,4,4}]CF_3COO$ interacts each other via the network. [88]

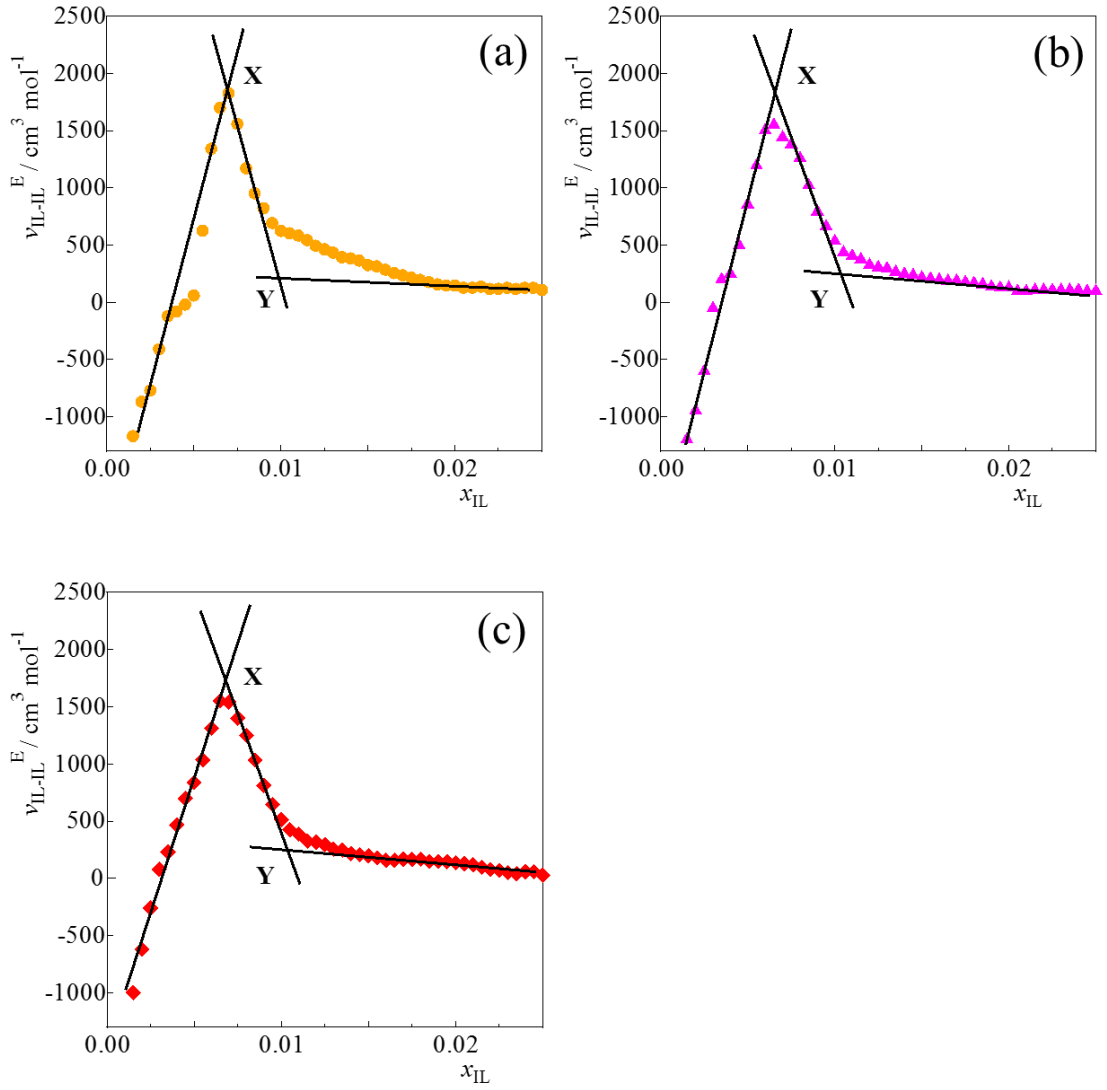

Figure 5-3 IL-IL interaction or the third derivative quantity of Gibbs energy in terms of volume, v^{E}_{IL-IL}, at (a)293, (b)298 and (c)301 K. v^{E}_{IL-IL} showed a peak type behavior against mole fraction of $[P_{4,4,4,4}]CF_3COO$ and two changing points of slope, point X and Y were obtained by approximation with three straight lines.

In previous studies, the loci of point X shift to a lower concentration with increasing temperature and define the Koga lines which approach to 353 K at the infinite dilution regardless of the identify and kind of solutes. [88], [123], [124] However from the obtained v^{E}_{IL-IL} in this study, the shift of point X with increasing temperature, though only by 8 K, was not observed. Since we applied graphical differentiation twice on the

raw density data to arrive at v^{E}_{IL-IL}, the temperature deviation as a function of T should be regarded with caution. Particularly so, for the loci of point Y. However, all peak type behaviors indicate points X and Y at similar concentrations. From differential thermodynamical analysis in terms of volume, point X at 298 K was observed around at x_{IL}= 0.0064 and point Y is around at x_{IL}= 0.0104. However we note that the post peak region may contain rather gradual decreases and points Y are have some inaccuracy.

5. 4. Enthalpic analysis

5. 4. 1. Experimental

Excess partial molar enthalpy of solute i, H^{E}_{i}, is one of the important thermodynamic quantities for studying aqueous solutions. For this purpose, isothermal titration calorimetry is used to our advantage. Namely, a small amount of a solute is titrated in the mixture and H^{E}_{i} is measured directly. H^{E}_{i} is the second derivative of Gibbs energy with respect to T and n_{i}. Then the third derivative quantity, H^{E}_{i}, is calculated by applying differentiation with respect to n_{i} only once.

However, as mentioned in 3. 3. 2., $[P_{4,4,4,4}]CF_3COO$ is a solid at room temperature. To measure the excess partial molar enthalpy of $[P_{4,4,4,4}]CF_3COO$, an mixture of $[P_{4,4,4,4}]CF_3COO$ and water was used as the titrant and added into pure water, successively. The mole fraction of $[P_{4,4,4,4}]CF_3COO$ for the titrant was 0.0461.The actual thermal effect by titration was obtained using a handmade calorimeter [125] at 298 K. Figure 5-4 shows a photo of the calorimeter used. The titrant solution was added into water using a syringe pump system with 25 mL gas-tight syringe. Details of the calorimeter and experimental conditions are reported in Appendix K.

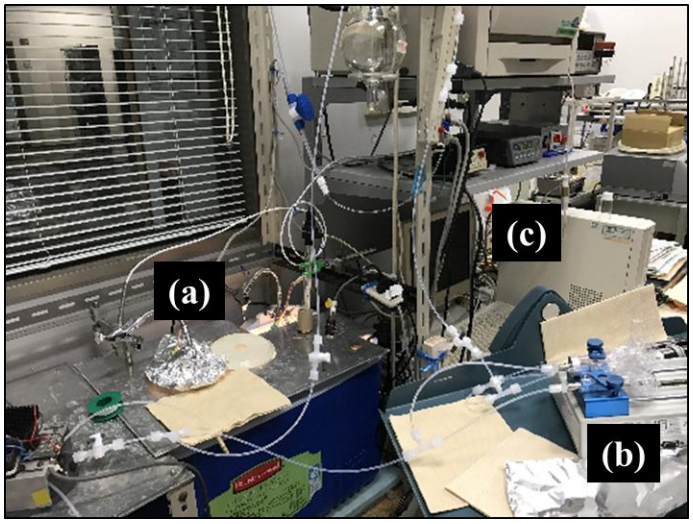

Figure 5-4 The photo of the calorimeter used; (a)the water bath at 298 K, (b)the syringe pump system and (c)the operation computer. The sample cell was set in (a).

To convert the apparent excess partial molar enthalpy to the excess partial molar enthalpy of $[P_{4,4,4,4}]CF_3COO$, we consider the case of titration of the titrant aqueous solution of $[P_{4,4,4,4}]CF_3COO$ into the mixture. [88] The initial base solvent contains n_{IL} mol $[P_{4,4,4,4}]CF_3COO$ and n_{W} mol water. The concentration of the titrant aqueous solution is constant at $x_{\mathrm{IL}}^{(\mathrm{t})}$. When small amount of titrant is added, $\delta n_{\mathrm{IL}}^{(\mathrm{t})}$ mol $[P_{4,4,4,4}]CF_3COO$ and $\delta n_{\mathrm{W}}^{(\mathrm{t})}$ mol water are added in the mixture. This thermal change, δq, is written as,

$$\delta q = H(n_{\mathrm{IL}} + \delta n_{\mathrm{IL}}, n_{\mathrm{W}} + \delta n_{\mathrm{W}}) - H(n_{\mathrm{IL}}, n_{\mathrm{W}}) - H^{(\mathrm{t})}\left(\delta n_{\mathrm{IL}}^{(\mathrm{t})}, \delta n_{\mathrm{W}}^{(\mathrm{t})}\right), \tag{57}$$

$$H^{(\mathrm{t})} = \delta n_{\mathrm{IL}}^{(\mathrm{t})} H_{\mathrm{IL}}^{(\mathrm{t})} + \delta n_{\mathrm{W}}^{(\mathrm{t})} H_{\mathrm{W}}^{(\mathrm{t})} = \text{constant}. \tag{58}$$

The superscript (t) indicates the titrant mixture. Define h, the apparent excess partial molar enthalpy, as the following,

$$h \equiv \left(\frac{\delta q}{\delta n_{\mathrm{IL}}}\right) = \frac{H\left(n_{\mathrm{IL}} + \delta n_{\mathrm{IL}}^{(\mathrm{t})}, n_{\mathrm{W}} + \delta n_{\mathrm{W}}^{(\mathrm{t})}\right) - H\left(n_{\mathrm{IL}}, n_{\mathrm{W}} + \delta n_{\mathrm{W}}^{(\mathrm{t})}\right)}{\delta n_{\mathrm{IL}}^{(\mathrm{t})}}$$

$$+ \frac{H\left(n_{\mathrm{IL}}, n_{\mathrm{W}} + \delta n_{\mathrm{W}}^{(\mathrm{t})}\right) - H(n_{\mathrm{IL}}, n_{\mathrm{W}})}{r\delta n_{\mathrm{W}}^{(\mathrm{t})}} - H_{\mathrm{IL}}^{(\mathrm{t})} - \frac{H_{\mathrm{W}}^{(\mathrm{t})}}{r}, \tag{59}$$

where

$$r = \frac{x_{\mathrm{IL}}^{(\mathrm{t})}}{1 - x_{\mathrm{IL}}^{(\mathrm{t})}} = \frac{\delta n_{\mathrm{IL}}^{(\mathrm{t})}}{\delta n_{\mathrm{W}}^{(\mathrm{t})}}. \tag{60}$$

In the limit of δn_{IL} and $\delta n_{\mathrm{W}} \to 0$, h is rewritten as,

$$h = H_{\mathrm{IL}} + \frac{H_{\mathrm{W}}}{r} - H_{\mathrm{IL}}^{(\mathrm{t})} - \frac{H_{\mathrm{W}}^{(\mathrm{t})}}{r}. \tag{61}$$

Figure 5-5 shows the results of the apparent excess partial molar enthalpy, h, at 298 K against mole fraction of $[P_{4,4,4,4}]CF_3COO$. We draw the smoothing curve as shown in the figure and read the values off the smooth curve drawn at the increment of δn_{IL}= 0.0002. All measured data are shown in Appendix L.

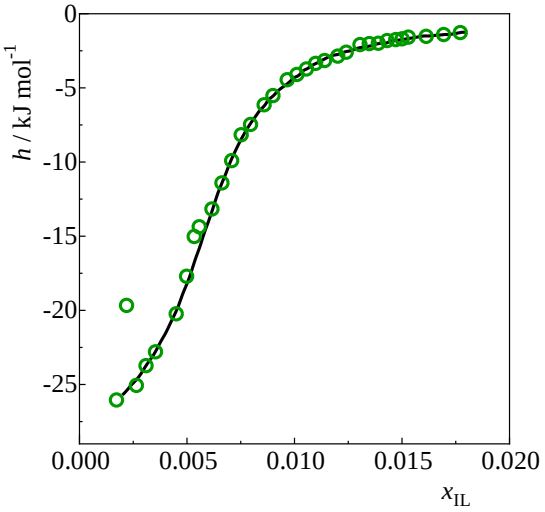

Figure 5-5 Apparent excess partial molar enthalpy, h, against mole fraction of $[P_{4,4,4,4}]CF_3COO$, x_{IL}, at 298 K. The black solid curve is the fitting curve drawn with a flexible ruler.

By considering variation of h between two adjustment points, δh, the constant terms are eliminated and δh is expressed by variation of partial molar enthalpy of $[P_{4,4,4,4}]CF_3COO$, that of water and mole fractions of the mixture. Using Gibbs-Duhem relation,

$$\delta h = \delta H_{\mathrm{IL}} + \frac{\delta H_{\mathrm{W}}}{r} = \delta H_{\mathrm{IL}} \left(1 - \frac{x_{\mathrm{IL}}}{r x_{\mathrm{W}}}\right) = \delta H_{\mathrm{IL}}^{\mathrm{E}} \left(1 - \frac{x_{\mathrm{IL}}}{r(1 - x_{\mathrm{IL}})}\right). \tag{62}$$

Hence,

$$\delta H_{\mathrm{IL}}^{\mathrm{E}} = \delta h \Big/ \left(1 - \frac{x_{\mathrm{IL}}}{r x_{\mathrm{W}}}\right), \tag{63}$$

and $H_{\mathrm{IL}}^{\mathrm{E}}$ is obtained if necessary as the sum of $\delta H_{\mathrm{IL}}^{\mathrm{E}}$.

$$H_{\mathrm{IL}}^{\mathrm{E}} = \sum \delta H_{\mathrm{IL}}^{\mathrm{E}} + C. \tag{64}$$

The constant value, C, should be obtained by determination of excess partial molar enthalpy of $[P_{4,4,4,4}]CF_3COO$ at a certain point directly. The required $H_{\mathrm{IL-IL}}^{\mathrm{E}}$ is then calculated using equation (63) as,

$$H_{\mathrm{IL-IL}}^{\mathrm{E}} = (1 - x_{\mathrm{IL}}) \left(\frac{\delta H_{\mathrm{IL}}^{\mathrm{E}}}{\delta x_{\mathrm{IL}}} \right). \tag{65}.$$

5. 4. 2. The third derivative quantity in terms of enthalpy

Figure 5-6 shows the concentration dependence of enthalpic interaction between $[P_{4,4,4,4}]CF_3COO$, the third derivative excess quantity of Gibbs energy in terms of enthalpy, $H_{\mathrm{IL-IL}}^{\mathrm{E}}$, at 298 K. The calculated values are shown in Appendix L. The peak type behavior of $H_{\mathrm{IL-IL}}^{\mathrm{E}}$ indicates that $[P_{4,4,4,4}]CF_3COO$ (the sum of contributions of $[P_{4,4,4,4}]^+$ and CF_3COO^-) has the hydrophobic contribution on the water network in the dilute concentration region. Point X, the end of the region of the mixing scheme I exists at x_{IL}= 0.0059 and point Y, the beginning of the concentration region of the mixing scheme II was found to be at x_{IL}= 0.0093.

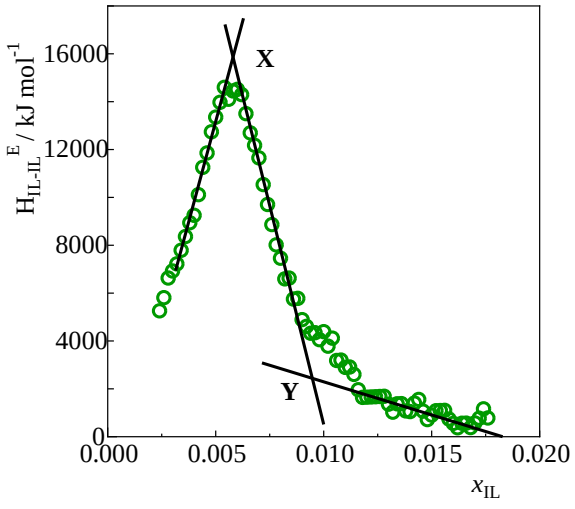

Figure 5-6 Concentration dependence of the enthalpic interaction between $[P_{4,4,4,4}]CF_3COO$, the third derivative excess quantity of Gibbs energy in terms of enthalpy, $H_{\mathrm{IL-IL}}^{\mathrm{E}}$, at 298 K. $H_{\mathrm{IL-IL}}^{\mathrm{E}}$ showed peak type behavior. Points X and Y determined by approximation with three straight lines indicate the boundaries of the mixing schemes.

In previous study, the value of enthalpic interaction between solutes at x_{IL}= 0 should be not zero because even at the infinite dilution, solutes have contribution on each other via the water network.[104] However, it seems that $H^{\mathrm{E}}_{\mathrm{IL-IL}}$ approaches zero at x_{IL}= 0. We observe the x_{IL} dependence pattern may not be simple straight line and two types of peak is overlapping. While such patterns with straight lines shown in figure 1 have been observed for a number of hydrophobes, for the aqueous solution of 2-butoxyethanol, a typical hydrophobe [88], [109], the double peaks appear to overlap[126] hinting intramolecular hydrogen bonding between the ether –O– and the end –OH, suggested by MD simulation [127], [128].

Comparing the third derivative quantities of Gibbs energy in terms of volume, $V^{\mathrm{E}}_{\mathrm{IL-IL}}$, and enthalpy, $H^{\mathrm{E}}_{\mathrm{IL-IL}}$, both quantities shows peak-type behavior against x_{IL} which indicate that the sum of contributions of each constituent ions is hydrophobic in the mixing scheme I. The loci of both point X and Y show similar values but values from $H^{\mathrm{E}}_{\mathrm{IL-IL}}$ are slightly smaller than those in terms of volume as shown in figure 5-7. However, taking into account of the fact that the volumetric third derivative was the result of double differentiation, while the enthalpic one was obtained by a single differentiation, the value resulting from enthalpy should be more accurate.

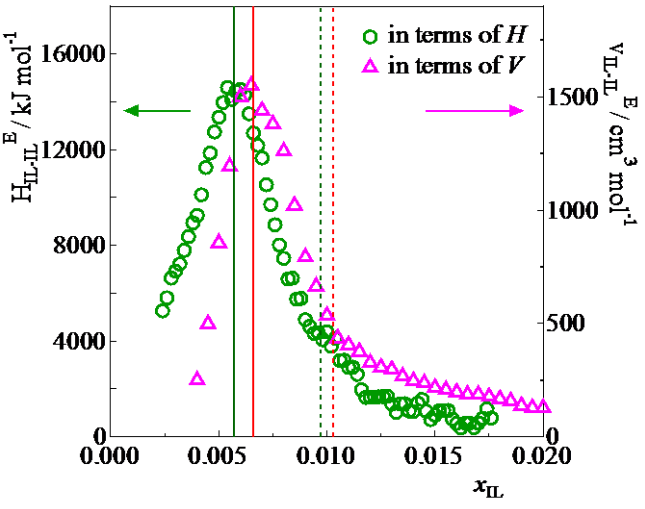

Figure 5-7 Comparison of third derivative quantities between those in terms of enthalpy, green circles, and in terms of volume, pink triangles. Loci of point X and Y of enthalpy shift to slightly smaller concentrations than those of volume.

5. 5. Characterization of $[P_{4,4,4,4}]^+$ and CF_3COO^- individual ions

5. 5. 1. 1-propanol probing methodology

Using the behavior of the interaction between solutes, S, in aqueous solution in terms of enthalpy, $H^{\mathrm{E}}_{\mathrm{S-S}}$, the 1-propanol (1P)-probing methodology was established to characterize the effect of the chosen solute on water network. [88], [104] In this method, hydrophobic and hydrophilic contributions of the chosen solute are evaluated by first measuring the excess partial molar enthalpy of the probing 1-propanol, $H^{\mathrm{E}}_{\mathrm{1P}}$, added into the aqueous solution of S. In the mixing scheme I, the effects of solutes work on water additively as discussed before.

Now consider the ternary system of 1-propanol, the solute S and water. The enthalpic interaction between 1-propanol, the third derivative quantity in terms of enthalpy, $H^{\mathrm{E}}_{\mathrm{1P-1P}}$, is written as,

$$H^{\mathrm{E}}_{\mathrm{1P-1P}} \equiv N\left(\frac{\partial H^{\mathrm{E}}_{\mathrm{1P}}}{\partial n_{\mathrm{1P}}}\right)_{p,T,n_{\mathrm{S}},n_{\mathrm{W}}} = (1-x_{\mathrm{1P}})\left(\frac{\partial H^{\mathrm{E}}_{\mathrm{1P}}}{\partial x_{\mathrm{1P}}}\right)_{p,T,N}, \tag{66}$$

where n_{1P}, n_{S} and n_{W} represent the molar amount of 1-propanol, the test solute and water, respectively. N is the total molar amount, i. e. $N = n_{\mathrm{1P}} + n_{\mathrm{S}} + n_{\mathrm{W}}$. x_{1P} is the mole fraction of 1-propanol, $x_{\mathrm{1P}} = n_{\mathrm{1P}}/N$. Partial molar enthalpy of 1-propanol is obtained experimentally by adding 1-propanol into the aqueous solution of the solute, S. The initial mole fraction of the test solute, x^0_{S}, is defined as,

$$x^0_{\mathrm{S}} = \frac{n_{\mathrm{S}}}{n_{\mathrm{S}} + n_{\mathrm{W}}}. \tag{67}$$

$H^{\mathrm{E}}_{\mathrm{1P-1P}}$ is determined by applying graphical or numerical differentiation on the measured $H^{\mathrm{E}}_{\mathrm{1P}}$ with respect to x_{1P}. 1-propanol is a typical hydrophobe and $H^{\mathrm{E}}_{\mathrm{1P-1P}}$ shows a peak type behavior against x_{1P} (see figure 5-1) without the presence of the test solute, S. The contributions of the test solute on water appear as the changes of the peak type behavior of $H^{\mathrm{E}}_{\mathrm{1P-1P}}$. Figure 5-8 shows the various pattern changes of $H^{\mathrm{E}}_{\mathrm{1P-1P}}$ depending on the nature of the test solute. When the test solute is a hydrophobe, the induced change is described as (a) of the figure. The pattern of $H^{\mathrm{E}}_{\mathrm{1P-1P}}$ shifts to the left side of the figure. By the presence of a hydrophilic test solute, point X of $H^{\mathrm{E}}_{\mathrm{1P-1P}}$ shifts downward of the figure as shown in (b). Amphiphile including both contributions of hydrophilicity and hydrophobicity, the pattern of $H^{\mathrm{E}}_{\mathrm{1P-1P}}$ shifts toward left as well as downward of figure 5-8 (c). When the test solute is a hydration center which shows similar effects to hydrophobe shown in figure 5-8 (a). In addition the values of $H^{\mathrm{E}}_{\mathrm{1P-1P}}$ at x_{1P}= 0 and at point X are fixed independent of the existence of the solute, S. From this observation, we

suggest that hydration centers do not have any effect on the hydrogen bond network in the bulk water away from hydration shells. In the 1P-probing methodology, the shift of point X toward lower $x_{1\mathrm{P}}$ against x_{S}^{0} is defined as the index of hydrophobicity and that toward lower $H_{1\mathrm{P}-1\mathrm{P}}^{\mathrm{E}}$ value is defined as that of hydrophilicity.

Also in the mixing scheme I, ion pairs are considered to be completely dissociated into anions and cations and their respective contributions are additive. The 1P-probing methodology is applied on characterization of an individual ion by choosing chloride or sodium for counter ions. Both chloride and sodium ions were found to be hydration centers [110], [111] Thus, we can characterize the hydrophobicity/hydrophilicity of any individual ion by choosing either Na^{+} or Cl^{-} as a counter ion. We then apply the 1P-probing methodology to the resulting salt. Then the results for the given ion are obtained by subtracting the effects of chosen counter ions.

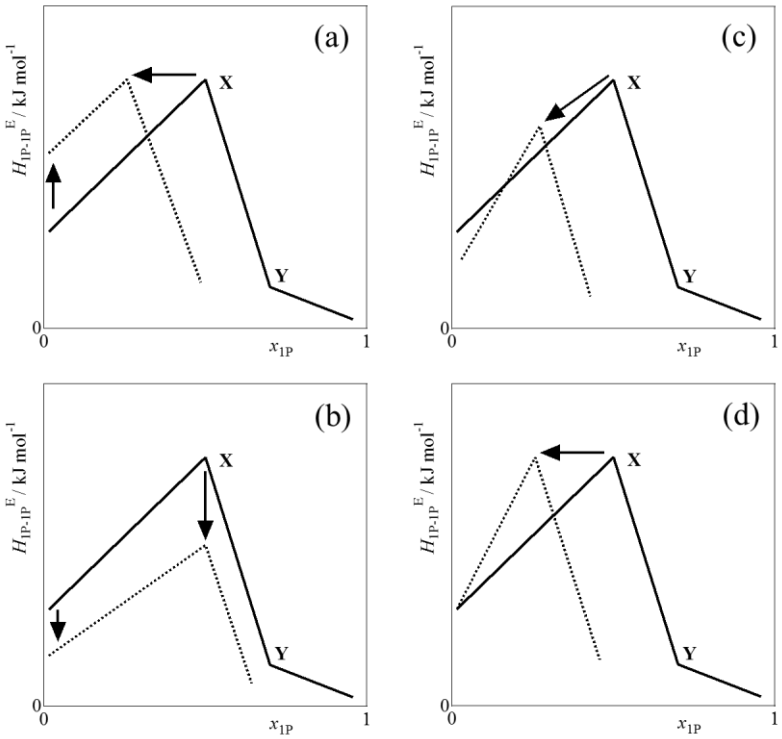

Figure 5-8 The shifts of enthalpic interaction between 1-propanol, $H_{1\mathrm{P}-1\mathrm{P}}^{\mathrm{E}}$, patterns by the effects of four kinds of solutes, (a)hydrophobes, (b)hydrophiles, (c)amphiphies and (d)hydration centers.

5. 5. 2. Experimental

To characterize tetrabutylphosphonium, $[P_{4,4,4,4}]^+$, and CF_3COO^- ions separately, the 1P-probing methodology was applied on aqueous solution of tetrabutylphosphonium chloride, $[P_{4,4,4,4}]Cl$, and that of sodium trifluroacetate, $NaCF_3COO$. [129] Two test solutes, $[P_{4,4,4,4}]Cl$ (Aldrich, > 98 %) and $NaCF_3COO$ (Sigma-Aldrich, > 96 %) are mixed with milliQ. Excess partial molar enthalpies of 1-propanol, H_{1P}^{E}, were measured using the isothermal titration calorimeter, TAM III (TA Instruments, New Castle, USA) at 298.15 K ± 0.0001 K and in the dynamic correction mode. 1-propanol as titrant was supplied from Sigma-Aldrich whose grade was Chromasolv for HPLC 99.9+%.

Figure 5-9 shows the partial molar enthalpies of 1-propanol, H_{1P}^{E}, for the aqueous solutions of $[P_{4,4,4,4}]Cl$ and $NaCF_3COO$ for various initial mole fraction of the test samples, x_S^0.[129] Symbols of blue diamond represent the result of binary system of 1-propanol and water. Adding salts, the changes were observed in H_{1P}^{E} pattern for both solutes, $[P_{4,4,4,4}]Cl$ and $NaCF_3COO$.

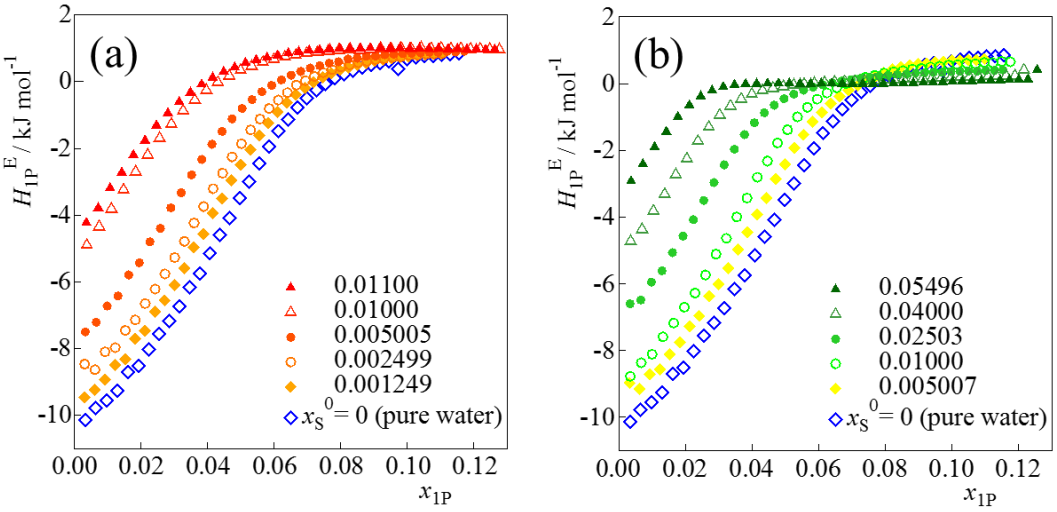

Figure 5-9 Partial molar enthalpies of 1-propanol, H_{1P}^{E}, on (a)$[P_{4,4,4,4}]Cl$ and (b)$NaCF_3COO$ for various x_S^0 against x_{1P}. [129] The blue plots correspond to the result of pure water.

5. 5. 3. Results

The excess enthalpic interaction between 1-propanol, $H^{\mathrm{E}}_{1\mathrm{P}-1\mathrm{P}}$, were obtained by numerical differentiation [129] of $H^{\mathrm{E}}_{1\mathrm{P}}$ with respect to $x_{1\mathrm{P}}$. The value of $H^{\mathrm{E}}_{1\mathrm{P}-1\mathrm{P}}$ at the i-th point is calculated with the (i+1)-th and (i-1)-th $H^{\mathrm{E}}_{1\mathrm{P}-1\mathrm{P}}$ values as,

$$H^{\mathrm{E}}_{1\mathrm{P}-1\mathrm{P}}(\mathrm{i}) = \left(1 - x_{1\mathrm{P}}(\mathrm{i})\right)\left(\frac{\partial H^{\mathrm{E}}_{1\mathrm{P}}(\mathrm{i})}{\partial x_{1\mathrm{P}}(\mathrm{i})}\right)_{p,T,N}$$

$$\approx \frac{1 - x_{1\mathrm{P}}(\mathrm{i})}{x_{1\mathrm{P}}(\mathrm{i}+1) - x_{1\mathrm{P}}(\mathrm{i}-1)} \times \left[\frac{H^{\mathrm{E}}_{1\mathrm{P}}(\mathrm{i}+1) - H^{\mathrm{E}}_{1\mathrm{P}}(\mathrm{i})}{x_{1\mathrm{P}}(\mathrm{i}+1) - x_{1\mathrm{P}}(\mathrm{i})}\left(x_{1\mathrm{P}}(\mathrm{i}) - x_{1\mathrm{P}}(\mathrm{i}-1)\right) + \frac{H^{\mathrm{E}}_{1\mathrm{P}}(\mathrm{i}) - H^{\mathrm{E}}_{1\mathrm{P}}(\mathrm{i}-1)}{x_{1\mathrm{P}}(\mathrm{i}) - x_{1\mathrm{P}}(\mathrm{i}-1)}\left(x_{1\mathrm{P}}(\mathrm{i}+1) - x_{1\mathrm{P}}(\mathrm{i})\right)\right]. \quad (68)$$

The $x_{1\mathrm{P}}$ interval from $x_{1\mathrm{P}}(\mathrm{i})$ to $x_{1\mathrm{P}}(\mathrm{i}+1)$, was approximately 0.003 in the present measurements. Figure 5-10 shows the results of $H^{\mathrm{E}}_{1\mathrm{P}-1\mathrm{P}}$ for aqueous solutions of (a)[$P_{4,4,4,4}$]Cl and (b)$NaCF_3COO$ for various x^0_{S}. [129] The symbols of blue diamond corresponding to the result for binary system of 1-propanol and pure water show a peak type behavior. For both test samples the loci of point X shifts toward both left side and down side in the figure. The results indicate both $[P_{4,4,4,4}]^+$ and CF_3COO^- are amphiphiles after subtracting the effects of counter ions.

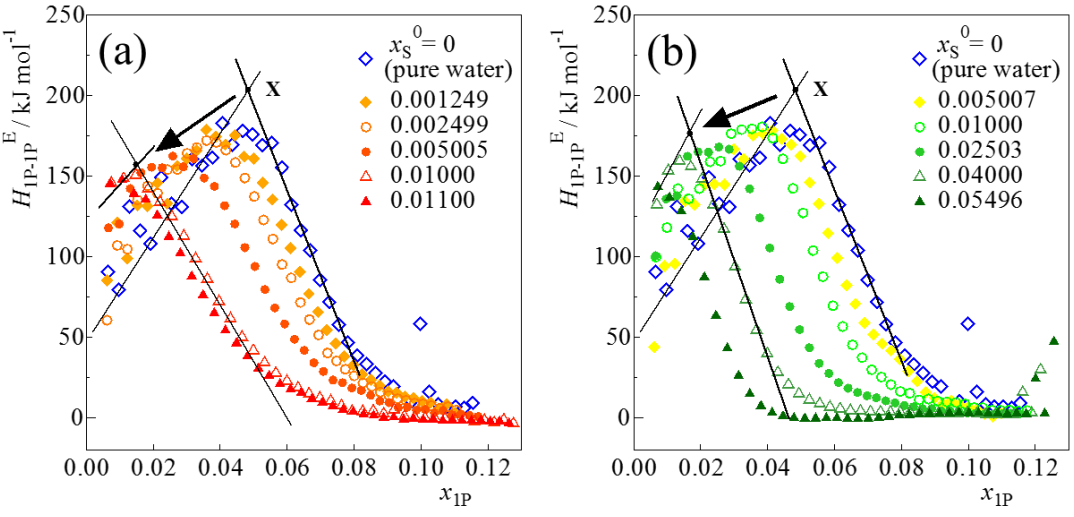

Figure 5-10 The shift of $H^{\mathrm{E}}_{1\mathrm{P}-1\mathrm{P}}$ with adding sample materials, (a)[$P_{4,4,4,4}$]Cl and (b)$NaCF_3COO$ at 298 K. [129] Points X for both systems shift toward both left and down side in the figure.

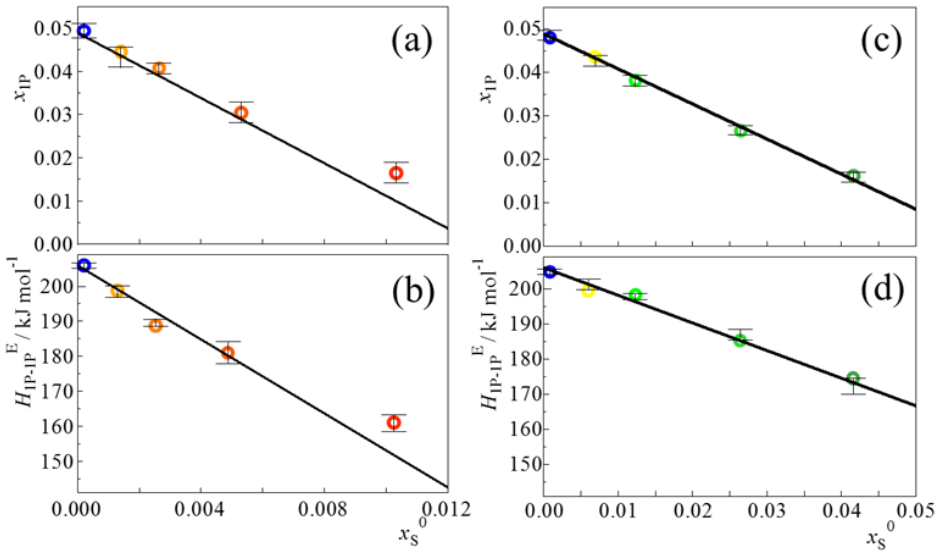

Figure 5-11 The dependences of the loci of point X on the initial mole fraction, x_S^0, for S= of $[P_{4,4,4,4}]Cl$ (a) in the x_{1P} direction and (b) in the H^{E}_{1P-1P} direction. Those for $NaCF_3COO$ (c) in the x_{1P} direction and (d) in the H^{E}_{1P-1P} direction. [129]

Figure 5-11 shows x_S^0-dependence of the loci of point X for the aqueous solution of $[P_{4,4,4,4}]Cl$ and $NaCF_3COO$. [129] To quantify the hydrophobic and hydrophilic contributions, their slope of leftward shift is defined as hydrophobicity, and that of downward shift hydrophilicity. [104] Then the slopes of the counter ions were subtracted to characterize the hydrophobicity/hydrophilicity of the individual test ions. Also the slope for x_{1P} direction reflects hydration number, n_H, calculated using the x_S^0 value at x_{1P}= 0 as discussed in ref. [104],

$$x_S^0(\text{at } x_{1P} = 0) = \frac{n_H}{1 + n_H}. \quad (69)$$

$[P_{4,4,4,4}]^+$ is characterized with hydrophobicity as -3.49 and hydrophilicity as -5337 kJ mol^{-1}. The larger the absolute values of hydrophobicity and hydrophilicity are, the stronger the effects of both ions are on water. The both contributions which are much stronger than other molecules or ions suggest that $[P_{4,4,4,4}]^+$ is a significant amphiphle. Hydration number is also large at 72. CF_3COO^- is also an amphiphile with hydrophobicity -0.49 and its hydrophilicity -767 kJ mol^{-1} and the hydration number is 10.

For $[P_{4,4,4,4}]^+$, the locus of point X at x_S^0= 0.0100 is deviated from the linear line. It hints that there could be a break point for the shift of point X. This may suggest that $[P_{4,4,4,4}]^+$ shows self-aggregation. While the H^{E}_{1P-1P} pattern retains a peak type indicates

the three component system is still in the mixing scheme I. This hints that for aqueous solution of original ionic liquid, i. e. $[P_{4,4,4,4}]CF_3COO$ an aggregation of the cation might occur, too.

5. 6. Discussion

Applying the differential thermodynamics on the aqueous solution of $[P_{4,4,4,4}]CF_3COO$, we found as discussed in 5. 4., that the third derivative quantities of Gibbs energy show a peak against the mole fraction of $[P_{4,4,4,4}]CF_3COO$. According to the obtained peak top, point X, the mixing scheme I of the aqueous solution of $[P_{4,4,4,4}]CF_3COO$ ends at x_{IL}= 0.0059. At lower concentrations than this mole fraction, $[P_{4,4,4,4}]CF_3COO$ should separate into $[P_{4,4,4,4}]^+$ cation and CF_3COO^- anion completely. Electric conductivity of the aqueous solution also shows the evidence for the separation of ions at very low concentrations. [129] By the peak-type behavior of both volumetric and enthalpic IL-IL interactions, V^{E}_{IL-IL} and H^{E}_{IL-IL}, the sum of contributions of each constituent ions, $[P_{4,4,4,4}]^+$ and CF_3COO^-, is strongly hydrophobic. However, H^{E}_{IL-IL} suggests H^{E}_{IL-IL} pattern is not able to be described with simple straight lines.

On the other hand, by the 1-propanol probing methodology, we found that both ions are characterized as amphiphiles separately. Especially $[P_{4,4,4,4}]^+$ is a significant amphiphile with a strong hydrophobicity and also strong hydrophilicity. Water forms hydration shells around $[P_{4,4,4,4}]^+$ with 72 water molecules. This value is three times larger than an imidazolium cation with butyl group, $[C_4mim]^+$. On the other hand, 10 water molecules form hydration shell around CF_3COO^-. Since, in a previous study, a single water molecule hydrates on the COO^- group of carboxylates and acts as the hydration center [130], nine water molecules must form the hydration shell around a hydrophobic trifluoromethyl group. Figure 5-12 is the two dimensional (2-D) map of hydrophobicity/hydrophilicity for typical ions composing ionic liquids. [110], [111], [129]–[134] The values of hydrophobicity/hydrophilicity of each ions in the figure are shown in Appendix M. The vertical axis shows hydrophilicity and the horizontal axis indicates hydrophobicity in the upper side of the figure and the hydration number in the lower axis. Water define the origin and the probing 1-propanol is necessarily located at (-1, 0). [104] As is evident in the figure, $[P_{4,4,4,4}]^+$ shows a stronger contribution on the water network.

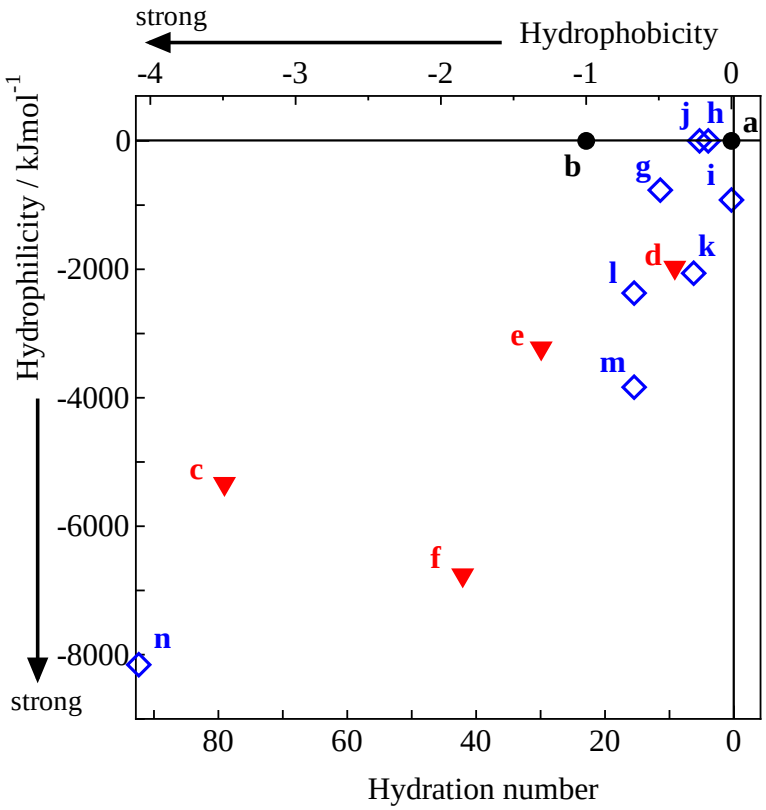

Figure 5-12 The 2-D map of hydrophobicity/hydrophlicity for typical cations (red symbols) and anions (blue symbols) composing ionic liquids; (c)$[P_{4,4,4,4}]^+$, (d)$[C_2mim]^+$, (e)$[C_4mim]^+$, (f)$[C_4C_1mim]^+$, (g)CF_3COO^-, (h)Cl^-, (i)Br^-, (j)CH_3COO^-, (k)BF_4^-, (l)OTf^-, (m)PF_6^- and (n)NTf_2^-. [110], [111], [129]–[134] Water (a) defines the origin and the probing 1-propanol (b) exists at (-1, 0).

In the 1-propanol probing methodology, the pattern changes of the third derivatives are observed, namely, the fourth derivative quantities of Gibbs energy are obtained. They should give deeper information of the system than the third derivatives. However, Cl^- and Na^+ were used for counter ions of $[P_{4,4,4,4}]CF_3COO$ in 1-propanol probing methodology. In the previous study [44], the IL–IL interactions, H^{E}_{IL-IL}, for 1-butyl-3-methylimidazolium tetrafluoroborate, $[C_4mim]BF_4$, and the iodide with the same cation, $[C_4mim]I$, in their aqueous solutions were reported. Comparing their patterns of H^{E}_{IL-IL} against IL mole fraction, much stronger hydrophobicity of the BF_4^- salt was observed than that of I^-.[44], [134] However, the results of characterization of BF_4^-[134] and I^- [111] separately by the 1-propanol probing methodology indicated they have similar hydrophilic contributions on the water network in the mixing scheme I with a small

hydrophobicity for BF_4^-[134]. So far, we are not able to discuss the contribution of pairing $[P_{4,4,4,4}]^+$ and CF_3COO^- on the total effects of $[P_{4,4,4,4}]CF_3COO$ on the water network. Characterization of $[P_{4,4,4,4}]CF_3COO$ by the 1-propanol probing methodology is necessary to understand why hydrophilic contribution was not observed from the third derivatives. As for hydrophobic contribution, both ions show hydrophobicity and lower the hydrogen bond probability in the bulk water away from hydration shells. The threshold of bond percolation of water network starts to break at point X, x_{IL}= 0.0059. Beyond point Y, x_{IL}= 0.0093, there are $[P_{4,4,4,4}]CF_3COO$-rich clusters and water-rich clusters. The loci of point X and Y for the aqueous solution of $[P_{4,4,4,4}]CF_3COO$ are at much lower mole fractions than those of aqueous solutions of normal molecules.

Chapter 6 Conclusion

In this thesis, the aqueous solution of tetrabutylphosphonium trifluoroacetate, $[P_{4,4,4,4}]CF_3COO$, was characterized from the viewpoints of fluctuation by means of small-angle X-ray (SAXS) study and of molecular level scenario by using differential thermodynamics. The aqueous solution shows the unique phase behavior, the LCST-type reversible phase separation with the critical point at the mole fraction of $[P_{4,4,4,4}]CF_3COO$, x_{IL}= 0.025 and at 302.35 K.

The density fluctuation and the concentration fluctuation for the aqueous solution around the critical point was determined in the concentration range, x_{IL}= 0.016-0.056 at 293, 298 and 301 K. Fluctuations were calculated by combination of three parameters, the zero-angle scattering intensity, the partial molar volumes of each components and the isothermal compressibility. Both fluctuations increased approaching to the critical point and, especially, the density fluctuation showed an extremely large value. Namely, the system shows an extremely large fluctuations toward the phase separation.

Using Kirkwood-Buff parameters, fluctuations for the entire system are divided into the individual density components and their correlation terms. Both of the individual density fluctuations for $[P_{4,4,4,4}]CF_3COO$ and water showed large degree of fluctuations toward the critical point. On the other hand, that of water was more than ten times greater than that of $[P_{4,4,4,4}]CF_3COO$. The extremely large difference of the partial molar volumes between $[P_{4,4,4,4}]CF_3COO$ and water must be closely related to the large density fluctuations and also to the large individual density fluctuation of water. Wang *et al.* reported the microemulsion-like aggregation of $[P_{4,4,4,4}]CF_3COO$ in water by NMR spectra, UV-Vis absorption spectra and freeze-fracture transmission electron microscopy. [135] In our study, the positive correlation terms of individual density fluctuations between $[P_{4,4,4,4}]CF_3COO$ and water suggests that a large number of water molecules hydrate $[P_{4,4,4,4}]CF_3COO$, and $[P_{4,4,4,4}]CF_3COO$ makes aggregates containing hydrating water molecules near the critical point.

Using differential thermodynamics, the concentration region of mixing scheme I and II for the aqueous solution of $[P_{4,4,4,4}]CF_3COO$ was obtained from the behavior of the third derivative quantities of Gibbs energy in terms of volume and of enthalpy at 298 K. For volume, the interaction among $[P_{4,4,4,4}]CF_3COO$, v^{E}_{IL-IL}, was obtained by applying differentiation with respect to the molar amount of $[P_{4,4,4,4}]CF_3COO$ on the measured

density data twice and, for enthalpy, H^{E}_{IL-IL} was obtained by a single differentiation of the measured apparent excess partial molar enthalpy of $[P_{4,4,4,4}]CF_3COO$. Both third derivative quantities indicate $[P_{4,4,4,4}]CF_3COO$ has a strong hydrophobic characteristics in the water network in the dilute concentration region. Namely, water molecules make hydration shells around $[P_{4,4,4,4}]CF_3COO$ and at the same time, the hydrogen bond probability of bulk water away from hydration shells decreases. From the break points of the third derivative quantities as a function of mole fraction, the end of the region of mixing scheme I and the beginning of the region of mixing scheme II were determined. Taking into account of experimental error and that coming from differentiation operation, the third derivative quantity in terms of enthalpy could be better than that in terms of volume. The former result indicates that mixing scheme I retains up to x_{IL}= 0.0059, and mixing scheme II in which $[P_{4,4,4,4}]CF_3COO$ interacts with each other directly is observed at higher than x_{IL}= 0.0093.

The critical point of phase separation at x_{IL}= 0.025 exists in the region of mixing II, in which there two types of clusters, water-rich and $[P_{4,4,4,4}]CF_3COO$-rich ones. This suggestion corresponds to a large individual fluctuations for each components and aggregation of $[P_{4,4,4,4}]CF_3COO$ containing water. Figure 6-1 shows the relationship between density fluctuation of the system and the mixing scheme drawn on the phase diagram. In this study the end of mixing scheme II or the beginning of mixing scheme III was not obtained. However the boundary of mixing scheme II and III should be at a higher concentration region than the concentration region shown in the figure.

In the region of the mixing scheme I, it is believed that $[P_{4,4,4,4}]CF_3COO$ is dissociated into cation and anion completely. Tetrabutylphosphoniu, $[P_{4,4,4,4}]^+$, and trifluoroacrtate, CF_3COO^-, were characterized separately by the 1-popanol probing methodology as their effects on water network within mixing scheme I. $[P_{4,4,4,4}]^+$ is a significant amphiphile with a strong hydrophobic and a strong hydrophilic contributions. Its hydration number 72 indicates water molecules form a large hydration shell. Also CF_3COO^- is an ampiphile and its hydration number is 10. These strong hydrophobic contributions of the composing ions on the water network corresponds to the behavior of the third derivatives for the binary system of $[P_{4,4,4,4}]CF_3COO$ and water. The existence of point X, the end of mixing scheme I, and Y, the beginning of mixing scheme II, the start of IL aggregation, were determined. However, by analysis of binary system, hydrophilicity of ions is not observed. The results indicate the contribution of $[P_{4,4,4,4}]CF_3COO$ ion pair is not able to describe by the sum of contributions of each cation and anion.

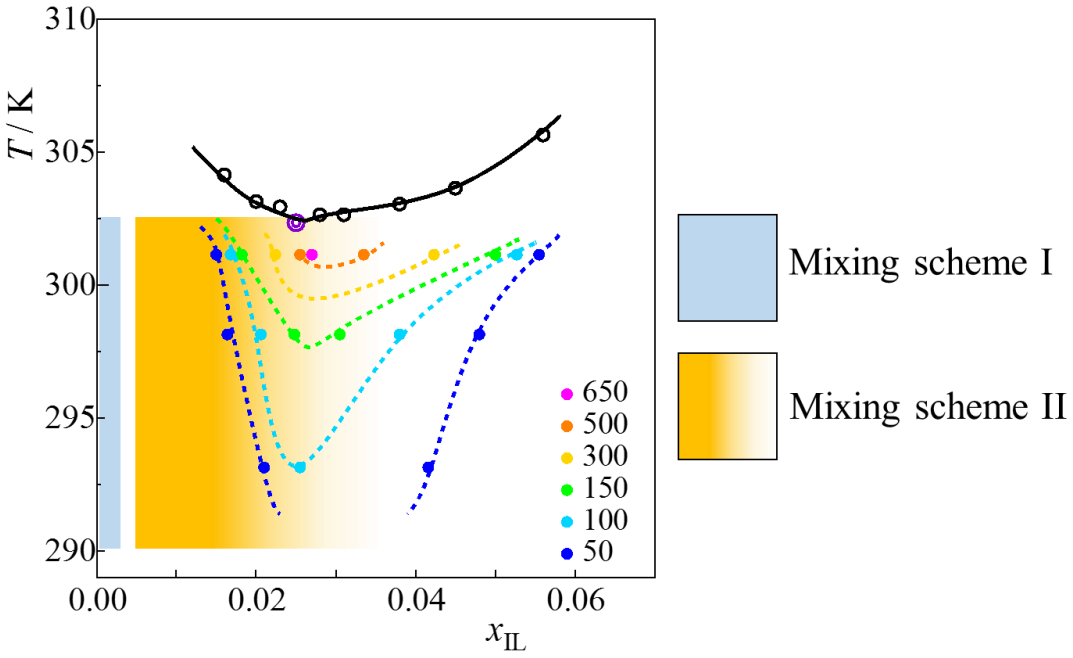

Figure 6-1 Mixing states of the aqueous solution of $[P_{4,4,4,4}]CF_3COO$. Black solid curve is the phase separation boundary and the contour lines represent distribution of the total density fluctuation. The blue concentration/temperature region corresponds to the region of mixing scheme I and the yellow region shows that of mixing scheme II. However the end of mixing scheme II is not known and may exist at a much higher concentration.

Using SAXS method, the drastic change of distribution of IL and water and information of IL aggregation were observed in the super critical region. Also, from the view point of the differential thermodynamics, the manner of interaction between ILs near the critical point was obtained. In dilute region, various ions composing ILs were characterized by the 1P-propbing methodology. These results should be valuable information for fundamental and applied study of aqueous solutions of IL. Comparing systematically the present results with various kinds of aqueous solutions of IL showing UCST-type phase separations and those not showing any phase separations is important.

Appendix

A. Sample preparation

Ionic liquid $[P_{4,4,4,4}]CF_3COO$ shows the melting point at 47 ºC and usually, it is solid state at room temperature. $[P_{4,4,4,4}]CF_3COO$ is needed a freeze dehydration because of its high hygroscopicity. First, glassy chunks or powders of $[P_{4,4,4,4}]CF_3COO$ in a vial container is frozen using liquid nitrogen completely. Then they are crashed and stirred $[P_{4,4,4,4}]CF_3COO$ is heated, temperature should be increased slowly up to 50-60 ºC. The IL shows the decomposition temperature at 178 ºC. During heating while water content is high, caution must be exercised not to bump a resulting highly viscous mixture. Until $[P_{4,4,4,4}]CF_3COO$ becomes powder-like, repeat freezing drying.

After drying under vacuum, the water content was determined by coulometric Karl-Fischer titration using the coulometer DL32 (Mettler Toledo) with Coulomat AG and CG reagents (Hydranal). A small amount of powders of $[P_{4,4,4,4}]CF_3COO$ was dissolved in dehydrated methanol which was determined water content beforehand. Water content of dried $[P_{4,4,4,4}]CF_3COO$ was smaller than 200 ppm.

Neat $[P_{4,4,4,4}]CF_3COO$ was put in a cold store chamber. Preparation of mixtures were performed after drying as soon as possible. First we mixed $[P_{4,4,4,4}]CF_3COO$ and water at x_{IL}= 0.07. Then the sample aqueous solutions was obtained by attenuation of the initial mixture. The mixture with too much high concentration need care for moisture absorption. Aqueous solutions of $[P_{4,4,4,4}]CF_3COO$ were stirred for 1 h and kept in a cool place because their phase separation points are near room temperature.

B. Conditions of SAXS measurements

All SAXS measurement was performed at the station BL-6A, PF. Table B-1 shows the conditions of experiments.

Table B-1

Date	2 June 2014
Sample	aqueous solution of $[P_{4,4,4,4}]CF_3COO$
Temperature	293 K
Camera length	2037.67 mm
Exposure time	300 s

Date	20 October 2015
Sample	aqueous solution of $[P_{4,4,4,4}]CF_3COO$
Temperature	298 and 301 K
Camera length	2036.55 mm
Exposure time	300 s

C. SAXS profiles and their fitting curves

All SAXS raw data for aqueous solutions of $[P_{4,4,4,4}]CF_3COO$ and their fitting curves are shown in figures C-1 to 3. The vertical axis is scattering intensity, $I(0)$ in arbitrary unit. Three types of fitting curves, straight line, even function and the Ornstein-Zernike equation with constant term as shown in equation (C1) to (C3) were applied on the data.

$$I(s) = a + bs, \tag{C1}$$

$$I(s) = c + ds^2 + es^4 + fs^6, \tag{C2}$$

$$I(s) = \frac{I(0)'}{1 + \xi^2 s^2} + \alpha. \tag{C3}$$

Equation (C1) was fitted on only the results of water. $I(0)$s were determined by applying equation (C3) near the critical point. Outside of this region, even functions, equation (C2), were fitted instead. These functions were applied on scattering intensity within $0.2 < s < 1.0$ nm^{-1}. The smaller edge of the region was determined based on the results of water. However, for the mixture of ionic liquid, unnecessary signals were obtained at smaller s region. Those signals were cut for fitting. One of the reasons is that the sample length which was determined based on absorption coefficient of water was wide for ionic liquid solutions. Table C-1 shows the used equations for fitting and the resulting absolute values of $I(0)$.

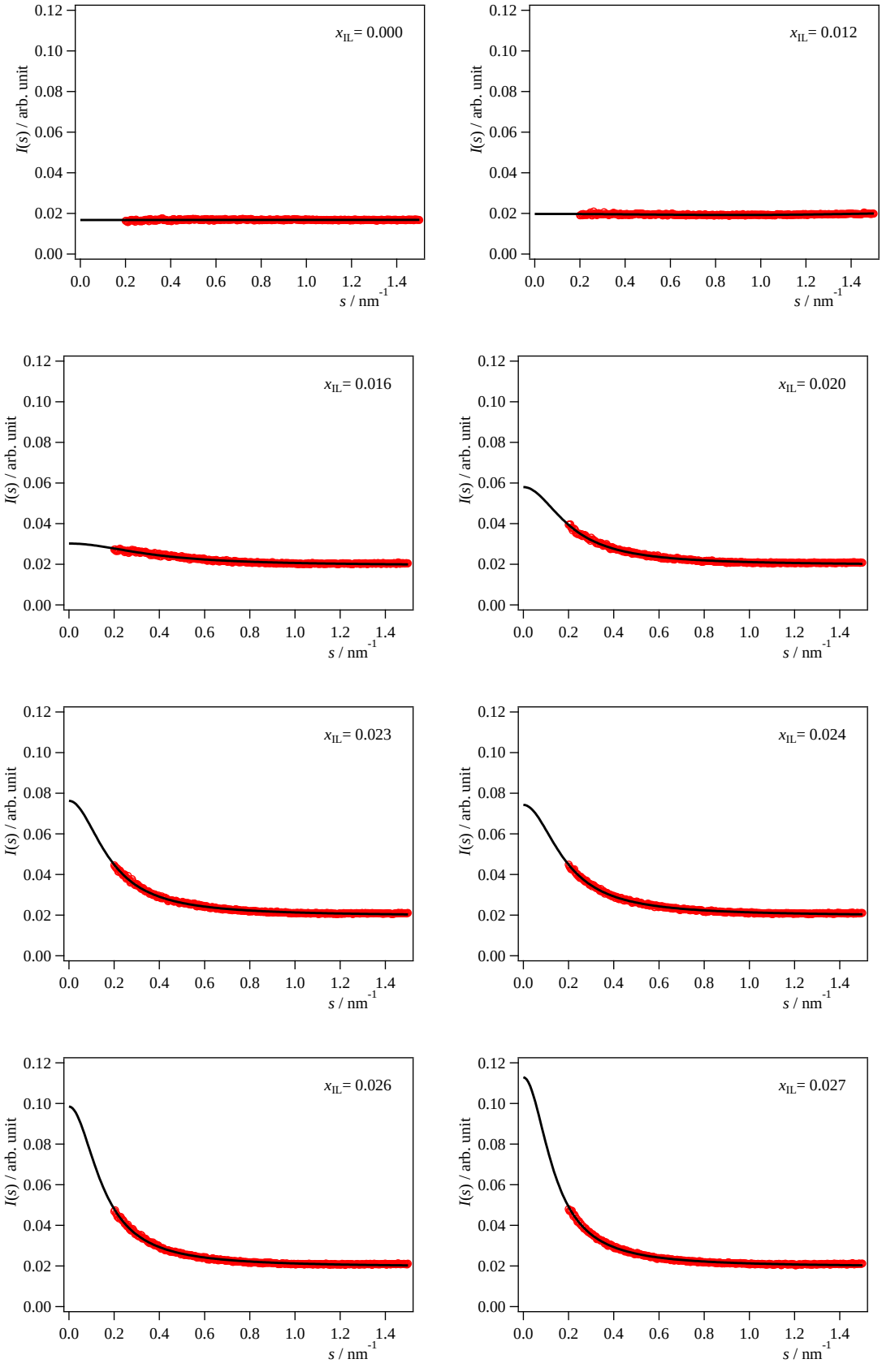
x_{IL}= 0.000
x_{IL}= 0.012
x_{IL}= 0.016
x_{IL}= 0.020
x_{IL}= 0.023
x_{IL}= 0.024
x_{IL}= 0.026
x_{IL}= 0.027
$I(s)$ / arb. unit
s / nm^{-1}
0.00
0.02
0.04
0.06
0.08
0.10
0.12
0.0
0.2
0.4
0.6
0.8
1.0
1.2
1.4

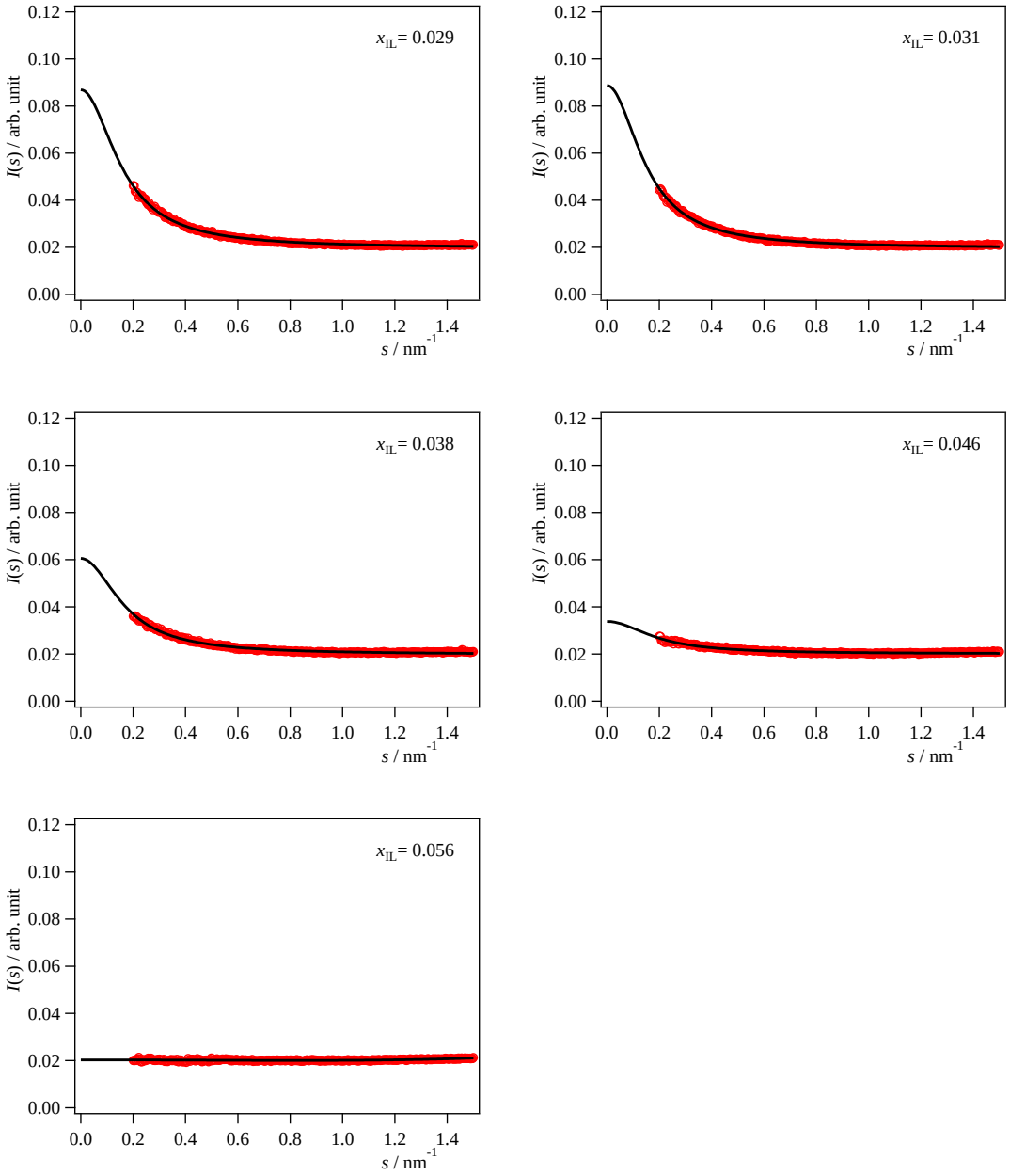

Figure C-1 SAXS raw data at 301 K. Black lines are the respective fitting functions. The equation numbers of used fitting functions were written below the concentrations.

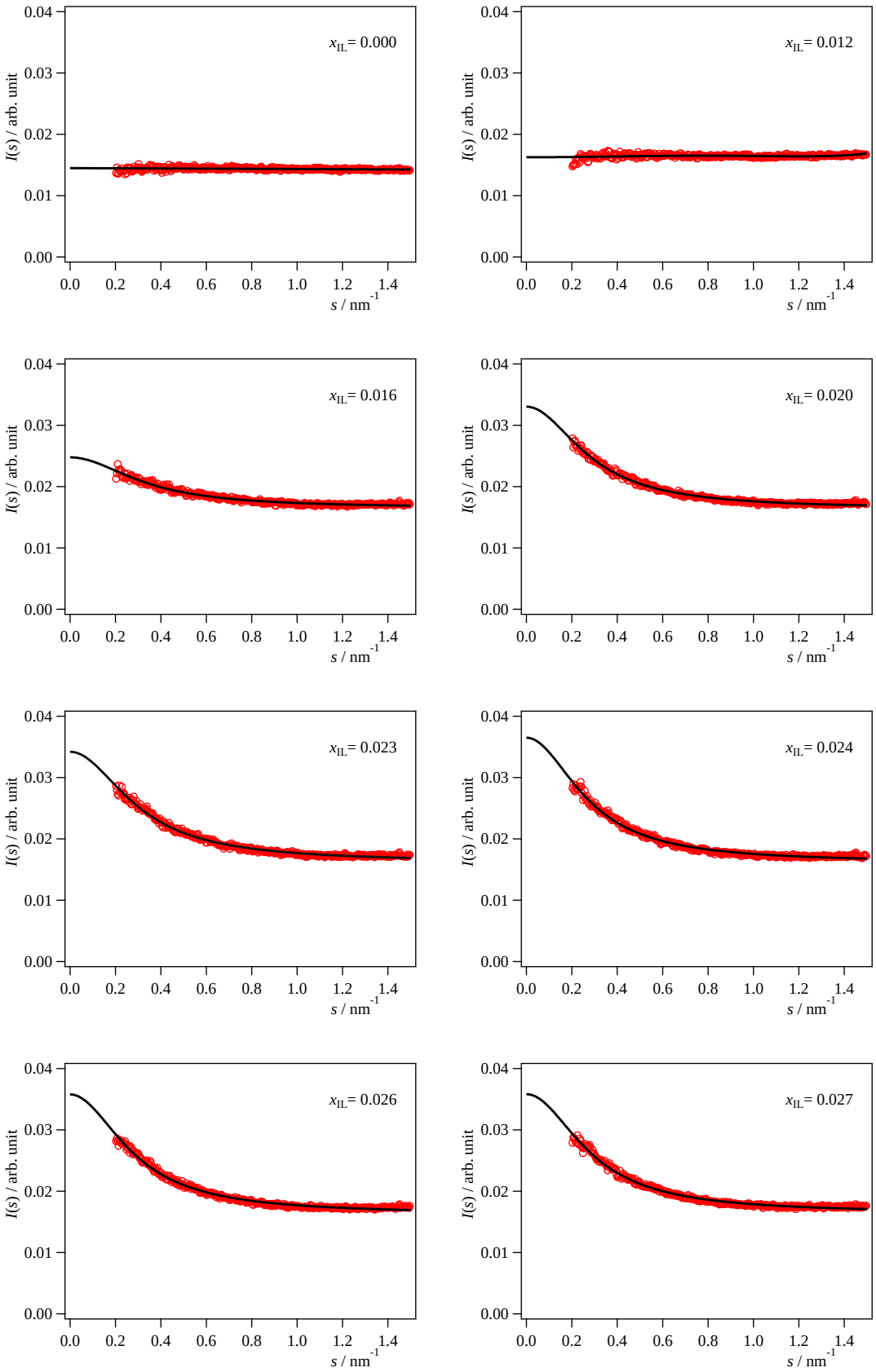
x_{IL}= 0.000
x_{IL}= 0.012
x_{IL}= 0.016
x_{IL}= 0.020
x_{IL}= 0.023
x_{IL}= 0.024
x_{IL}= 0.026
x_{IL}= 0.027
I(s) / arb. unit
s / nm^{-1}
0.00
0.01
0.02
0.03
0.04
0.0
0.2
0.4
0.6
0.8
1.0
1.2
1.4

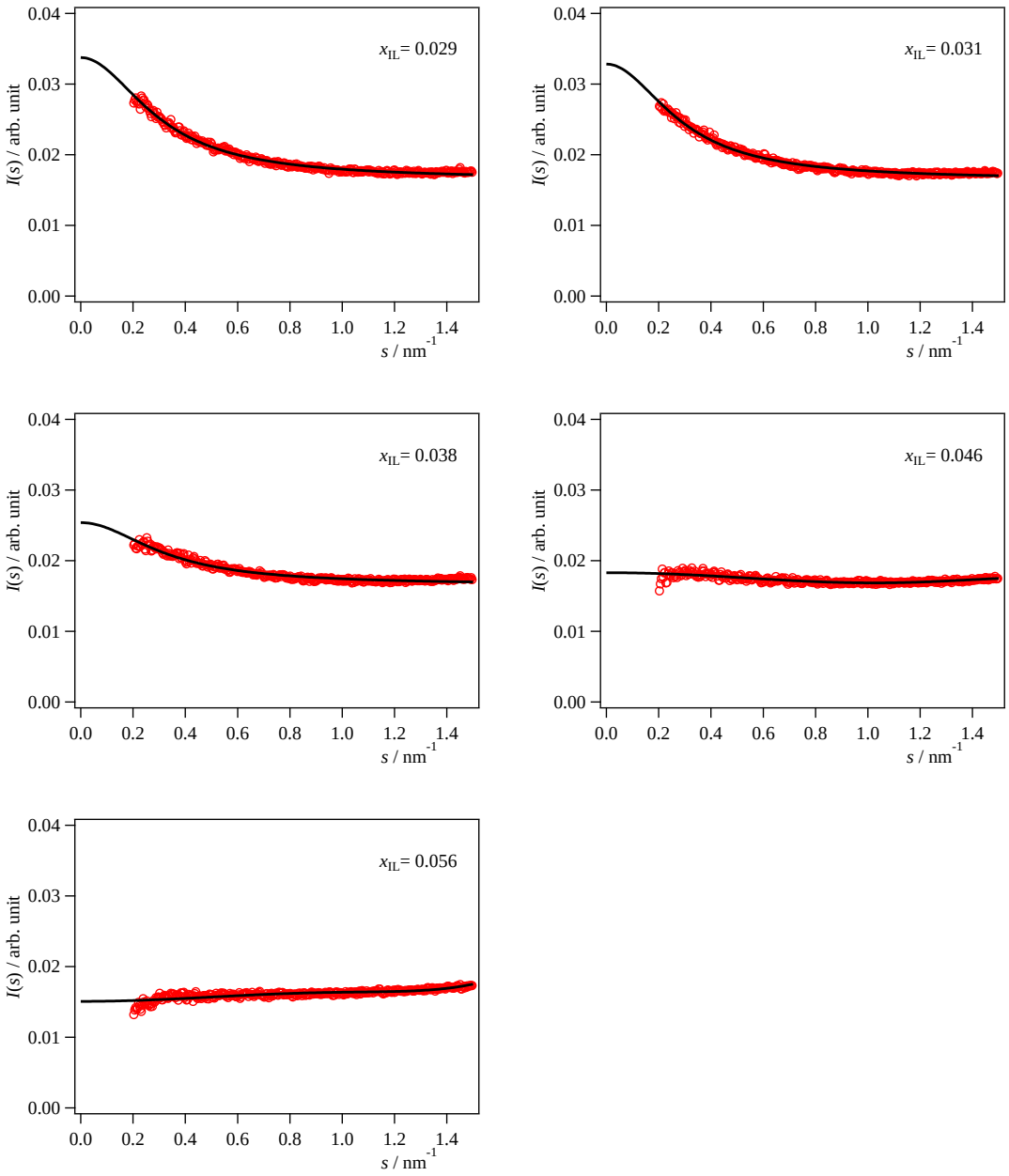

Figure C-2 SAXS raw data at 298 K. Black lines are the respective fitting functions. The equation numbers of used fitting functions were written below the concentrations.

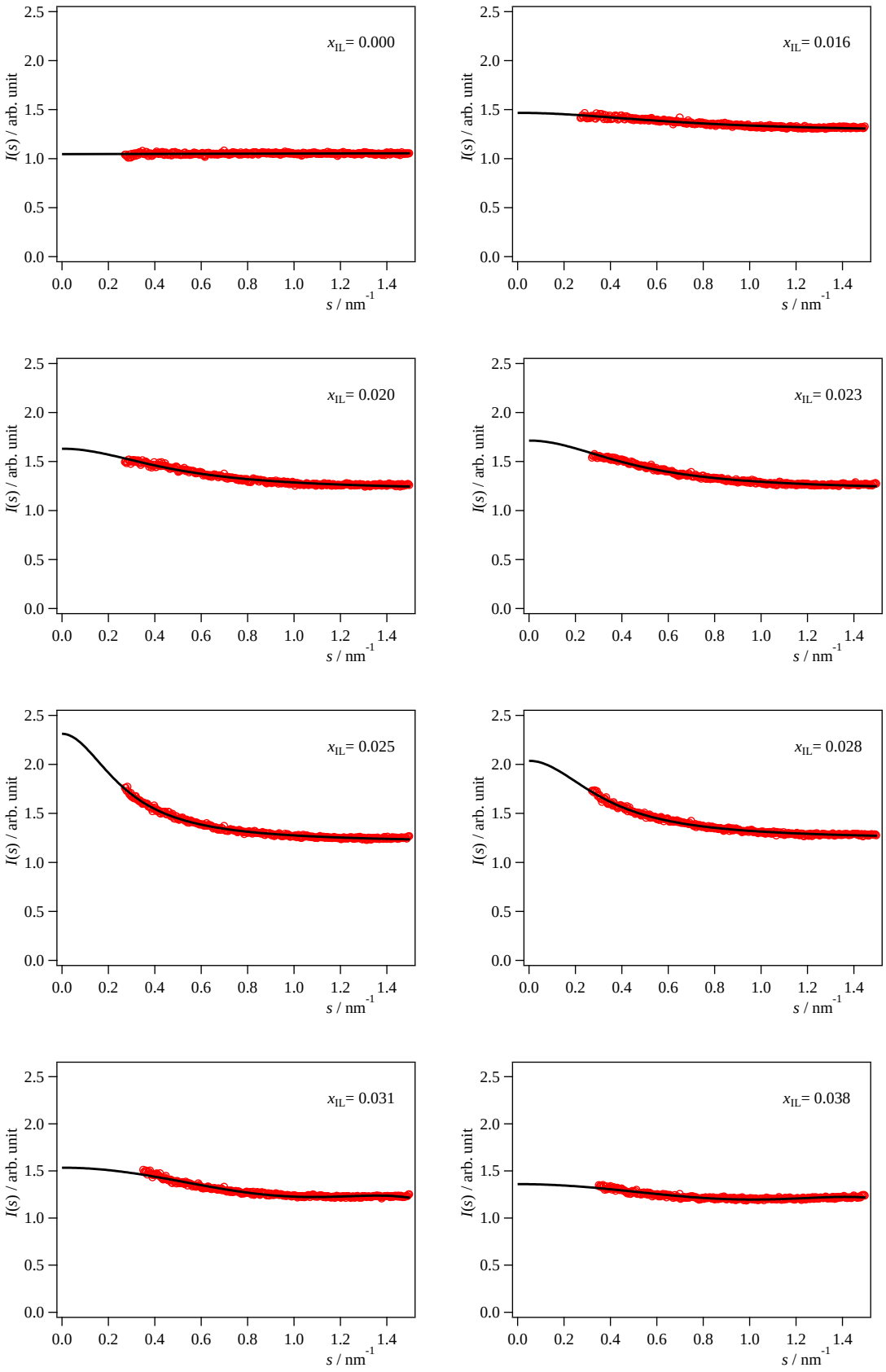
x_{IL}= 0.000
x_{IL}= 0.016
x_{IL}= 0.020
x_{IL}= 0.023
x_{IL}= 0.025
x_{IL}= 0.028
x_{IL}= 0.031
x_{IL}= 0.038
I(s) / arb. unit
s / nm^{-1}
0.0
0.5
1.0
1.5
2.0
2.5
0.2
0.4
0.6
0.8
1.2
1.4

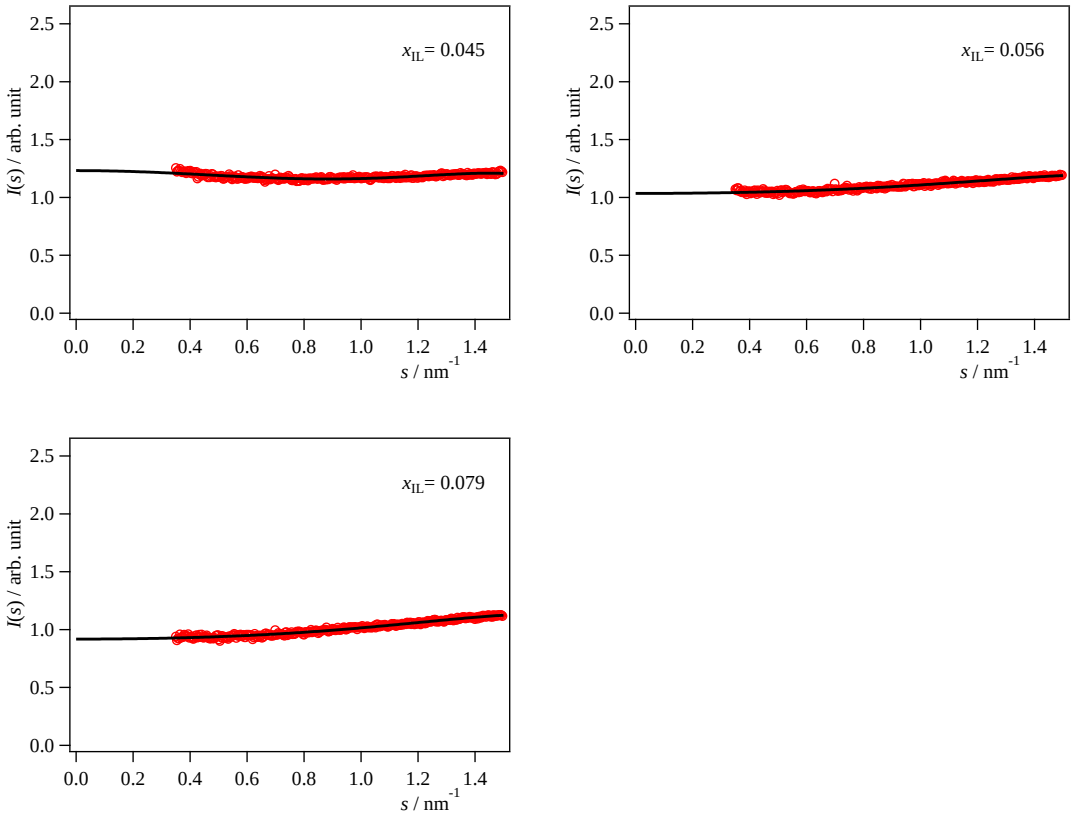

Figure C-3 SAXS raw data at 293 K. Black lines are the respective fitting functions. The equation numbers of used fitting functions were written below the concentrations.

Table C-1

x_{IL}	Equation	$I(0)$ / 10^{23} e.u. cm^{-3}	x_{IL}	Equation	$I(0)$ / 10^{23} e.u. cm^{-3}
301 K			298 K		
0.000	(C1)	2.07	0.000	(C1)	2.06
0.012	(C2)	2.05	0.012	(C2)	2.32
0.016	(C3)	3.72	0.016	(C3)	3.53
0.020	(C3)	7.15	0.020	(C3)	4.71
0.023	(C3)	9.40	0.023	(C3)	4.88
0.024	(C3)	9.15	0.024	(C3)	5.20
0.026	(C3)	12.14	0.026	(C3)	5.10
0.027	(C3)	13.91	0.027	(C3)	5.11
0.029	(C3)	10.71	0.029	(C3)	4.81
0.031	(C3)	10.94	0.031	(C3)	4.68
0.038	(C3)	7.46	0.038	(C3)	3.62
0.046	(C3)	4.17	0.046	(C2)	2.61
0.056	(C2)	2.58	0.056	(C2)	2.15
293 K					
0.000	(C1)	2.06			
0.016	(C3)	2.54			
0.020	(C3)	3.22			
0.023	(C3)	3.38			
0.025	(C3)	4.57			
0.028	(C3)	4.02			
0.031	(C2)	3.03			
0.038	(C2)	2.68			
0.045	(C2)	2.43			
0.056	(C2)	2.04			
0.079	(C2)	1.81			

D. Details of high-pressure density meter

Pressure dependence of density for the aqueous solution of $[P_{4,4,4,4}]CF_3COO$ was measured using high-pressure density meter DMA HP (Anton Paar). The values were displayed on DMA 4500. The oscillating period of a Hastelloy U-tube was corrected by nitrogen gas and liquid water at each temperature and pressure. Nitrogen was injected by gas cylinder and liquids were by pump system shown in figure D-1. Pressure was monitored. Temperature was controlled by cooling water and monitored by pressure gage.

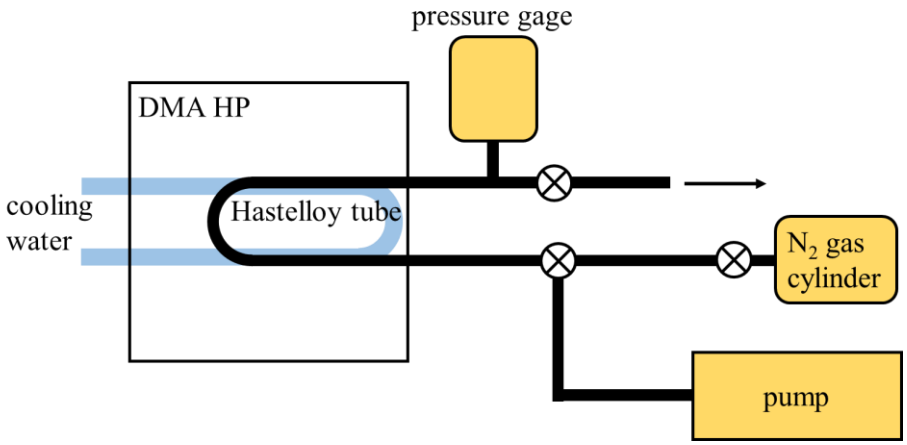

Figure D-1 Layout of liquid and gas injection system.

Table D-1 shows the measured oscillating periods of nitrogen and water at 293 and 301 K. Their values of density data sets are referred to the NIST data base [136]. Both measurements with pressure increasing direction and that with decreasing direction showed the same value. To determine the value at 0.1 MPa carefully, the measurements were performed with increasing pressure. Table D-2 shows apparatus constants A and B as equation (39).

Table D-1

p / MPa	Period / μs		Density / g cm^{-3}	
	N_2	water	N_2	water
293 K				
0.1	2485.23	2690.47	0.001147	0.99799
1.0	2487.44	2690.57	0.011486	0.99841
2.0	2489.92	2690.69	0.023010	0.99886
3.0	2492.40	2690.81	0.034555	0.99931

4.0	2494.88	2690.92	0.046104	0.99977
5.0	2497.36	2691.03	0.057638	1.0002
6.0	2499.82	2691.16	0.069141	1.0007
7.0	2502.27	2691.27	0.080593	1.0011
301 K				
0.1	2488.90	2692.60	0.001119	0.99624
1.0	2491.09	2692.71	0.011205	0.99664
2.0	2493.47	2692.82	0.022433	0.99708
3.0	2495.87	2692.93	0.033670	0.99753
4.0	2498.27	2693.05	0.044900	0.99797
5.0	2500.61	2693.18	0.056106	0.99842
6.0	2503.02	2693.27	0.067272	0.99886
7.0	2505.41	2693.37	0.078382	0.99930
8.0	2507.82	2693.49	0.089421	0.99974
9.0	2510.12	2693.60	0.10037	1.00018
10.0	2512.45	2693.69	0.11122	1.00062
11.0	2514.72	2693.81	0.12195	1.00105
12.0	2517.00	2693.93	0.13256	1.00149

Table D-2

p / MPa	A	B	p / MPa	A	B
293 K			301 K		
0.1	9.3842	-5.7949	0.1	9.4282	-5.8393
1.0	9.3831	-5.7942	1.0	9.4286	-5.8397
2.0	9.3822	-5.7937	2.0	9.4271	-5.8387
3.0	9.3811	-5.7931	3.0	9.4264	-5.8384
4.0	9.3807	-5.7929	4.0	9.4255	-5.8379
5.0	9.3803	-5.7927	5.0	9.4215	-5.8352
6.0	9.3790	-5.7919	6.0	9.4233	-5.8365
7.0	9.3778	-5.7912	7.0	9.4244	-5.8374
			8.0	9.4262	-5.8389
			9.0	9.4243	-5.8376
			10.0	9.4260	-5.8388
			11.0	9.4244	-5.8379
			12.0	9.4247	-5.8383

E. Concentration dependence of density

Concentration dependence of density for the aqueous solution of $[P_{4,4,4,4}]CF_3COO$ at 293, 298 and 301 K measured by the vibration tube density meter, DMA 4500 and DMA 4100 (Anton Paar). The accuracy of temperature is ±0.03 ºC and that of density is ±0.00005 g cm^{-3} for DMA 4500. For DMA 4100, temperature is ±0.05 ºC and density is ±0.0001 g cm^{-3}. The glass tubes were cleaned by pure water, methanol and acetone to remove ionic liquid before each measurement. After drying with air, check the density value of air at 20 ºC.

Table E-1 shows the raw density data at 293, 298 and 301 K using DMA 4500. Table E-2 shows those using DMA 4100. Both results showed good agreement.

Table E-1

x_{IL}	Molar mass	Density / g cm^{-3}		
		293 K	298 K	301 K
0.000000	18.020	0.99820	0.99704	0.99623
0.002402	18.871	1.00176	1.00042	0.99950
0.004862	19.743	1.00534	1.00376	1.00270
0.007505	20.680	1.00875	1.00683	1.00558
0.010038	21.578	1.01135	1.00915	1.00775
0.012579	22.479	1.01352	1.01111	1.00960
0.015910	23.659	1.01592	1.01330	1.01166
0.022918	26.143	1.02000	1.01703	1.01520
0.024982	26.874	1.02099	1.01796	1.01608
0.028066	27.967	1.02241	1.01927	1.01733
0.032179	29.425	1.02404	1.02079	1.01879
0.038260	31.580	1.02616	1.02278	1.02070
0.045182	34.034	1.02811	1.02461	1.02248
0.077637	45.537	1.03390	1.03013	1.02786

Table E-2

x_{IL}	Molar mass	Density / g cm^{-3}		
		293 K	298 K	301 K
0.000000	18.020	0.9983	0.9971	0.9963
0.001004	18.376	0.9998	0.9985	0.9977
0.002218	18.806	1.0016	1.0003	0.9994
0.002872	19.038	1.0025	1.0012	1.0002
0.003905	19.404	1.0041	1.0026	1.0016
0.004175	19.500	1.0044	1.0030	1.0019
0.004986	19.787	1.0056	1.0040	1.0030
0.005443	19.949	1.0062	1.0046	1.0035
0.006039	20.160	1.0070	1.0053	1.0042
0.006721	20.402	1.0078	1.0060	1.0048
0.007482	20.672	1.0088	1.0069	1.0057
0.008803	21.140	1.0102	1.0082	1.0069
0.009859	21.515	1.0112	1.0091	1.0077
0.010878	21.876	1.0122	1.0099	1.0085
0.011959	22.259	1.0131	1.0107	1.0093
0.012876	22.584	1.0138	1.0114	1.0099
0.013941	22.961	1.0146	1.0121	1.0106
0.015102	23.373	1.0154	1.0129	1.0113
0.016013	23.696	1.0161	1.0135	1.0118
0.019455	24.916	1.0182	1.0154	1.0136
0.023012	26.176	1.0201	1.0172	1.0153
0.023825	26.464	1.0205	1.0175	1.0157
0.025274	26.978	1.0212	1.0182	1.0163
0.025973	27.226	1.0215	1.0185	1.0166
0.026857	27.539	1.0219	1.0188	1.0169
0.028139	27.994	1.0226	1.0195	1.0176
0.031195	29.077	1.0237	1.0205	1.0185
0.037292	31.238	1.0259	1.0226	1.0205
0.044608	33.831	1.0280	1.0246	1.0225
0.056365	37.998	1.0310	1.0274	1.0252
0.064871	41.013	1.0322	1.0285	1.0263
0.079021	46.028	1.0341	1.0304	1.0281

F. Differentiation by graphical curve fitting with a flexible ruler

To differentiate apparent excess molar volumes, we draw a smooth curve using a flexible ruler. Redlich-Kister polynomial [137] is known as one of the famous fitting functions of excess quantities for binary systems as,

$$V_{\mathrm{m}}^{\mathrm{E}}(x) = x(1-x)\sum_{\mathrm{i}=0}^{\mathrm{n}} A_{\mathrm{i}}(2x-1)^{\mathrm{i}}, \qquad \text{(F1)}$$

where x is mole fraction of a component, A_{i} are the polynomial coefficients and n is the polynomial degree. For this system, equation (F1) was not suitable at low concentration region as shown in figure F-1. Accurate fitting curve is important at such low concentration region for the differential thermos dynamics.

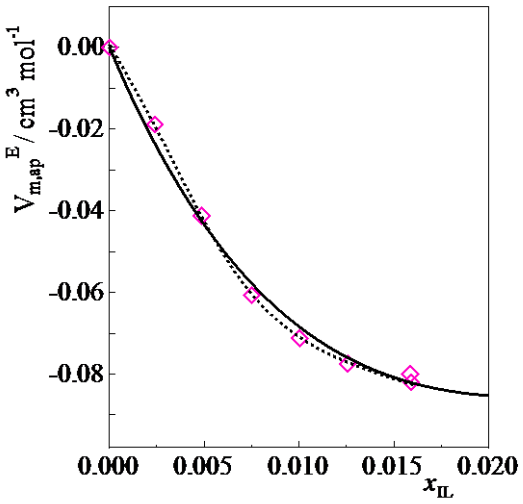

Figure F-1 Smooth curve fitted on the measured apparent excess partial molar volume, $V_{\mathrm{m}}^{\mathrm{E,ap}}$, at 298 K. the solid line was obtained by Redlich-Kister polynomial and the dotted line is drawn using a flexible ruler.

Numerical differentiation as equation (68) is the best method because it reflects experimental fact well without any assumptions. However, for the apparent excess molar volume, their value was too small and the experimental error was too large. And for partial molar enthalpy, the number of measured points was few. Because of them, the numerical differentiation was inappropriate.

G. Differentiation of volume with respect to mole fraction

Raw density data shown in Appendix E were converted to molar volume, V_m. Then using the two data point at x_{IL}= 0.000 and 0.079 in table D-2, the apparent excess molar volume, $V^E_{m,ap}$, was calculated. Figure G-1 shows $v^E_{m,ap}$ at 293 and 301 and their fitting curves drawn by a flexible ruler. At x_{IL}> 0.05, the volumetric ratio of $[P_{4,4,4,4}]CF_3COO$ is larger than that of water and $[P_{4,4,4,4}]CF_3COO$ ion pairs occupy the volume of aqueous solution. Then, the molar volume of the mixture of $[P_{4,4,4,4}]CF_3COO$ and water increased almost linearly and, at high concentration region, there were larger error as seen in the figure. Table G-1 shows the values of resulting partial molar volumes of $[P_{4,4,4,4}]CF_3COO$, v_{IL}, and water, v_W.

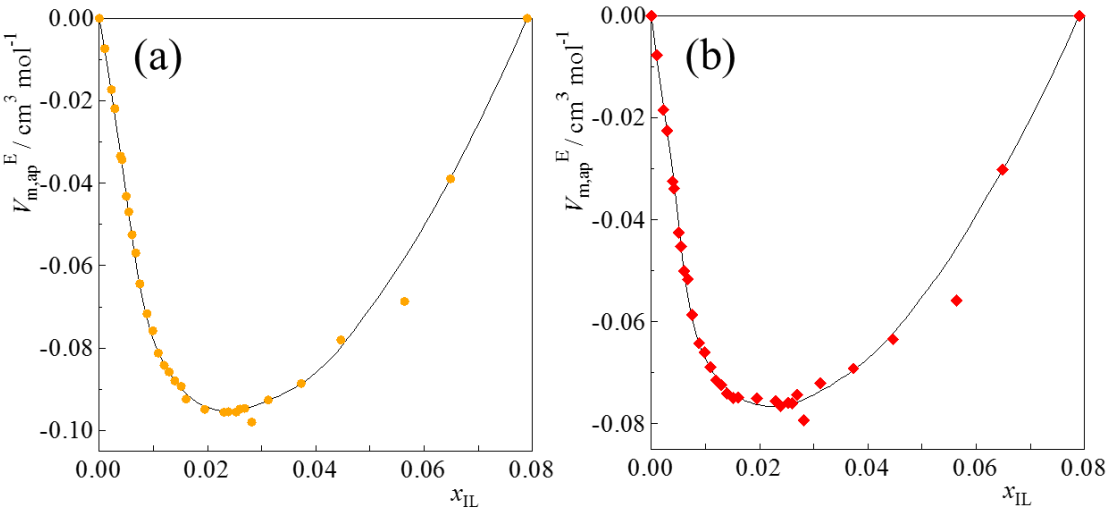

Figure G-1 The apparent excess molar volume of the aqueous solution of $[P_{4,4,4,4}]CF_3COO$, $V^E_{m,ap}$, at (a)293 and (b)301 K against x_{IL}. The solid lines are fitting curves drawn with a flexible ruler.

Table G-1

x_{IL}	v_{IL} / cm^3 mol^{-1}			v_W / cm^3 mol^{-1}		
	293 K	298 K	301 K	293 K	298 K	301 K
0.002	344.50	346.29	347.98	18.05	18.07	18.07
0.004	343.75	345.84	347.26	18.05	18.07	18.08
0.006	344.24	347.16	348.18	18.05	18.07	18.07
0.008	346.53	349.67	351.38	18.03	18.05	18.05
0.010	348.93	351.62	353.37	18.01	18.03	18.03
0.012	350.32	352.71	354.23	18.00	18.02	18.02
0.014	351.06	353.28	354.82	17.99	18.01	18.01
0.016	351.57	353.67	355.07	17.98	18.01	18.01
0.018	351.99	353.99	355.19	17.97	18.00	18.01
0.020	352.31	354.26	355.46	17.97	18.00	18.00
0.024	352.85	354.65	355.83	17.95	17.99	17.99
0.028	353.19	354.99	356.10	17.95	17.98	17.99
0.032	353.36	355.19	356.29	17.94	17.97	17.98
0.036	353.53	355.33	356.39	17.93	17.97	17.98
0.040	353.89	355.57	356.58	17.92	17.96	17.97
0.044	354.27	355.86	356.82	17.90	17.94	17.96
0.048	354.51	356.17	357.01	17.89	17.93	17.95
0.052	354.61	356.24	357.06	17.89	17.93	17.95
0.056	354.75	356.43	357.27	17.88	17.92	17.93
0.060	354.96	356.53	357.46	17.87	17.91	17.92
0.064	355.12	356.50	357.39	17.85	17.91	17.93
0.068	355.29	356.62	357.60	17.84	17.90	17.91
0.072	355.43	356.76	357.72	17.83	17.89	17.90
0.076	355.57	356.81	357.92	17.82	17.89	17.89

To obtain the third derivative quantity, smooth curves drawn again on apparent excess partial molar volumes of $[P_{4,4,4,4}]CF_3COO$, $v^{E}_{IL,ap}$. Figure G-2 shows $v^{E}_{IL,ap}$ at 293 and 301 and their fitting curves by the same manner. And table G-2 shows the values of calculated the third derivative quantity in terms of volume or volumetric interaction among $[P_{4,4,4,4}]CF_3COO$, v^{E}_{IL-IL}.

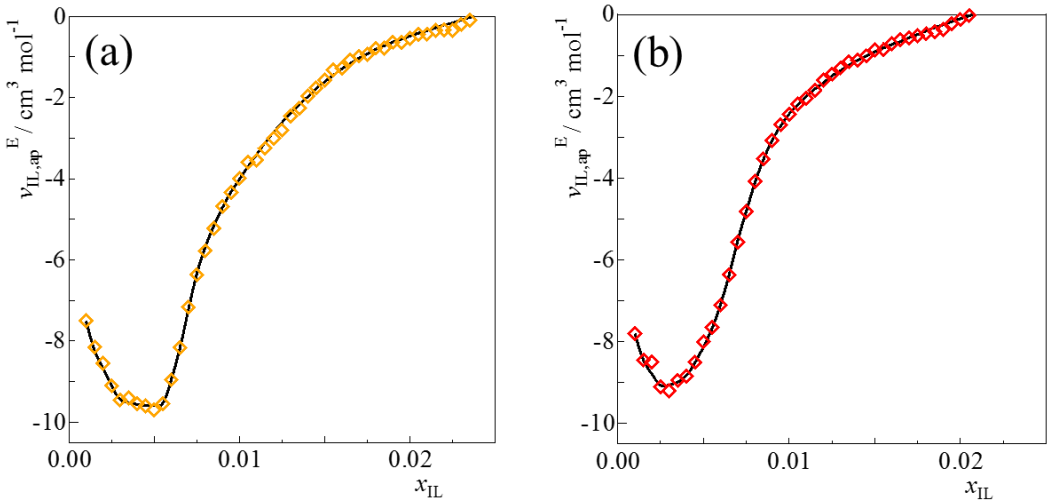

Figure G-2 Excess partial molar volumes of $[P_{4,4,4,4}]CF_3COO$, $v^{E}_{IL,ap}$, in dilute region at (a)293 and (b)301 K. The solid lines are the fitting curve drawn with a flexible ruler.

Table G-2

x_{IL}	$v^{\mathrm{E}}_{\mathrm{IL-IL}}$			x_{IL}	$v^{\mathrm{E}}_{\mathrm{IL-IL}}$		
	293 K	298 K	301 K		293 K	298 K	301 K
0.0015	-1046.73	-1196.35	-697.75	0.0155	315.04	206.75	177.21
0.0020	-946.28	-946.38	-647.73	0.0160	285.36	196.80	157.44
0.0025	-895.71	-600.89	-699.65	0.0165	255.71	186.87	157.36
0.0030	-298.45	-53.09	47.31	0.0170	235.92	186.77	167.11
0.0035	-99.50	199.30	368.70	0.0175	216.15	176.85	167.03
0.0040	-198.20	249.00	527.88	0.0180	196.40	166.94	166.94
0.0045	-153.61	497.75	696.85	0.0185	176.67	157.04	147.23
0.0050	64.87	855.70	835.80	0.0190	156.96	137.34	147.15
0.0055	745.87	1193.40	1034.28	0.0195	147.08	127.47	147.08
0.0060	1341.90	1500.94	1312.08	0.0200	147.00	127.40	137.20
0.0065	1698.89	1549.86	1549.86	0.0205	127.34	97.95	127.34
0.0070	1827.12	1439.85	1539.15	0.0210	127.27	97.90	117.48
0.0075	1558.23	1379.58	1399.43	0.0215	136.99	107.64	97.85
0.0080	1170.56	1259.84	1249.92	0.0220	117.36	107.58	78.24
0.0085	951.84	1021.25	1031.16	0.0225	117.30	107.53	68.43
0.0090	822.53	792.80	812.62	0.0230	127.01	107.47	48.85
0.0095	693.35	663.63	643.82	0.0235	117.18	107.42	39.06
0.0100	623.70	534.60	514.80	0.0240	126.88	107.36	58.56
0.0105	603.59	435.38	425.49	0.0245	126.82	97.55	58.53
0.0110	583.51	405.49	385.71	0.0250	107.25	97.50	29.25
0.0115	543.67	375.63	326.21	0.0255	107.20	87.70	19.49
0.0120	494.00	326.04	316.16	0.0260	107.14	87.66	19.48
0.0125	464.13	306.13	296.25	0.0265	107.09	97.35	19.47
0.0130	434.28	296.10	256.62	0.0270	107.03	97.30	9.73
0.0135	394.60	266.36	246.63	0.0275	116.70	97.25	0.00
0.0140	384.54	246.50	216.92	0.0280	126.36	97.20	0.00
0.0145	364.64	236.52	206.96	0.0285	116.58	97.15	9.71
0.0150	325.05	216.70	197.00	0.0290	116.52	87.39	9.71

H. Determination of isothermal compressibility

Table H-1 shows the oscillation periods measured with the high pressure density meter, DMA HP, at 293 K and 301 K. These data were converted into density using the apparatus constants A and B shown in Appendix D.

Table H-1

p / MPa	Period / μs				
293 K					
$x_{\mathrm{IL}} =$	0.016	0.02	0.023	0.025	0.028
0.1	2693.73	2694.24	2694.5	2694.77	2694.99
1.0	2693.84	2694.35	2694.6100	2694.87	2695.1
2.0	2693.95	2694.46	2694.7000	2694.99	2695.22
3.0	2694.06	2694.57	2694.8200	2695.1	2695.33
4.0	2694.17	2694.68	2694.9400	2695.21	2695.44
5.0	2694.28	2694.79	2695.0500	2695.32	2695.55
6.0	2694.39	2694.91	2695.1700	2695.43	2695.66
7.0	2694.50	2695.02	2695.2800	2695.54	2695.77
$x_{\mathrm{IL}} =$	0.031	0.038	0.045	0.056	0.079
0.1	2695.25	2695.72	2696.16	2696.74	2697.17
1.0	2695.36	2695.83	2696.27	2696.86	2697.28
2.0	2695.48	2695.95	2696.39	2696.97	2697.4
3.0	2695.59	2696.06	2696.5	2697.09	2697.51
4.0	2695.69	2696.18	2696.62	2697.22	2697.63
5.0	2695.81	2696.29	2696.72	2697.32	2697.74
6.0	2695.91	2696.4	2696.84	2697.42	2697.85
7.0	2696.02	2696.51	2696.95	2697.54	2697.97
301 K					
$x_{\mathrm{IL}} =$	0.016	0.02	0.023	0.025	0.028
0.1	2695.65	2696.06	2696.28	2696.49	2696.73
1.0	2695.76	2696.17	2696.40	2696.60	2696.84
2.0	2695.87	2696.28	2696.52	2696.72	2696.95
3.0	2695.98	2696.39	2696.63	2696.83	2697.07
4.0	2696.09	2696.50	2696.74	2696.94	2697.18

5.0	2696.20	2696.62	2696.86	2697.06	2697.30
6.0	2696.32	2696.73	2696.98	2697.17	2697.41
7.0	2696.42	2696.84	2697.08	2697.28	2697.52
8.0	2696.52	2696.95	2697.19	2697.39	2697.64
9.0	2696.63	2697.06	2697.30	2697.50	2697.75
10.0	2696.74	2697.17	2697.41	2697.61	2697.86
11.0	2696.85	2697.28	2697.53	2697.72	2697.97
12.0	2696.97	2697.39	2697.65	2697.83	2698.08
$x_{\mathrm{IL}} =$	0.031	0.038	0.045	0.056	0.079
0.1	2696.97	2697.37	2697.71	2698.17	2698.82
1.0	2697.08	2697.48	2697.83	2698.28	2698.94
2.0	2697.19	2697.60	2697.95	2698.40	2699.05
3.0	2697.30	2697.71	2698.06	2698.53	2699.16
4.0	2697.41	2697.82	2698.17	2698.63	2699.29
5.0	2697.53	2697.93	2698.28	2698.75	2699.41
6.0	2697.64	2698.05	2698.39	2698.86	2699.52
7.0	2697.76	2698.16	2698.51	2698.97	2699.64
8.0	2697.87	2698.28	2698.62	2699.09	2699.75
9.0	2697.98	2698.39	2698.74	2699.20	2699.87
10.0	2698.09	2698.51	2698.85	2699.31	2699.99
11.0	2698.20	2698.64	2698.98	2699.42	2700.10
12.0	2698.32	2698.73	2699.08	2699.54	2700.22

Table H-2

x_{IL}	κ_T / 10^{-4} MPa^{-1}		x_{IL}	κ_T / 10^{-4} MPa^{-1}	
	293 K	298 K		293 K	298 K
0.000	4.5825	4.4840	0.028	4.2193	4.4665
0.016	4.1750	4.3004	0.031	4.1368	4.4378
0.020	4.2369	4.3849	0.038	4.2948	4.5112
0.023	4.2723	4.4712	0.045	4.2678	4.4897
0.025	4.1842	4.4033	0.056	4.3071	4.4722
			0.079	4.3027	4.6009

I. Fluctuations of the aqueous solution of $[P_{4,4,4,4}]CF_3COO$

The fluctuations of the aqueous solution of $[P_{4,4,4,4}]CF_3COO$ was obtained by SAXS method at 293, 298 and 301 K. Table I-1 shows the calculated values of density fluctuation, $\langle(\Delta N)^2\rangle/\bar{N}$, concentration fluctuation, $\bar{N}\langle(\Delta x)^2\rangle$, and their cross term, $\langle\Delta N\Delta x\rangle$, from combination of forward scattering intensities, $I(0)$, partial molar volumes and isothermal compressibilies.

Table I-1

x_{IL}	$\bar{N}\langle(\Delta x)^2\rangle$	$\frac{\langle(\Delta N)^2\rangle}{\bar{N}}$	$\langle\Delta N\Delta x\rangle$	x_{IL}	$\bar{N}\langle(\Delta x)^2\rangle$	$\frac{\langle(\Delta N)^2\rangle}{\bar{N}}$	$\langle\Delta N\Delta x\rangle$
301 K				298 K			
0.016	0.47	97.10	-6.74	0.012	0.04	10.19	-0.67
0.020	1.92	357.91	-26.25	0.016	0.32	65.74	-4.57
0.023	3.45	593.11	-45.24	0.020	0.79	145.79	-10.71
0.024	3.60	603.23	-46.60	0.023	1.04	178.23	-13.62
0.026	5.80	924.60	-73.25	0.024	1.24	206.31	-15.97
0.027	7.38	1148.02	-92.07	0.026	1.37	217.60	-17.27
0.029	6.11	905.29	-74.39	0.027	1.48	228.82	-18.39
0.031	6.89	972.75	-81.87	0.029	1.52	224.15	-18.45
0.038	6.06	730.80	-66.57	0.031	1.60	224.98	-18.96
0.046	3.88	395.91	-39.18	0.038	1.38	166.44	-15.18
0.056	1.43	120.75	-13.14	0.046	0.83	85.04	-8.42
				0.056	0.15	12.78	-1.39
293 K							
0.016	0.09	19.37	-1.35				
0.020	0.28	51.72	-3.81				
0.023	0.40	68.11	-5.22				
0.025	0.84	136.59	-10.73				
0.028	0.81	121.15	-9.87				
0.031	0.48	67.66	-5.71				
0.038	0.48	57.52	-5.25				
0.045	0.50	51.83	-5.09				
0.056	0.08	6.44	-0.70				

J. Individual density fluctuations

Table J-1 shows the Kirkwood-Buff parameters, $G_{\mathrm{IL-IL}}$, $G_{\mathrm{W-W}}$ and $G_{\mathrm{IL-W}}$, individual fluctuations of $[P_{4,4,4,4}]CF_3COO$, $\langle(\Delta N_{\mathrm{IL}})^2\rangle/\overline{N_{\mathrm{IL}}}$, those of water, $\langle(\Delta N_{\mathrm{W}})^2\rangle/\overline{N_{\mathrm{W}}}$, and the cross term of individual fluctuations, $\langle\Delta N_{\mathrm{IL}}\Delta N_{\mathrm{W}}\rangle/\overline{N_{\mathrm{IL}}}$, at 293, 298 and 301 K. The units of the Kirkwood-Buff parameters are cm^3 $molecule^{-1}$.

Table J-1

x_{IL}	$G_{\mathrm{IL-IL}}$	$G_{\mathrm{W-W}}$	$G_{\mathrm{IL-W}}$	$\frac{\langle(\Delta N_{\mathrm{IL}})^2\rangle}{\overline{N_{\mathrm{IL}}}}$	$\frac{\langle(\Delta N_{\mathrm{W}})^2\rangle}{\overline{N_{\mathrm{W}}}}$	$\frac{\langle\Delta N_{\mathrm{IL}}\Delta N_{\mathrm{W}}\rangle}{\overline{N_{\mathrm{IL}}}}$
301 K						
0.016	39646	4287	18727	17.31	109.49	473.95
0.020	102627	16961	63544	50.91	405.21	1514.33
0.023	134374	29463	101028	73.20	673.48	2305.90
0.024	127001	30420	101626	71.29	685.64	2287.23
0.026	170664	48046	152913	100.75	1053.02	3348.19
0.027	199136	60544	188403	120.36	1308.76	4069.50
0.029	138931	49123	146668	88.27	1034.11	3084.60
0.031	133757	54289	156040	88.68	1113.43	3197.43
0.038	71728	44809	115133	54.21	842.46	2162.06
0.046	28035	26816	62305	24.14	460.11	1066.74
0.056	5503	9149	19289	6.02	141.78	296.81
298 K						
0.012	4421	387	2248	2.45	11.45	60.70
0.016	26241	2886	12686	11.82	74.16	321.55
0.020	40786	6874	25878	20.87	165.11	617.79
0.023	39249	8809	30342	22.13	202.44	693.86
0.024	42440	10358	34738	24.53	234.56	783.33
0.026	39019	11254	35963	23.85	247.89	788.93
0.027	38517	12012	37527	24.13	260.94	812.10
0.029	33333	12107	36285	21.98	256.11	764.59
0.031	29877	12499	36061	20.62	257.59	740.27
0.038	15345	10146	26188	12.41	191.92	492.80
0.046	5081	5703	13360	5.20	98.85	229.22
0.056	-394	908	2036	0.64	15.01	31.40

301 K						
0.016	6074	821	3734	3.51	21.86	94.89
0.020	13227	2406	9171	7.46	58.59	219.52
0.023	13923	3331	11580	8.52	77.39	265.55
0.025	25682	6928	22743	15.69	155.50	507.23
0.028	18469	6412	19699	12.40	138.34	421.91
0.031	7960	3714	10823	6.24	77.49	222.88
0.038	4443	3461	9029	4.31	66.34	170.45
0.045	2756	3400	8115	3.26	60.20	141.27
0.056	-736	424	1021	0.32	7.56	15.80

K. Details of the handmade isothermal titration calorimeter

The excess partial molar enthalpy was measured using a handmade isothermal titration calorimeter of a design similar to an LKB Bromma 8700 calorimetry system. [125] Figure K-1 shows a sketch of the sample cell and figure K-2 shows a schematic diagram of the electrical circuity. The sample cell was set in a metallic container and then, the container was put in 25 ºC water bath. Temperature was controlled within ±0.02 ºC.

The volume of initial base solvent in the sample cell was about 50 cm^3. The titrant was injected into the sample cell by a syringe pump system (CX07100, ISIS Co.) with 25 mL gas-tight syringe (1025TLL, Hamilton). Temperature change following titration was monitored by a 2 kΩ thermistor. To convert the temperature change to energy, the sample mixture was heated with a known energy before and after titration. The energy input of heating was determined by using a standard resistance connected on series of the heater.

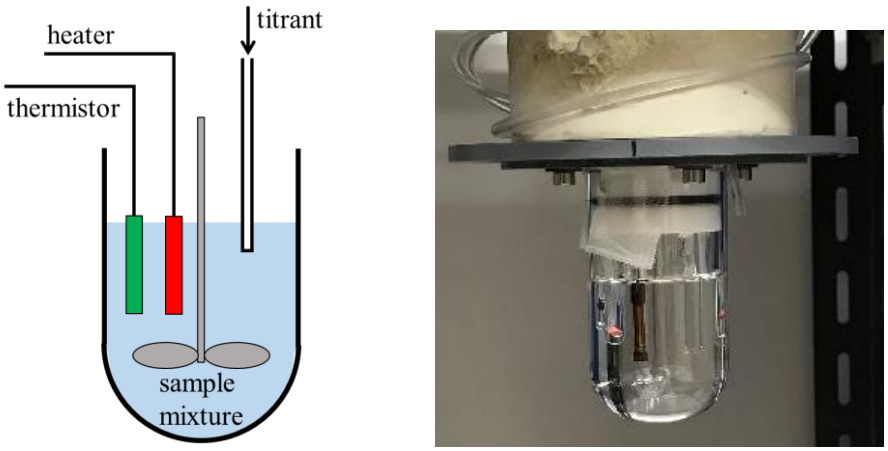

Figure K-1 A sketch and photo of the sample cell. The titrant was injected by the syringe pump system (CX07100, ISIS Co.) with 25 mL gas-tight syringe (1025TLL, Hamilton). The glass stirrer ensures mixing. To obtain energy change by titration, the temperature change at the titration was calibrated using the heating runs before and after the titration.

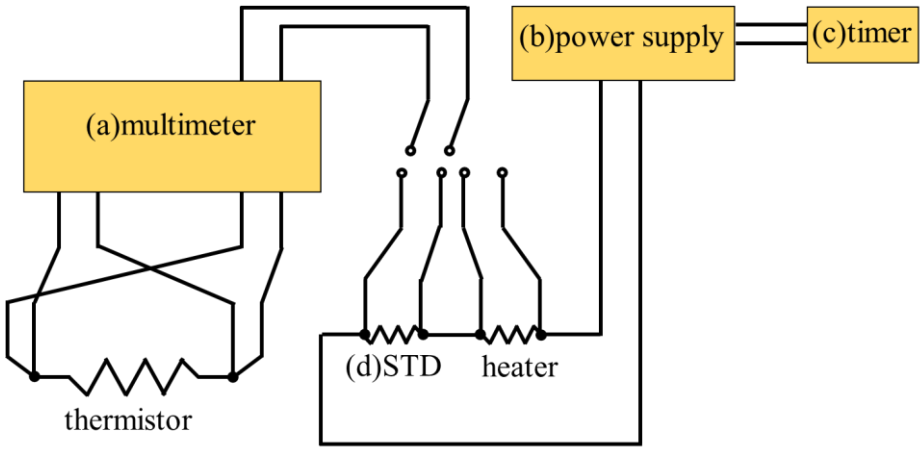

Figure K-2 The schematic diagram of the electric circuitry; (a)multimeter (HP34401A, Hewlett Packrd), (b)power supply (PA18-2A, TEXIO), (c)timer (Matsushita Electric Works) and (d)metallic foil resister with 99.991 Ω at 25 ºC (Alpha Electronics).

Figure K-3 shows the trace of the resistance of the thermistor as a function of time. The computer programs for data acquisition and analysis were written by J. Lai, Y. Koga and I. Lai.

Figure K-3 A photo displaying the time dependent of the value of thermistor. The first and third steps indicate the temperature traces by calibration heating before and after the titration. The second shows an exotherm by the titration.

L. Excess partial molar enthalpy of $[P_{4,4,4,4}]CF_3COO$

Excess partial molar enthalpy of $[P_{4,4,4,4}]CF_3COO$ was measured by the isothermal titration calorimetry mentioned in Appendix K. Because of the high melting point of the ionic liquid, an aqueous solution of $[P_{4,4,4,4}]CF_3COO$ (x_{IL}= 0.0461) was used for titrant. At the concentration, viscosity of the titrant is low enough and the mole fraction is far from the critical point. The 1.0204 g of titrant (= 0.01373 mol of $[P_{4,4,4,4}]CF_3COO$) was injected at one time. The mole fraction change was 0.0003-0.0005. Table L-1 shows the apparent excess partial molar enthalpy, h, converted from the raw data using equation (61) in 5. 4. 1. Smoothing curve was fitted on h with a flexible ruler as shown in figure 5-5. The values were read off from the smooth curve drawn and calculate δh in steps of δx_{IL}= 0.0006. Then the third derivative H^{E}_{IL-IL} was calculated as shown in Table L-2.

Table L-1

x_{IL}	h / kJ mol^{-1}	x_{IL}	h / kJ mol^{-1}
0.001721	-26.040	0.009662	-4.449
0.002189	-19.665	0.010113	-4.091
0.002647	-25.058	0.010553	-3.723
0.003096	-23.727	0.010982	-3.346
0.003535	-22.794	0.011402	-3.153
0.004498	-20.232	0.012012	-2.856
0.004981	-17.701	0.012407	-2.593
0.005337	-15.018	0.013045	-2.079
0.005570	-14.362	0.013478	-2.014
0.006160	-13.164	0.013899	-1.988
0.006625	-11.406	0.014310	-1.809
0.007079	-9.902	0.014710	-1.742
0.007522	-8.159	0.015005	-1.691
0.007956	-7.464	0.015292	-1.576
0.008588	-6.137	0.016123	-1.523
0.008998	-5.517	0.016938	-1.403
		0.017710	-1.270

Table L-2

x_{IL}	$H^{\mathrm{E}}_{\mathrm{IL-IL}}$ / kJ mol^{-1}	x_{IL}	$H^{\mathrm{E}}_{\mathrm{IL-IL}}$ / kJ mol^{-1}
0.002400	5260.6	0.01040	4120.0
0.002600	5810.9	0.01060	3185.8
0.002800	6631.2	0.01080	3202.6
0.003000	6925.7	0.01100	2897.6
0.003200	7222.8	0.01120	2913.1
0.003400	7791.0	0.01140	2603.3
0.003600	8364.2	0.01160	1963.0
0.003800	8942.4	0.01180	1644.7
0.004000	9253.5	0.01200	1653.7
0.004200	10114.1	0.01220	1662.8
0.004400	11256.8	0.01240	1672.0
0.004600	11858.1	0.01260	1681.3
0.004800	12741.8	0.01280	1690.8
0.005000	13355.3	0.01300	1360.3
0.005200	13974.2	0.01320	1026.0
0.005400	14598.8	0.01340	1375.8
0.005600	14101.1	0.01360	1383.7
0.005800	14448.8	0.01380	1078.6
0.006000	14515.1	0.01400	1049.9
0.006200	14296.2	0.01420	1408.1
0.006400	13500.8	0.01440	1558.1
0.006600	12698.0	0.01460	1068.6
0.006800	12177.7	0.01480	716.7
0.007000	11652.5	0.01500	901.3
0.007200	10537.0	0.01520	1088.1
0.007400	9705.0	0.01540	1094.8
0.007600	8865.1	0.01560	1101.5
0.007800	8017.1	0.01580	738.9
0.008000	7459.2	0.01600	557.6
0.008200	6596.1	0.01620	374.1
0.008400	6628.5	0.01640	564.7
0.008600	5752.9	0.01660	568.3
0.008800	5781.4	0.01680	381.3
0.009000	4892.9	0.01700	575.7

0.009200	4610.1	0.01720	772.6
0.009400	4324.5	0.01740	1166.5
0.009600	4346.5	0.01760	782.8
0.009800	4056.7	0.01325	-176.5
0.010000	4391.2	0.00885	15213.6
0.010200	3783.4	0.00895	15251.5
		0.00450	9866.8

M. Hydrophobicity/hydrophilicity of typical ions composing ionic liquids

The effects on water of typical cations and anions composing ILs are characterized by the 1-propanol probing methodology. Table M-1 shows their value of hydrophobicity, hydrophilicity and hydration number, n_{H}.

Table M-1

	Ions	character	Hydrophobicity	n_{H}	Hydrophilicity	Ref.
	Cations					
c	$[P_{4,4,4,4}]^+$	Amphiphile	-3.49	72	-5337	[129]
d	$[C_2mim]^+$	Amphiphile	-0.39	7	-1970	[131]
e	$[C_4mim]^+$	Amphiphile	-1.31	26	-3227	[133]
f	$[C_4C_1mim]^{+(a}$	Amphiphile	-1.85	37	-6760	[131]
	Anions					
g	CF_3COO^-	Amphiphile	-0.49	10	-767	[129]
h	Cl^-	Hydration center	-0.16	2.3	0	[110], [111]
i	Br^-	Hydrophile	0	0	-920	[111]
j	CH_3COO^-	Hydrophobe	-0.22	3.7	0	[130]
k	BF_4^-	Hydrophile	-0.26	5.5	-2060	[134]
l	$[OTf]^{-(b}$	Amophiphile	-0.67	13	-2370	[133]
m	PF_6^-	Amophiphile	-0.67	13	-3835	[133]
n	$[NTf_2]^-$	Amphiphile	-4.08	84	-8156	[132]

a) 1-butyl-2,3-dimethyl imidazolium

b) Trifluoromethylsulfonate

N. Fluctuations for the aqueous solution of [C4mim]BF4

Ionic Liquid 1-butyl 3-methyl imidazolium tetrafluoroborate, [C4mim]BF4, is one of the most popular imidazolium-based ILs and its aqueous solution shows UCST-type phase separation. The critical point is shown at x_{IL}= 0.07 and at 277 K, where x_{IL} is the mole fraction of [C4mim]BF4.[33] The fluctuations of aqueous solution of [C4mim]BF4 at 298 and 284 K (and only one point at 278 K) were determined by SAXS method. As discussed in 2. 2., fluctuations were obtained by combination of the zero-angle scattering intensity, $I(0)$, partial molar volumes, v_i, and isothermal compressibility, κ_T. However, κ_T of water was used for calculation of the fluctuation of the mixtures. Because it was difficult to control the temperature of high-pressure density meter DMA HP at low temperature. For this system, the contribution of κ_T on the fluctuations is small as discussed in 3. 3. 3. Other parameters were obtained in same technique as for the aqueous solution of [P4,4,4,4]CF3COO.

Figure N-1 shows the density fluctuation, $\langle(\Delta N)^2\rangle/\bar{N}$, and the concentration fluctuation, $\bar{N}\langle(\Delta x)^2\rangle$, for the aqueous solution. The system becomes fluctuating approaching to the critical point. $\langle(\Delta N)^2\rangle/\bar{N}$ shows a large value. The size difference between [C4mim]BF4 and water has a large contribution probably. Almásy *et al.* determined the concentration fluctuation of the aqueous solution by SANS method[54] as shown in Appendix O.

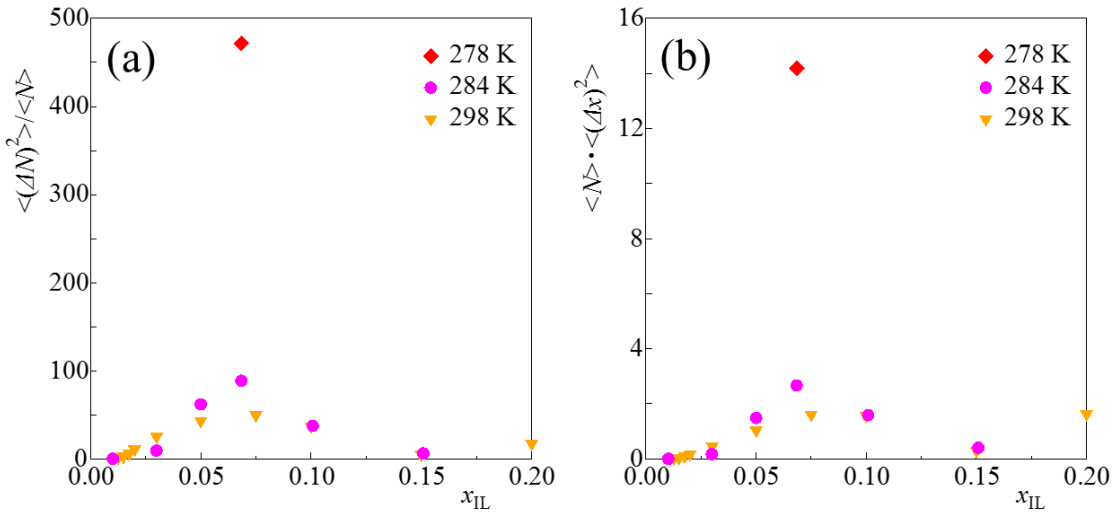

Figure N-1 Mole fraction dependence of (a)density fluctuation, $\langle(\Delta N)^2\rangle/\bar{N}$, and (b)cncentration fluctuation, $\bar{N}\langle(\Delta x)^2\rangle$, for the aqueous solution of [C4mim]BF4 at 298, 284 and 278 K.

Using Kirkwood-Buff parameters, the individual density fluctuations of $[C_4mim]BF_4$, $\langle(\Delta N_{IL})^2\rangle/\overline{N_{IL}}$, and water, $\langle(\Delta N_W)^2\rangle/\overline{N_W}$, and their cross term, $\langle\Delta N_{IL}\Delta N_W\rangle/\overline{N_{IL}}$, were also obtained as shown in figure N-2. The individual density fluctuations of $[C_4mim]BF_4$ shows slightly larger value than that of water. Furthermore, the cross term showed negative value near the critical point. It indicate that each $[C_4mim]BF_4$ and water show aggregations of each. However, the accuracy of these value is poor especially around the critical point. Because the critical temperature is too low to keep the system stable.

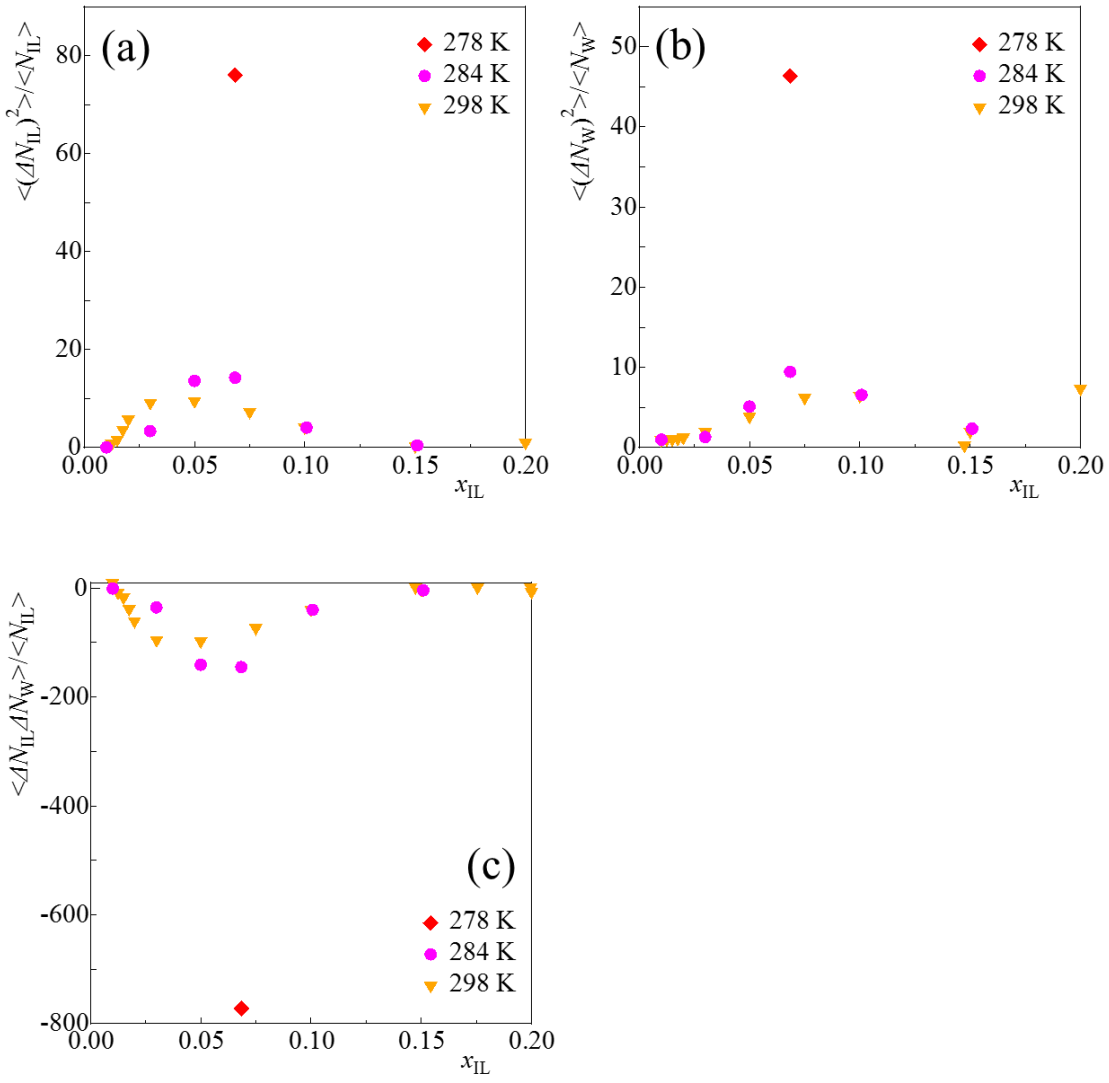

Figure N-2 Individual density fluctuations for (a)$[C_4mim]BF_4$, $\langle(\Delta N_{IL})^2\rangle/\overline{N_{IL}}$, (b)water, $\langle(\Delta N_W)^2\rangle/\overline{N_W}$, and (c)their coross term, $\langle\Delta N_{IL}\Delta N_W\rangle/\overline{N_{IL}}$, in the aqueous solution of $[C_4mim]BF_4$ at 298, 284 and 278 K.

Figure N-3 shows the excess molar volume, V_m^E, and the partial molar volumes for [C_4mim]BF_4,v_{IL}. [C_4mim]BF_4 is a liquid at room temperature and the actual excess molar volume can be measured. V_m^E shows positive value almost entirely including the critical point excluding in the dilute region around at x_{IL} = 0.010 where V_m^E is negative. However, the deep analysis of the dilute region is done yet. On the other hand, the poor accuracy of V_m^E at higher concentration region may be the effect of the high hygroscopicity of IL.

By differentiation with respect to x_{IL} using a flexible ruler, v_{IL} and v_W are obtained. Figure N-4 shows the concentration dependence of v_{IL} at 298 K. There is a large size difference between them as for [$P_{4,4,4,4}$]CF_3COO and water. However, v_{IL} decreases and v_W (about 18 cm^3 mol^{-1} in pure water) increases with x_{IL} increasing. There is repulsive force between [C_4mim]BF_4 and water.

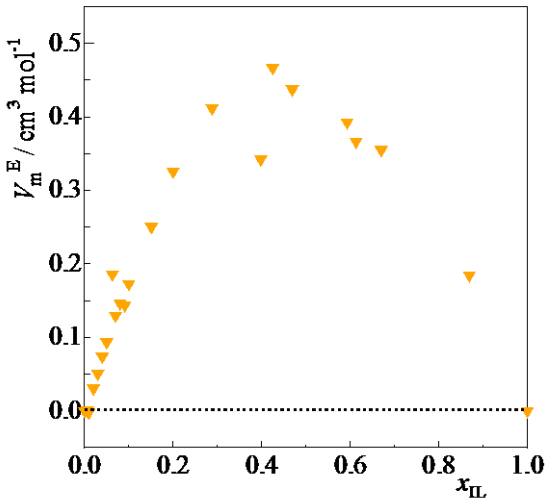

Figure N-3 Mole fraction dependence of the excess molar volume, V_m^E, at 298 K.

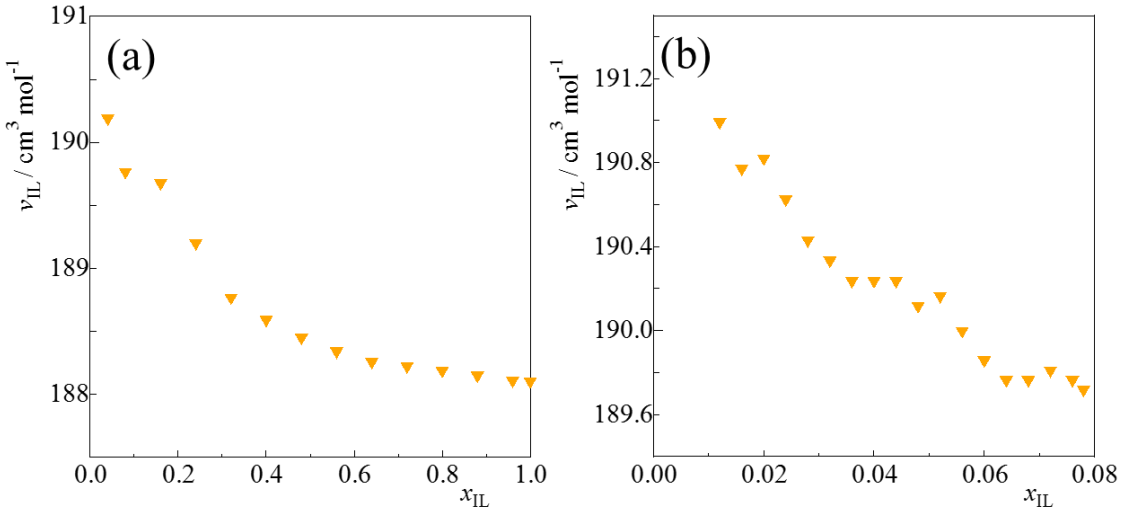

Figure N-4 The partial molar volumes of $[C_4mim]BF_4$, v_{IL}, at 298 K (a)for entire concentration region and (b)for dilute concentration region including the critical concentration, x_{IL}= 0.07.

These results indicate the aqueous solutions of $[P_{4,4,4,4}]CF_3COO$ with the LCST-type phase separation and $[C_4mim]BF_4$ with the UCST-type phase separation show different mixing state completely.

O. Comparison of fluctuations of various aqueous solutions

Table O-1 shows values of the density and the concentration fluctuation for various aqueous solutions as a function of mole fraction of solute, x; 1-butyl-3-methylimidazolium tetrafluoroborate ([C_4mim]BF_4) [54], acetonitrile [81] and ethanol [138]. Aqueous solutions of [C_4mim]BF_4 and acetonitrile shows UCST-type phase separation. To compare those with the aqueous solution of [$P_{4,4,4,4}$]CF_3COO, the relative temperature, T_r, and mole fraction, x_r, is defined as,

$$T_r = \frac{|T - T_c|}{T_c}, \tag{O1}$$

$$x_r = \frac{|x|}{x_c}, \tag{O2}$$

where subscripts c indicate the value at critical point. At the critical point, T_r is equal to 0 and x_r to 1.

Table O-1

x	x_r	$\bar{N}\langle(\Delta x)^2\rangle$	$\frac{\langle(\Delta N)^2\rangle}{\bar{N}}$	x	x_r	$\bar{N}\langle(\Delta x)^2\rangle$	$\frac{\langle(\Delta N)^2\rangle}{\bar{N}}$
[C_4mim]BF_4 (UCST T_c= 277 K, x_c= 0.075) [54]							
	T_r= 0.076						
0.01	0.13	0.017		0.06	0.80	1.029	
0.02	0.27	0.048		0.07	0.93	1.249	
0.03	0.40	0.167		0.08	1.07	1.436	
0.04	0.53	0.428		0.10	1.33	1.314	
0.05	0.67	0.761		0.12	1.60	1.061	
				0.16	2.13	0.624	
Acetonitrile (UCST T_c= 272 K, x_c= 0.38) [81]							
	T_r= 0.0036				T_r= 0.025		
0.20	0.53	5.0	9.0	0.20	0.53	3.4	6.2
0.30	0.79	22.1	33.4	0.30	0.79	12.6	19.1
0.35	0.92	49.0	66.4	0.35	0.92	18.6	25.3
0.38	1.00	65.9	83.4	0.38	1.00	20.5	26.0
0.40	1.05	46.8	57.0	0.40	1.05	18.8	23.0
0.45	1.18	39.1	39.1	0.45	1.18	16.2	17.8
0.50	1.32	17.0	17.0	0.50	1.32	10.3	10.3

		T_r= 0.095					
0.20	0.53	1.70	3.34	0.38	1.00	6.17	8.08
0.30	0.79	4.82	7.52	0.40	1.05	6.17	7.77
0.35	0.92	6.17	8.63	0.45	1.18	5.86	6.67
				0.50	1.32	4.40	4.55
			Ethanol (water miscible at 293 K) [138]				
0.05		0.036	0.17	0.32		0.76	1.40
0.09		0.089	0.30	0.40		0.96	1.45
0.15		0.17	0.48	0.50		0.88	1.11
0.18		0.28	0.71	0.72		0.42	0.39
0.24		0.47	1.05	1.00		0.00	0.049
			$[P_{4,4,4,4}]CF_3COO$ (LCST T_c= 302 K, x_c= 0.025)				
		T_r= 0.0044				T_r= 0.014	
0.016	0.64	0.47	97.1	0.012	0.48	0.04	10.19
0.02	0.80	1.92	357.91	0.016	0.64	0.32	65.74
0.023	0.92	3.45	593.11	0.02	0.80	0.79	145.79
0.024	0.96	3.6	603.23	0.023	0.92	1.04	178.23
0.026	1.04	5.8	924.6	0.024	0.96	1.24	206.31
0.027	1.08	7.38	1148.02	0.026	1.04	1.37	217.6
0.029	1.16	6.11	905.29	0.027	1.08	1.48	228.82
0.031	1.24	6.89	972.75	0.029	1.16	1.52	224.15
0.038	1.52	6.06	730.8	0.031	1.24	1.6	224.98
0.046	1.84	3.88	395.91	0.038	1.52	1.38	166.44
0.056	2.24	1.43	120.75	0.046	1.84	0.83	85.04
				0.056	2.24	0.15	12.78
		T_r= 0.031					
0.016	0.64	0.09	19.37	0.028	1.12	0.81	121.15
0.02	0.80	0.28	51.72	0.031	1.24	0.48	67.66
0.023	0.92	0.4	68.11	0.038	1.52	0.48	57.52
0.025	1.00	0.84	136.59	0.045	1.80	0.5	51.83
				0.056	2.24	0.08	6.44

P. NMR method

NMR (Nuclear Magnetic Resonance) method is one of the powerful tool to analysis the chemical structure at atomic level. To determine the sites of water molecules on $[P_{4,4,4,4}]CF_3COO$, concentration and temperature dependence of ^1H chemical shift was obtained. The measurement were performed using JNM-ECA500 spectrometer (JEOL). The sample aqueous solutions were contained in the inner NMR tube and deuterated chloroform, $CDCl_3$, with tetramethylsilane, TMS, was filled in the outer tube. TMS was used as internal reference. Figure O-1 shows the 1H spectrum at x_{IL}= 0.025 and at 298 K. Water showed a much stronger signal because the mole fraction x_{IL} too small.

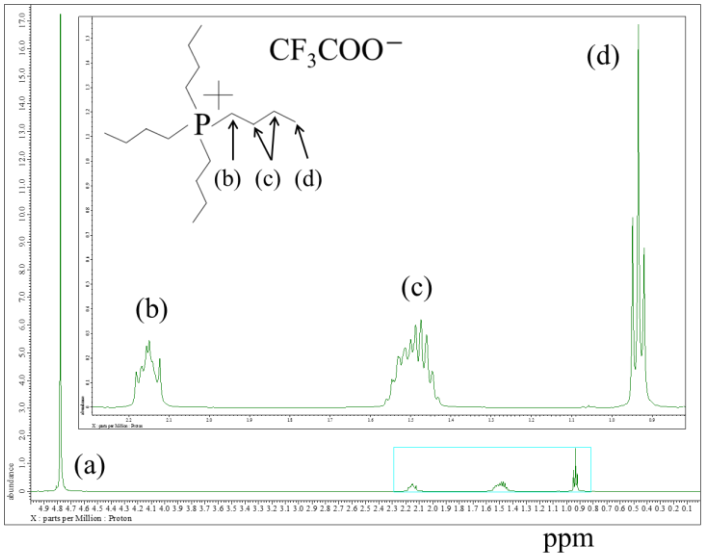

Figure O-1 ^1H NMR spectrum of aqueous solution of $[P_{4,4,4,4}]CF_3COO$ at x_{IL}= 0.025 and at 298 K; (a)H of water and (b)(c)(d)H on butyl chains of $[P_{4,4,4,4}]^+$. The inset focuses on the spectra of the cation.

Focusing on the chemical shift of (a) and (d), the change of chemical shifts at x_{IL}= 0.025 and 0.070 from 294 to 305 K. H atom on the terminal of the butyl chains may be sensitive to surroundings. Figure O-2 shows the temperature dependence of those chemical shifts of ^1H on water and on terminal of butyl chains. Both of them became smaller with temperature increasing monotonically. For various protons and carbons ^{13}C, the change of chemical shifts with temperature were measured. The changes of them were too small to discuss. Also concentration dependence of chemical shifts of them showed linear behavior. We were not able to know which site on $[P_{4,4,4,4}]CF_3COO$ had strong interaction with water molecule when $[P_{4,4,4,4}]CF_3COO$ showed aggregation near the

critical point. Probably, the critical point are shown at very small mole fraction because of the large size difference between $[P_{4,4,4,4}]CF_3COO$ and water.

However, at x_{IL}=0.025, the chemical shift of (d) deviated from the linear change at 303 K beyond the critical point. The signal of water split into two at the same temperature. This result indicates there are two type water molecules in different surroundings after phase separation, in water-rich phase and in $[P_{4,4,4,4}]CF_3COO$-rich phase.

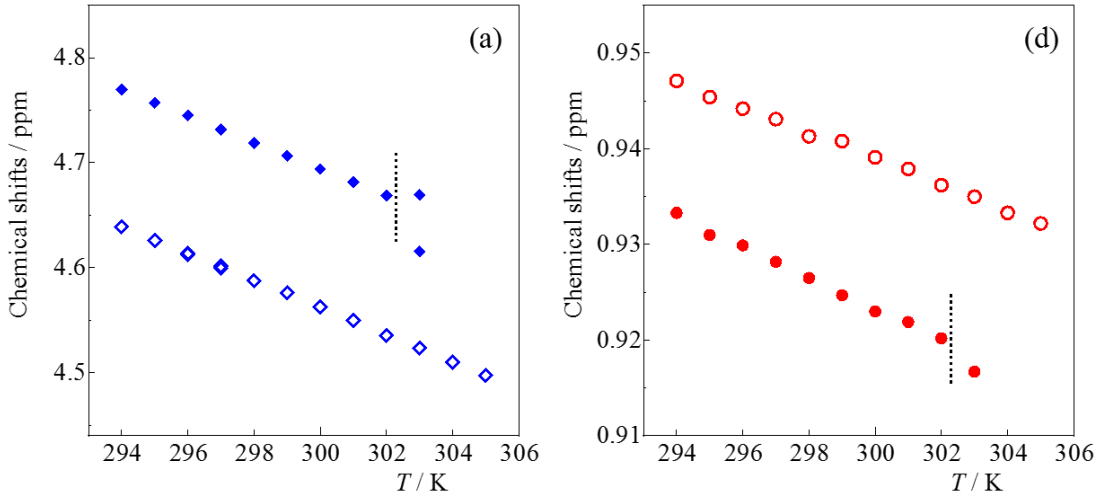

Figure O-2 Temperature dependence of chemical shifts of ^1H (a)on water and (d)on terminal of butyl chains for the aqueous solution of $[P_{4,4,4,4}]CF_3COO$. The filled markers are the results at x_{IL}= 0.025 and the opened markers are at x_{IL}= 0.070. The dashed lines for the results x_{IL}= 0.025 indicate the phase separation temperature, namely the critical temperature 302 K. For the mixture at x_{IL}= 0.070, the phase separation temperature is higher than measured temperature region.

References

[1] R. D. Rogers and K. R. Seddon, “Ionic Liquids - Solvents of the Future?,” *Science*, vol. 302, pp. 792–793, 2003.

[2] K. R. Seddon, “Ionic liquids: A taste of the future,” *Nat. Mater*, vol. 2, pp. 363–365, 2003.

[3] J. S. Wilkes and M. J. Zaworotko, “Air and water stable 1-ethyl-3-methylimidazolium based ionic liquids,” *J. Chem. Soc. Chem. Commun.*, pp. 965–967, 1992.

[4] T. Welton, “Room-temperature ionic liquids. Solvent for synthesis and catalysis,” *Chem. Rev*, vol. 99, pp. 2071–2083, 1999.

[5] N. V Plechkova and K. R. Seddon, “Applications of ionic liquids in the chemical industry.,” *Chem. Soc. Rev.*, vol. 37, pp. 123–150, 2008.

[6] H. V. R. Annapureddy, H. K. Kashyap, P. M. De Biase, and C. J. Margulis, “What is the Origin of the Prepeak in the X-ray Scattering of Imidazolium-Based Room-Temperature Ionic Liquids?,” *J. Phys. Chem. B*, vol. 114, pp. 16838–16846, 2010.

[7] A. Triolo, O. Russina, H.-J. Bleif, and E. Di Cola, “Nanoscale segregation in room temperature ionic liquids.,” *J. Phys. Chem. B*, vol. 111, pp. 4641–4644, 2007.

[8] A. Triolo, O. Russina, B. Fazio, G. B. Appetecchi, M. Carewska, and S. Passerini, “Nanoscale organization in piperidinium-based room temperature ionic liquids,” *J. Chem. Phys.*, vol. 130, no. 164521, 2009.

[9] J. N. A. C. Lopes and A. A. H. Pdua, “Nanostructural Organization in Ionic Liquids Nanostructural Organization in Ionic Liquids,” vol. 110, pp. 3330–3335, 2006.

[10] C. P. Fredlake, J. M. Crosthwaite, D. G. Hert, S. N. V. K. Aki, and J. F. Brennecke, “Thermophysical Properties of Imidazolium-Based Ionic Liquids,” *J. Chem. Eng. Data*, vol. 49, pp. 954–964, 2004.

[11] Y. Shimizu, Y. Wachi, K. Fujii, M. Imanari, and K. Nishikawa, “NMR Study on Ion Dynamics and Phase Behavior of a Piperidinium-Based Room-Temperature Ionic Liquid: 1-Butyl-1-methylpiperidinium Bis(fluorosulfonyl)amide,” *J. Phys. Chem. B*, vol. 120, pp. 5710–5719, 2016.

[12] J. S. Wilkes, “A short history of ionic liquids—from molten salts to neoteric solvents,” *Green Chem.*, vol. 4, pp. 73–80, 2002.

[13] E. D. Bates, R. D. Mayton, I. Ntai, and J. H. Davis, “CO_2 Capture by a Task-Specific Ionic Liquid,” *J. Am. Chem. Soc.*, vol. 124, pp. 926–927, 2002.

[14] N. V Plechkova and K. R. Seddon, “Applications of ionic liquids in the chemical industry,” *Chem Soc Rev*, vol. 37, pp. 123–150, 2008.

[15] M. Armand, F. Endres, D. R. MacFarlane, H. Ohno, and B. Scrosati, “Ionic-liquid materials for the electrochemical challenges of the future,” *Nat. Mater*, vol. 8, pp. 621–629, 2009.

[16] R. P. Swatloski, S. K. Spear, J. D. Holbrey, and R. D. Rogers, “Dissolution of cellulose with ionic liquids,” *J. Am. Chem. Soc.*, vol. 124, pp. 4974–4975, 2002.

[17] I. J. B. Lin and C. S. Vasam, “Metal-containing ionic liquids and ionic liquid crystals based on imidazolium moiety,” *J. Organomet. Chem.*, vol. 690, pp. 3498–3512, 2005.

[18] M. Yoshizawa, M. Hirao, K. Ito-Akita, and H. Ohno, “Ion conduction in zwitterionic-type molten salts and their polymers,” *J. Mater. Chem.*, vol. 11, pp. 1057–1062, 2001.

[19] H. Ohno and K. Ito, “Room-Temperature Molten Salt Polymers as a Matrix for Fast Ion Conduction.,” *Chemistry Letters*, vol. 27. pp. 751–752, 1998.

[20] M. Yoshio, T. Mukai, K. Kanie, M. Yoshizawa, H. Ohno, and T. Kato, “Layered ionic liquids: Anisotropic ion conduction in new self-organized liquid-crystalline materials,” *Adv. Mater.*, vol. 14, pp. 351–354, 2002.

[21] K. N. Marsh, J. a. Boxall, and R. Lichtenthaler, “Room temperature ionic liquids and their mixtures - A review,” *Fluid Phase Equilib.*, vol. 219, pp. 93–98, 2004.

[22] K. N. Marsh, A. Deev, A. C.-T. Wu, E. Tran, and A. Klamt, “Room temperature ionic liquids as replacements for conventional solvents – A review,” *Korean J. Chem. Eng.*, vol. 19, pp. 357–362, 2002.

[23] A. Stoppa, J. Hunger, and R. Buchner, “Conductivities of Binary Mixtures of Ionic Liquids with Polar Solvents Conductivities of Binary Mixtures of Ionic Liquids with Polar Solvents,” *J. Chem. Eng. Data*, vol. 54, pp. 472–479, 2009.

[24] C. A. S. Trindade, Z. P. Visak, R. Bogel-ŁUkasik, E. Bogel-ŁUkasik, and M. N. Da Ponte, “Liquid-liquid equilibrium of mixtures of imidazolium-based ionic liquids with propanediols or glycerol,” *Ind. Eng. Chem. Res.*, vol. 49, pp. 4850–4857, 2010.

[25] V. Najdanovic-Visak, J. M. S. S. Esperança, L. P. N. Rebelo, M. Nunes da Ponte, H. J. R. Guedes, K. R. Seddon, H. C. de Sousa, and J. Szydlowski, “Pressure, Isotope, and Water Co-solvent Effects in Liquid−Liquid Equilibria of (Ionic Liquid + Alcohol) Systems,” *J. Phys. Chem. B*, vol. 107, pp. 12797–12807, 2003.

[26] M. B. Shiflett, A. Yokozeki, E. Station, D. Fluoroproducts, and E. Procedures, “Liquid - Liquid Equilibria in Binary Mixtures of 1 , 3-Propanediol + Ionic Liquids,” *J. Chem. Eng. Data*, vol. 52, pp. 1302–1306, 2007.

[27] J. L. Anthony, E. J. Maginn, and J. F. Brennecke, “Solution Thermodynamics of Imidazolium-Based Ionic Liquids and Water Solution Thermodynamics of Imidazolium-Based Ionic Liquids and Water,” *J. Phys. Chem. B*, vol. 105, pp. 10942–10949, 2001.

[28] J. N. C. Lopes, M. F. C. Gomes, P. Husson, A. H. P. Agílio, L. P. N. Rebelo, S. Sarraute, and M. Tariq, “Polarity , Viscosity , and Ionic Conductivity of Liquid Mixtures Containing [C_4C_1im][Ntf_2] and a Molecular Component,” *J. Phys. Chem. B*, vol. 115, pp. 6088–6099, 2011.

[29] G. Hong, J. Jacquemin, P. Husson, M. F. C. Gomes, M. Deetlefs, M. Nieuwenhuyzen, O. Sheppard, C. Hardacre, and B. Pascal, “Effect of Acetonitrile on the Solubility of Carbon Dioxide in 1-Ethyl-3-methylimidazolium Bis (trifluoromethylsulfonyl) amide,” *Ind. Eng. Chem. Res.*,

vol. 45, pp. 8180–8188, 2006.

[30] J. N. Canongia Lopes, T. C. Cordeiro, J. M. S. S. Esperança, H. J. R. Guedes, S. Huq, L. P. N. Rebelo, and K. R. Seddon, "Deviations from ideality in mixtures of two ionic liquids containing a common ion," *J. Phys. Chem. B*, vol. 109, pp. 3519–3525, 2005.

[31] F. Qi and H. Wang, "Application of Prigogine-Flory-Patterson theory to excess molar volume of mixtures of 1-butyl-3-methylimidazolium ionic liquids with N-methyl-2-pyrrolidinone," *J. Chem. Thermodyn.*, vol. 41, pp. 265–272, 2009.

[32] Y. Kohno and H. Ohno, "Ionic liquid/water mixtures: from hostility to conciliation," *Chem. Commun.*, vol. 48, pp. 7119–7130, 2012.

[33] L. P. N. Rebelo, V. Najdanovic-Visak, Z. P. Visak, M. Nunes da Ponte, J. Szydlowski, C. a. Cerdeiriña, J. Troncoso, L. Romaní, J. M. S. S. Esperança, H. J. R. Guedes, and H. C. de Sousa, "A detailed thermodynamic analysis of $[C_4mim][BF_4]$ + water as a case study to model ionic liquid aqueous solutions," *Green Chem.*, vol. 6, pp. 369–381, 2004.

[34] H. M. Lin, H. Y. Tien, Y. T. Hone, and M. J. Lee, "Solubility of selected dibasic carboxylic acids in water, in ionic liquid of [Bmim][BF_4], and in aqueous [Bmim][BF_4] solutions," *Fluid Phase Equilib.*, vol. 253, pp. 130–136, 2007.

[35] Y. Kohno, S. Saita, Y. Men, J. Yuan, H. Ohno, Y. KohnYo, S. Saita, Y. Men, J. Yuan, and H. Ohno, "Thermoresponsive polyelectrolytes derived from ionic liquids," *Polym. Chem.*, vol. 6, pp. 2163–2178, 2015.

[36] K. Fukumoto and H. Ohno, "LCST-type phase changes of a mixture of water and ionic liquids derived from amino acids," *Angew. Chem. Int. Ed.*, vol. 46, pp. 1852–1855, 2007.

[37] W. Liu, L. Cheng, Y. Zhang, H. Wang, and M. Yu, "The physical properties of aqueous solution of room-temperature ionic liquids based on imidazolium: Database and evaluation," *J. Mol. Liq.*, vol. 140, pp. 68–72, 2008.

[38] H. Zhao, "Are ionic liquids kosmotropic or chaotropic? An evaluation of available thermodynamic parameters for quantifying the ion kosmotropicity of ionic liquids," *J. Chem. Technol. Biotechnol.*, vol. 81, pp. 877–891, 2006.

[39] E. Rilo, J. Pico, S. García-Garabal, L. M. Varela, and O. Cabeza, "Density and surface tension in binary mixtures of CnMIM-BF4 ionic liquids with water and ethanol," *Fluid Phase Equilib.*, vol. 285, pp. 83–89, 2009.

[40] Q. G. Zhang, F. Xue, J. Tong, W. Guan, and B. Wang, "Studies on volumetric properties of concentrated aqueous solutions of the ionic liquid $BMIBF_4$," *J. Solution Chem.*, vol. 35, pp. 297–309, 2006.

[41] I. Bou Malham, P. Letellier, A. Mayaffre, and M. Turmine, "Part I: Thermodynamic analysis of volumetric properties of concentrated aqueous solutions of 1-butyl-3-methylimidazolium tetrafluoroborate, 1-butyl-2,3-dimethylimidazolium tetrafluoroborate, and ethylammonium nitrate

based on pseudo-lattice theory," *J. Chem. Thermodyn.*, vol. 39, pp. 1132–1143, 2007.

[42] E. Gómez, B. González, A. Domínguez, E. Tojo, and J. Tojo, "Dynamic viscosities of a series of 1-alkylimidazolium chloride ionic liquids and their binary mixtures with water at several temperatures," *J. Chem. Eng. Data*, vol. 51, pp. 696–701, 2006.

[43] D. G. Archer, J. A. Widegren, D. R. Kirklin, and J. W. Magee, "Enthalpy of solution of 1-Octyl-3-methylimidazolium tetrafluoroborate in water and in aqueous sodium fluoride," *J. Chem. Eng. Data*, vol. 50, pp. 1484–1491, 2005.

[44] H. Katayanagi, K. Nishikawa, H. Shimozaki, K. Miki, P. Westh, and Y. Koga, "Mixing Schemes in Ionic Liquid−H_2O Systems: A Thermodynamic Study," *J. Phys. Chem. B*, vol. 108, pp. 19451–19457, 2004.

[45] H. Kato, K. Nishikawa, H. Murai, T. Morita, and Y. Koga, "Chemical potentials in aqueous solutions of some ionic liquids with the 1-ethyl-3-methylimidazolium cation," *J. Phys. Chem. B*, vol. 112, pp. 13344–13348, 2008.

[46] C. Fernandez and A. Bald, "Conductance Studies of Aqueous Ionic Liquids Solutions [emim][BF_4] and [bmim][BF_4] at Temperatures from (283.15 to 318.15) K," *Int. J. Electrochem. Sci.*, 1vol. 10, pp. 2120–2129, 2015.

[47] E. Rilo, J. Vila, J. Pico, S. García-Garabal, L. Segade, L. M. Varela, and O. Cabeza, "Electrical conductivity and viscosity of aqueous binary mixtures of 1-alkyl-3-methyl imidazolium tetrafluoroborate at four temperatures," *J. Chem. Eng. Data*, vol. 55, pp. 639–644, 2010.

[48] J. Vila, P. Ginés, E. Rilo, O. Cabeza, and L. M. Varela, "Great increase of the electrical conductivity of ionic liquids in aqueous solutions," *Fluid Phase Equilib.*, vol. 247, pp. 32–39, 2006.

[49] N. Sieffert and G. Wipff, "The [BMI][Tf_2N] ionic liquid/water binary system: A molecular dynamics study of phase separation and of the liquid-liquid interface," *J. Phys. Chem. B*, vol. 110, pp. 13076–13085, 2006.

[50] C. E. S. Bernardes, M. E. Minas Da Piedade, and J. N. Canongia Lopes, "The structure of aqueous solutions of a hydrophilic ionic liquid: The full concentration range of 1-ethyl-3-methylimidazolium ethylsulfate and water," *J. Phys. Chem. B*, vol. 115, pp. 2067–2074, 2011.

[51] S. Cha, M. Ao, W. Sung, B. Moon, B. Ahlström, P. Johansson, Y. Ouchi, and D. Kim, "Structures of ionic liquid-water mixtures investigated by IR and NMR spectroscopy.," *Phys. Chem. Chem. Phys.*, vol. 16, pp. 9591–601, 2014.

[52] M. Nakakoshi, S. Ishihara, H. Utsumi, H. Seki, Y. Koga, and K. Nishikawa, "Anomalous dynamic behavior of ions and water molecules in dilute aqueous solution of 1-butyl-3-methylimidazolium bromide studied by NMR," *Chem. Phys. Lett.*, vol. 427, pp. 87–90, 2006.

[53] H. Abe, T. Takekiyo, M. Shigemi, Y. Yoshimura, S. Tsuge, T. Hanasaki, K. Ohishi, S. Takata, and J. Suzuki, "Direct Evidence of Con fi ned Water in Room-Temperature Ionic Liquids by

Complementary Use of Small-Angle X-ray and Neutron Scattering," *Chem. Phys. Lett.*, vol. 5, pp. 1175–1180, 2014.

[54] L. Almásy, M. Turmine, and a Perera, "Structure of aqueous solutions of ionic liquid 1-butyl-3-methylimidazolium tetrafluoroborate by small-angle neutron scattering.," *J. Phys. Chem. B*, vol. 112, no. 8, pp. 2382–2387, 2008.

[55] J. Bowers, C. P. Butts, P. J. Martin, M. C. Vergara-Gutierrez, and R. K. Heenan, "Aggregation behavior of aqueous solutions of ionic liquids.," *Langmuir*, vol. 20, pp. 2191–2198, 2004.

[56] T. Singh and A. Kumar, "Cation-anion-water interactions in aqueous mixtures of imidazolium based ionic liquids," *Vib. Spectrosc.*, vol. 55, pp. 119–125, 2011.

[57] W. Li, Z. Zhang, B. Han, S. Hu, Y. Xie, and G. Yang, "Effect of Water and Organic Solvents on the Ionic Dissociation of Ionic Liquids," *J. Phys. Chem. B*, vol. 111, pp. 6452–6456, 2007.

[58] S. Katsuta, R. Ogawa, N. Yamaguchi, T. Ishitani, and Y. Takeda, "Ion pair formation of 1-alkyl-3-methylimidazolium salts in water," *J. Chem. Eng. Data*, vol. 52, pp. 248–251, 2007.

[59] M. Tariq, F. Moscoso, F. J. Deive, A. Rodriguez, M. A. Sanromán, J. M. S. S. Esperança, J. N. Canongia Lopes, and L. P. N. Rebelo, "Probing the self-aggregation of ionic liquids in aqueous solutions using density and speed of sound data," *J. Chem. Thermodyn.*, vol. 59, pp. 43–48, 2013.

[60] N. V. Sastry, N. M. Vaghela, and V. K. Aswal, "Effect of alkyl chain length and head group on surface active and aggregation behavior of ionic liquids in water," *Fluid Phase Equilib.*, vol. 327, pp. 22–29, 2012.

[61] W. Jiang, Y. Wang, and G. A. Voth, "Molecular dynamics simulation of nanostructural organization in ionic liquid/water mixtures," *J. Phys. Chem. B*, vol. 111, pp. 4812–4818, 2007.

[62] N. V. Sastry, N. M. Vaghela, P. M. Macwan, S. S. Soni, V. K. Aswal, and A. Gibaud, "Aggregation behavior of pyridinium based ionic liquids in water - Surface tension, ^{1}H NMR chemical shifts, SANS and SAXS measurements," *J. Colloid Interface Sci.*, vol. 371, pp. 52–61, 2012.

[63] D. E. TomŠík and P. N. Gospodinova, "Water in Ionic Liquids: Correlation between Anion Hydrophilicity and Near-Infrared Fingerprints," *Chem. Phys. Phys. Chem.*, vol. 17, pp. 1586–1590, 2016.

[64] L. Cammarata, S. G. Kazarian, P. a. Salter, and T. Welton, "Molecular states of water in room temperature ionic liquidsElectronic Supplementary Information available. See http://www.rsc.org/suppdata/cp/b1/b106900d/," *Phys. Chem. Chem. Phys.*, vol. 3, pp. 5192–5200, 2001.

[65] J. Gao and N. J. Wagner, "Water Nanocluster Formation in the Ionic Liquid 1-Butyl-3-methylimidazolium Tetrafluoroborate ([C_4mim][BF_4])-D_2O Mixtures," *Langmuir*, vol. 32, pp. 5078–5084, 2016.

[66] B. Fazio, A. Triolo, and G. Di Marco, "Local organization of water and its effect on the structural

heterogeneities in room-temperature ionic liquid/H2O mixtures," *J. Raman Spectrosc.*, vol. 39, pp. 233–237, 2008.

[67] P. Ludley and N. Karodia, "Phosphonium tosylates as solvents for the Diels-Alder reaction," *Tetrahedron Lett.*, vol. 42, pp. 2011–2014, 2001.

[68] C. Comyns, N. Karodia, S. Zeler, and J.-A. Andersen, "Clean catalysis with clean solvents - phosphonium tosylates for transfer hydrogenation reactions.," *Catal. Letters*, vol. 67, pp. 113–115, 2000.

[69] Y. Kohno, H. Arai, S. Saita, and H. Ohno, "Material design of ionic liquids to show temperature-sensitive LCST-type phase transition after mixing with water," *Aust. J. Chem.*, vol. 64, pp. 1560–1567, 2011.

[70] A. Okafuji, Y. Kohno, and H. Ohno, "Thermoresponsive Poly(Ionic Liquid)s in Aqueous Salt Solutions: Salting-Out Effect on Their Phase Behavior and Water Absorption/Desorption Properties," *Macromol. Rapid Commun.*, vol. 37, pp. 1130–1134, 2016.

[71] Y. Deguchi, Y. Kohno, and H. Ohno, "A Fine Tuning of LCST-type Phase Transition of Poly(ionic liquid)s in Water," *Chem. Lett.*, vol. 44, pp. 238–240, 2015.

[72] S. Saita, Y. Mieno, Y. Kohno, and H. Ohno, "Ammonium based zwitterions showing both LCST- and UCST-type phase transitions after mixing with water in a very narrow temperature range," *Chem. Commun.*, vol. 50, pp. 15450–15452, 2014.

[73] K. Nishikawa and T. Morita, "Solution Chemistry Based on the Concept of Fluctuations," *Mol. Sci.*, vol. 6, A0054, 2012.

[74] N. Ito, T. Fujiyama, and Y. Udagawa, "A Study of Local Structure Formation in Binary Solutions of 2-butoxyethanol and Water by Rayleigh Scattering and Raman Spectra," *Bull. Chem. Soc. Jpn.*, vol. 56. pp. 379–385, 1983.

[75] A. B. Bhatia and D. E. Thornton, "Structural aspects of the electrical resistivity of binary alloys," *Phys. Rev. B*, vol. 2, pp. 3004–3012, 1970.

[76] T. Morita, H. Murai, S. Kase, and K. Nishikawa, "Small-angle X-ray scattering study on the fluctuations of supercritical aqueous solution of n-pentane along the critical isotherm of water," *Chem. Phys. Lett.*, vol. 543, pp. 68–71, 2012.

[77] H. Hayashi and Y. Udagawa, "SAXS Curve Shape Analysis of 2-Butoxyethanol Aqueous Solutions.," *Bulletin of the Chemical Society of Japan*, vol. 65, pp. 600–602, 1992.

[78] K. Nishikawa and T. Iijima, "Structural Study of fed-Butyl Alcohol and Water Mixtures by X-ray Diffraction," *J. Phys. Chem.*, vol. 94, pp. 6227–6231, 1990.

[79] H. Hayashi, K. Nishikawa, and T. Iijima, "Small-angle x-ray scattering study of fluctuations in 1-propanol-water and 2-propanol-water systems," *J. Phys. Chem.*, vol. 94, no. 21, pp. 8334–8338, 1990.

[80] J. Hu, C. A. Haynes, A. H. Wu, C. M. Cheung, M. M. Chen, E. G. Yee, T. Ichioka, K. Nishikawa,

P. Westh, and Y. Koga, “Chemical potential and concentration fluctuation in some aqueous alkane-mono-ols at 25 ºC,” *Can. J. Chem.*, vol. 81, pp. 141–149, 2003.

[81] K. Nishikawa, Y. Kasahara, and T. Ichioka, “Inhomogeneity of mixing in acetonitrile aqueous solution studied by small-angle X-ray scattering,” *J. Phys. Chem. B*, vol. 106, pp. 693–700, 2002.

[82] Y. Koga, K. Nishikawa, K. Yoshino, I. Tanaka, Y. Xu, and Y. Amemiya, “Anomalous X-ray scattering from aqueous 2-butoxyethanol at X_{BE} = 0.06 near freezing,” *Chem. Phys. Lett.*, vol. 228, pp. 53–56, 1994.

[83] T. Zemb and P. Lindner, *Neutron, X-rays and Light. Scattering Methods Applied to Soft Condensed Matter, 1st Edition*. Elsevier, 2002.

[84] R.-J. Roe, *Methods of X-ray and Neutron Scattering in Polymer Science*. OXFORD University Press, 2000.

[85] Y. Amemiya and Y. Shinohara, “X 線小角散乱の基礎と今後の展開 Principle of Small-Angle X-ray Scattering and a Perspective,” 放射光, vol. 19, pp. 338–348, 2006.

[86] H. Hayashi, K. Nishikawa, and T. Iijima, “Easy derivation of the formula relating the fluctuations of a binary system to the X-ray scattering intensity extrapolated to s = 0,” *J. Appl. Crystallogr.*, vol. 23, pp. 134–135, 1990.

[87] Y. Koga, “Vapor Pressures of Aqueous 2-Butoxyethanol Solutions at 25 ºC: Transition in Mixing Schemes,” *J. Phys. Chem.*, vol. 95, pp. 4119–4126, 1991.

[88] Y. Koga, *Solution Thermodynamics and its Application to Aqueous Solutions, 1st Edition A Differential Approach*. Elsevier Science, 2007.

[89] J. G. Kirkwood and F. P. Buff, “The Statistical Mechanical Theory of Solutions. I,” *J. Chem. Phys.*, vol. 19, pp. 774–777, 1951.

[90] A. Ben-Naim, “Inversion of the Kirkwood–Buff theory of solutions: Application to the water–ethanol system,” *J. Chem. Phys.*, vol. 67, p. 4884, 1977.

[91] K. Nishikawa, “Simple relationship between the Kirkwood-Buff parameters and the fluctuations in the particle number and concentration obtained by small-angle X-ray scattering,” *Chem. Phys. Lett.*, vol. 132, pp. 50–54, 1986.

[92] N. Shimizu, T. Mori, N. Igarashi, H. Ohta, Y. Nagatani, T. Kosuge, and K. Ito, “Refurbishing of Small-Angle X-ray Scattering Beamline, BL-6A at the Photon Factory,” *J. Phys. Conf. Ser.*, vol. 425, no. 20, 202008, 2013.

[93] T. Morita, Y. Tanaka, K. Ito, Y. Takahashi, and K. Nishikawa, “Apparatus for the simultaneous measurement of the X-ray absorption factor developed for a small-angle X-ray scattering beamline,” *J. Appl. Crystallogr.*, vol. 40, pp. 791–795, 2007.

[94] E. B. Saloman, J. H. Hubbell, and J. H. Scofield, “X-ray attenuation cross sections for energies 100 eV to 100 keV and elements Z = 1 to Z = 92,” *At. Data Nucl. Data Tables*, vol. 38, pp. 1–196, 1988.

[95] M. J. Berger, J. H. Hubbell, S. M. Seltzer, J. Chang, J. S. Coursey, R. Sukumar, D. S. Zucker, and K. Olsen, “NIST Standard Reference Database 8 (XGAM).” [Online]. Available: https://www.nist.gov/pml/xcom-photon-cross-sections-database.

[96] A. P. Hammersley, “ESRF Internal Report, ESRF98HA01 T, FIT2D V9.129, V3.1 RM.,” 1998.

[97] A. P. Hammersley, S. O. Svensson, M. Hanfland, A. N. Fitch, and D. Hausermann, “Two-dimensional detector software: From real detector to idealised image or two-theta scan,” *High Press. Res.*, vol. 14, 1996.

[98] H. E. Stanley, *Introduction to Phase Transitions and Critical Phenomena*. OXFORD University Press, 1987.

[99] J. N. Canongia Lopes, M. F. Costa Gomes, and A. A. H. Pádua, “Nonpolar, polar, and associating solutes in ionic liquids,” *J. Phys. Chem. B*, vol. 110, pp. 16816–16818, 2006.

[100] T. Morita and M. Ushio, “SAXS intensity of pure $[P_{4,4,4,4}]CF_3COO$,” 2012.

[101] D. Pečar and V. Doleček, “Volumetric properties of ethanol-water mixtures under high temperatures and pressures,” *Fluid Phase Equilib.*, vol. 230, pp. 36–44, 2005.

[102] G. S. Kell, “Density, Thermal Expansivity, and Compressibility of Liquid Water from 0" to 150 ºC: Correlations and Tables for Atmospheric Pressure and Saturation Reviewed and Expressed on 1968 Temperature Scale,” *J. Chem. Eng. Data*, vol. 20, pp. 97–105, 1975.

[103] A. Nitta, “イミダゾリウム系イオン液体$[C_4mim]BF_4$-水混合系のゆらぎ,” Master Thesis, 2014.

[104] Y. Koga, “1-Propanol probing methodology: two-dimensional characterization of the effect of solute on H_2O.,” *Phys. Chem. Chem. Phys.*, vol. 15, pp. 14548–14565, 2013.

[105] Y. Koga, “Two-dimensional characterization of the effect of solute on H_2O: A thermodynamic probing methodology,” *J. Mol. Liq.*, vol. 205, pp. 31–36, 2015.

[106] Y. Koga, “Mixing Schemes in Aqueous Solutions of Nonelectrolytes: A Thermodynamic Approach,” *J. Phys. Chem.*, vol. 100, pp. 5172–5181, 1996.

[107] Y. Koga, W. W. Y. Siu, and T. Y. H. Wong, “Excess Partial Molar Free Energies and Entroples In Aqueous tert-Butyl Alcohol Solutions at 25 ºC,” *J. Phys. Chem.*, vol. 94, pp. 7700–7706, 1990.

[108] S. H. Tanaka, H. I. Yoshihara, A. W.-C. Ho, F. W. Lau, P. Westh, and Y. Koga, “Excess partial molar enthalpies of alkane-mono-ols in aqueous solutions,” *Can. J. Chem.*, vol. 74, pp. 713–721, 1996.

[109] Y. Koga, J. Kristiansen, and A. Hvidt, “Excess partial molar volumes of $\{xCH_3(CH_2)_3O(CH_2)_2OH + (1-x)H_2O\}$ in the water-rich region,” *Journal of Chemical Thermodynamics*, vol. 25. pp. 51–56, 1993.

[110] H. Matsuo, E. C. H. To, D. C. Y. Wong, S. Sawamura, Y. Taniguchi, and Y. Koga, “Excess Partial Molar Enthalpy of 1-Propanol in 1-Propanol−NaCl−H_2O at 25 ºC: The Effect of NaCl on Molecular Organization of H_2O,” *J. Phys. Chem. B*, vol. 103, pp. 2981–2983, 1999.

[111] P. Westh, H. Kato, K. Nishikawa, and Y. Koga, “Toward understanding the Hofmeister series. 3. Effects of sodium halides on the molecular organization of H_2O as probed by 1-propanol,” *J. Phys. Chem. A*, vol. 110, pp. 2072–2078, 2006.

[112] N. Galamba, “Water tetrahedrons, hydrogen-bond dynamics, and the orientational mobility of water around hydrophobic solutes,” *J. Phys. Chem. B*, vol. 118, pp. 4169–4176, 2014.

[113] N. Galamba, “Water’s Structure around Hydrophobic Solutes and the Iceberg Model,” *J. Phys. Chem. B*, vol. 117, pp. 2153–2159, 2013.

[114] H. S. Frank and M. W. Evans, “Free Volume and Entropy in Condensed Systems III. Entropy in Binary Liquid Mixtures; Partial Molal Entropy in Dilute Solutions; Structure and Thermodynamics in Aqueous Electrolytes,” *J. Chem. Phys.*, vol. 13, pp. 507–532, 1945.

[115] Y. Koga, “Mixing Schemes in Binary Aqueous Solutions of Non-electrolytes,” *Netsu Sokutei*, vol. 30, pp. 54–65, 2003.

[116] J. Hu, W. M. Chiang, P. Westh, D. Heng, C. Chen, C. A. Haynes, and Y. Koga, “Additive Effect of 1-Propanol and 2-Propanol on Molecular Organiza- tion of H_2O in the Water-Rich Region : Excess Chemical Potential, Partial Molar Enthalpy and Volume of 1-Propanol in 1-Propanol–2-Propanol–H_2O at 25 ºC,” *Bull. Chem. Soc. Jpn.*, vol. 74, pp. 809–816, 2001.

[117] D. H. C. Chen, P. M. Chu, S. H. Tanaka, E. C. H. To, and Y. Koga, “Excess chemical potentials, partial molar enthalpies and entropies in binary aqueous acetone and tetramethyl urea at 25 ºC,” *Fluid Phase Equilib.*, vol. 175, pp. 35–43, 2000.

[118] J. T. W. Lai, F. W. Lau, D. Robb, P. Westh, G. Nielsen, C. Trandum, A. Hvidt, and Y. Koga, “Excess partial molar enthalpies, entropies, Gibbs energies, and volumes in aqueous dimethylsulfoxide,” *J. Solution Chem.*, vol. 24, pp. 89–102, 1995.

[119] M. T. Parsons, F. W. Lau, E. G. M. Yee, and Y. Koga, “Excess chemical potentials and partial molar enthalpies in aqueous 1,2-and 1,3-propanediols at 25 ºC,” *J. Solution Chem.*, vol. 32, pp. 137–153, 2003.

[120] W. W. Y. Siu, T. Y. H. Wong, L. C. F. Chao, and Y. Koga, “Excess Partial Molar Enthalpies in the Water-Rich Region of the Isobutyric Acid–Water-System,” *Can. J. Chem*, vol. 69, pp. 1065–1069, 1991.

[121] Y. Koga, P. Westh, K. Nishikawa, and S. Subramanian, “Is a methyl group always hydrophobic? Hydrophilicity of trimethylamine-N-oxide, tetramethyl urea and tetramethylammonium ion,” *J. Phys. Chem. B*, vol. 115, pp. 2995–3002, 2011.

[122] Y. Koga, “Transition of mixing scheme in the water-rich region of aqueous 2-butoxyethanol: Partial molar volumes and their derivatives,” *J. Phys. Chem.*, vol. 96, pp. 10466–10468, 1992.

[123] A. Perera, “Aqueous SolutionssTheory and Experiments,” in *85th CSC Conf. Exhib., Vancouver, Canada*, 2002.

[124] K. Nishikawa, K. Kusano, A. A. Arai, and T. Morita, “Density fluctuation of a van der Waals

fluid in supercritical state," *J. Chem. Phys.*, vol. 118, p. 1341, 2003.

[125] Y. Koga, "Excess partial molar enthalpies of tert-butanol in water-tert-butanol mixtures," *Can. J. Chem.*, vol. 66, pp. 1187–1193, 1988.

[126] K. Yoshida, S. Baluja, A. Inaba, and Y. Koga, "Acceleration of the effect of solute on the entropy-volume cross fluctuation density in aqueous 2-butoxyethanol, 1-propanol, and glycerol: The fourth derivative of Gibbs energy," *J. Chem. Phys.*, vol. 134, 214502, 2011.

[127] R. Gupta and G. N. Patey, "Association and microheterogeneity in aqueous 2-butoxyethanol solutions," *J. Phys. Chem. B*, vol. 115, pp. 15323–15331, 2011.

[128] R. Gupta and G. N. Patey, "How aggregation in aqueous 2-butoxyethanol solutions is influenced by temperature," *J. Mol. Liq.*, vol. 177, pp. 102–109, 2013.

[129] T. Morita, K. Miki, A. Nitta, H. Ohgi, and P. Westh, "Effects of Constituent Ions of a Phosphonium-based Ionic Liquid on Molecular Organization of H_2O as Probed by 1-Propanol: Tetrabutylphosphonium and Trifluoroacetate Ions," *Phys. Chem. Chem. Phys.*, vol. 17, pp. 22170–22178, 2015.

[130] T. Kondo, Y. Miyazaki, A. Inaba, and Y. Koga, "Effects of Carboxylate Anions on the Molecular Organization of H_2O as Probed by 1-Propanol," *J. Phys. Chem. B*, vol. 116, pp. 3571–3577, 2012.

[131] H. Kato, K. Miki, T. Mukai, and K. Nishikawa, "Ions : Toward Characterization of Room Temperature Ionic Liquids," *J. Phys. Chem. B*, vol. 113, pp. 14754–14760, 2009.

[132] H. Kato, K. Nishikawa, and Y. Koga, "Relative hydrophobicity and hydrophilicity of some 'ionic liquid' anions determined by the 1-propanol probing methodology: A differential thermodynamic approach," *J. Phys. Chem. B*, vol. 112, pp. 2655–2660, 2008.

[133] K. Miki, P. Westh, K. Nishikawa, and Y. Koga, "Effect of an 'ionic liquid' cation, 1-butyl-3-methylimidazolium, on the molecular organization of H_2O," *J. Phys. Chem. B*, vol. 109 pp. 9014–9019, 2005.

[134] T. Morita, A. Nitta, K. Nishikawa, P. Westh, and Y. Koga, "Characterization of BF_4^- in terms of its effect on water by the 1-propanol probing methodology," *J. Mol. Liq.*, vol. 198, pp. 211–214, 2014.

[135] R. Wang, W. Leng, Y. Gao, and L. Yu, "Microemulsion-like aggregation behaviour of an LCST-type ionic liquid in water," *RSC Adv.*, vol. 4, pp. 14055–14062, 2014.

[136] NIST, "Thermophysical Properties of Fluid Systems." [Online]. Available: http://webbook.nist.gov/chemistry/fluid/.

[137] O. Redlich and A. T. Kister, "Algebraic Representation of Thermodynamic Properties and the Classification of Solutions," *Ind. Eng. Chem.*, vol. 40, pp. 345–348, 1948.

[138] K. Nishikawa and T. Iijima, "Small-Angle X-ray Scattering Study of Fluctuations in Ethanol and Water Mixtures," vol. 97, pp. 10824–10828, 1993.

Acknowledgments

I would like to express the deepest appreciation to Professor Takeshi Morita for his helpful guidance through the course of this work. He gave me many chances for my valuable experiences and he instructed me experimental technique. Without his support, this thesis would not be materialized.

I would like to express my sincerest appreciation to Professor Keiko Nishikawa for her continuous support. She gave the opportunity to study on the aqueous solution of ionic liquid.

I am indebted to Dr. Yoshikata Koga (The University of British Columbia) for his instruction of differential thermodynamics. Also I developed my English skill by his lesson on writing papers.

I would like to express my gratitude to Professor Hiroyuki Ohno (Tokyo University of Agriculture and Technology) for donation of the sample ionic liquid tetrabutylphosphonium trifluoroacetate.

I thank to High Energy Accelerator Research Organization (KEK). All Small-Angle X-ray Scattering measurements were performed under the approval of the Photon Factory Program Advisory Committee (Proposal No. 2014G689).

And special thanks to my family for their support in everyday life.